

# February 6, 2023 Kahramanmaraş Earthquakes in Türkiye

## Reconnaissance Report

Canadian  
Association  
for Earthquake  
Engineering  
and Seismology



L'Association  
Canadienne  
du Génie  
Parasismique et  
de la Sismologie

## CAEES/ACGPS Field Team Members (Alphabetical Order)

Jason Dowling	Associated Engineering
Emre Insel	University of Ottawa
Yavuz Kaya	British Columbia Ministry of Transportation and Infrastructure
Tuna Onur	Onur Seemann Consulting, Inc. University of Victoria
Bora Pulatsu	Carleton University
Murat Saatcioglu	University of Ottawa
Ali Senturk	STFA Group
Cheryl Sewell	AtkinsRéalis
Tyler Southam	Tetra Tech Canada Inc.
Thuraisamy Thavaraj	Klohn Crippen Berger
Helene Tischer	Arup
Martin Zaleski	BGC Engineering

## Table of Contents

<b>Table of Contents</b>	<b>1</b>
<b>Introduction</b>	<b>7</b>
<b>1. Earthquake Sequence Summary</b>	<b>8</b>
<b>2. Geology and Tectonic Setting</b>	<b>10</b>
<b>3. Ground Rupture and Surface Faulting</b>	<b>11</b>
<b>3.1. East Anatolian Fault</b>	<b>11</b>
3.1.1. Kırıkhan, Hatay	12
3.1.2. Altınüzüm, Gaziantep	14
3.1.3. Ağabey, Gaziantep	16
3.1.4. Islahiye, Gaziantep	16
3.1.5. Şekeroba, Kahramanmaraş	18
3.1.6. Türkoğlu, Kahramanmaraş	18
3.1.7. Çiğli, Kahramanmaraş	20
3.1.8. Balkar, Adıyaman	24
3.1.9. Çelikhan, Adıyaman	24
<b>3.2. Narlı Fault</b>	<b>27</b>
3.2.1. Bahçelievler, Kahramanmaraş	27
3.2.2. Tetirlik, Kahramanmaraş	28
<b>3.3. Sürgü-Çardak Fault</b>	<b>28</b>
3.3.1. Barış, Kahramanmaraş	28
3.3.2. Polatdere, Doğanşehir	29
<b>4. Ground Motions</b>	<b>32</b>
<b>5. Geotechnical Observations</b>	<b>34</b>
<b>5.1. Liquefaction and Lateral Spreading</b>	<b>35</b>
5.1.1. İskenderun, Hatay	35
5.1.1.1. Liquefaction Settlements	35
5.1.1.2. Lateral Spreading	40
5.1.1.3. Ejecta	41

5.1.2.	Orontes River Bridges, Demirköprü, Hatay	42
5.1.3.	Gölbashi, Adiyaman	44
5.1.3.1.	Liquefaction Settlements	44
5.1.3.2.	Lateral Spreading	44
5.1.3.3.	Ejecta	45
5.1.4.	Roadway Lateral Spreading, Malatya-Kahramanmaraş Road	49
<b>5.2.</b>	<b>Performance of Earth Dams</b>	<b>51</b>
5.2.1.	Büyük Karaçay Dam, Hatay	51
5.2.2.	Karamanli Göleti Dam, Hatay	52
5.2.3.	Kartalkaya Dam, Kahramanmaraş	53
5.2.4.	Sürgü Dam, Malatya	54
5.2.5.	Sultansuyu Dam, Malatya	55
<b>5.3.</b>	<b>Performance of Retaining Structures</b>	<b>56</b>
<b>5.4.</b>	<b>Landslides, Rockfall, and Slope Stability</b>	<b>57</b>
5.4.1.	D420 Transmission Tower Block Slide, Hancağiz, Hatay	57
5.4.2.	Olive Grove Block Slide, Tepehan, Hatay	57
5.4.3.	Tektuğ Erkenek hes Hydroelectric Facility, Adiyaman	60
5.4.4.	O-52 Underpass Embankment Failure, Çöçelli, Kahramanmaraş	63
5.4.5.	Rockfall outside of Nurhak, Kahramanmaraş	64
5.4.6.	Bulam 2 Bridge, Adiyaman-Çelikhan Road, Adiyaman	65
<b>5.5.</b>	<b>Karst Failures</b>	<b>66</b>
<b>6.</b>	<b>Performance of Building Structures</b>	<b>68</b>
<b>6.1.</b>	<b>Overview</b>	<b>68</b>
6.1.1.	Typical Structural Systems in Türkiye	69
6.1.2.	Evolution of Turkish Seismic Design Codes for Buildings	69
6.1.3.	Design Response Spectra for Selected Locations Visited	74
<b>6.2.</b>	<b>General Overview of Observed Damage</b>	<b>78</b>
6.2.1.	PGA Intensity	80
6.2.2.	Soil Conditions	80
6.2.3.	Building characteristics	80
<b>6.3.</b>	<b>Observed Damage Based on Locations Visited</b>	<b>80</b>

<b>6.4.</b>	<b>Reinforced Concrete (RC) Structures</b>	<b>93</b>
6.4.1.	RC Buildings constructed prior to 2000	93
6.4.2.	RC Buildings constructed since 2000	94
6.4.3.	Effects of Structural Irregularities	97
6.4.3.1.	Stiffness Irregularity	97
6.4.3.2.	Cantilevered floors	100
6.4.4.	Damage to Stairs	101
<b>6.5.</b>	<b>Reinforced Concrete Tunnel Form Shear Wall Buildings</b>	<b>102</b>
<b>6.6.</b>	<b>Precast Concrete Buildings</b>	<b>106</b>
<b>6.7.</b>	<b>Steel Buildings</b>	<b>113</b>
<b>6.8.</b>	<b>Hospitals</b>	<b>117</b>
<b>6.9.</b>	<b>Schools</b>	<b>121</b>
<b>6.10.</b>	<b>Performance of Non-Structural Components</b>	<b>131</b>
<b>6.11.</b>	<b>Pounding and Impact Damage</b>	<b>136</b>
<b>6.12.</b>	<b>Effects of Soft Soils and Liquefaction</b>	<b>138</b>
<b>7.</b>	<b>Traditional Residential Buildings and Cultural Heritage</b>	<b>139</b>
7.1.	Introduction	139
7.2.	Damage and Failure Mechanisms of Unreinforced Masonry Buildings	140
7.3.	Traditional Timber-Laced and Infill-Frame Masonry Buildings	144
7.4.	Post-Earthquake Observations on the Local and Global Failure Mechanisms of Historical Constructions	147
7.5.	Final Remarks	153
<b>8.</b>	<b>Lifelines</b>	<b>156</b>
8.1.	Performance of Roadway Network	156
8.2.	Performance of Bridges	156
8.2.1.	Typical Highway Underpasses	156
8.2.2.	Pedestrian Bridges	159
8.2.3.	Other Bridges	161
8.2.4.	Summary List	165

<b>8.3.</b>	<b>Airports and Ports</b>	<b>168</b>
<b>8.4.</b>	<b>Pipelines</b>	<b>169</b>
<b>9.</b>	<b>Recovery and Reconstruction Efforts</b>	<b>170</b>
<b>9.1.</b>	<b>Environmental Impact</b>	<b>170</b>
<b>9.2.</b>	<b>Emergency Response, and Temporary Shelters</b>	<b>171</b>
9.2.1.	Tent Camps and Container Settlements	171
	<b>References</b>	<b>174</b>

## Executive Summary

A M7.8 earthquake occurred in southeast Türkiye, 33 km south-east of Kahramanmaraş on February 6, 2023 at 4:17 local time at a depth of 10 km. A second earthquake with M7.6 hit the region only 9 hours later at 13:24 local time, 62 km north-east of Kahramanmaraş at a depth of 9 km. The earthquakes occurred along the East-Anatolian fault and affected 11 provinces, resulting in over 50,000 casualties and over 110,000 injuries. More than 100,000 buildings were either collapsed or heavily damaged. Shallow nature of the earthquakes, coupled with strong shakings, as well as the proximity to urban areas and unfavourable soil conditions resulted in widespread devastation. According to the World Bank rapid assessment report released on February 27, 2023 the earthquakes caused an estimated \$34.2 billion in direct physical damages in Türkiye, the equivalent of 4% of the country's 2021 GDP. Turkish Government declared on March 17, 2023 that the total loss was \$103.6 billion. The Canadian Association for Earthquake Engineering and Seismology/L'Association Canadienne du Genie Parasismique et de la Sismologie sent a reconnaissance team to investigate the performance of engineering infrastructure. The team consisted of 12 members covering expertise in seismology, geology, as well as geotechnical and structural engineering. Their findings are presented in this reconnaissance report.

The earthquakes imposed high seismic force and deformation demands on structures. In many cases the seismic resistance of the buildings was below the design force levels prescribed in the current Turkish Seismic Code. The Turkish seismic codes followed the global seismic design practices closely. However, there appears to be challenges with the implementation of seismic design requirements in the field, indicating potential lack of code enforcement practices. Furthermore, the prevailing soil conditions in large segments of the disaster region were not suitable for earthquake resistant construction without the implementation of appropriate geotechnical measures. Therefore, significant amplifications of ground motions were recorded. The geo-seismic impacts included ground rupture, liquefaction-induced lateral spreading, and settlements, rockfalls, and landslides. These impacts caused widespread damage to buildings, bridges, earth dams, port structures, and lifelines. In general, the damage to buildings was much greater than the damage observed in other infrastructure. A number of earth dams suffered various degrees of damage. The bridge infrastructure experienced limited damage, but some damage was observed in other lifelines, including road surface failures and airport runway failures. Hatay airport was constructed on the former Amik Lake with unfavourable soil conditions, and its runway was damaged due to the surface rupture.

The quality of construction materials and practices were observed to have improved over the years. The predominant form of building construction was cast-in-place reinforced concrete frames with infill masonry walls, having between 5 to 18 stories. Most of the buildings were built prior to the implementation of the 2019 seismic code. The damage observed in the majority of buildings was attributed to commonly used irregular structural layouts and lack of appropriate design and detailing practices. The increased use of reinforced concrete shear walls

and wall-like wide columns in recent years improved the seismic performance. The unreinforced masonry infill walls suffered extensive damage, often in the form of diagonal tension cracking and the crushing of masonry units. The region had diverse traditional residential and heritage building stock which was severely affected by the earthquakes. The damage observed were attributed to lack of proper connections among the load-bearing walls, which were poorly constructed, though a significant number of these traditional buildings performed exceptionally well.

Emergency response efforts and temporary shelters were observed in the areas visited, with tent camps and container settlements, indicating well-coordinated post-disaster measures.

## Acknowledgements

The CAEES/ACGPS reconnaissance trip started with a visit to the Middle East Technical University (METU) in Ankara, Türkiye to meet with the members of the METU team who had been in the disaster region immediately after the earthquakes. The assistance received and the valuable insight provided were extremely valuable in planning and conducting the reconnaissance investigation. The meeting was organized by Professor Erdem Canbay, Chair, Department of Civil Engineering at METU. The authors gratefully acknowledge the contributions of colleagues who were involved in the exchange of information, including Professors Ayşegül Askan, Erdem Canbay, Güney Özcebe and Onur Pekcan. In addition, Mr. Serhat Erinmez provided logistical support and Mr. Ali Kürşad Bozbaş provided help for visiting the industrial facilities in Gaziantep.

Appreciations are extended to AFAD (Disaster and Emergency Management Presidency of the Ministry of Interior of the Government of Türkiye) for granting the permission to visit the disaster area and the facilities in the region. In particular, Dr. Recep Çakır of Washington Geological Survey was instrumental in requesting the permission, Ms. Tuba Kadiroğlu and Mr. Murat Doruk Şentürk of AFAD facilitated the permission process with the letter of permission received from the General Director of AFAD Seismic Risk Reduction Directorate, Dr. Orhan Tatar.

The authors acknowledge information shared by USGS (United States Geological Survey), CGS (California Geological Survey), and GEER (Geotechnical Extreme Events Reconnaissance) team members involved in early post-earthquake desktop-level analysis and field reconnaissance, whose findings informed this trip's reconnaissance targets, especially Kate Allstadt, Timothy Dawson, Alexandra Hatem, Richard Koehler, Ben Mason, Nadine Reitman, and Kate Thomas. The authors also acknowledge information on fault surface rupture provided by Kandilli Observatory and Earthquake Research Institute, which was visited by some members in İstanbul, Türkiye prior to the trip.

Finally, the financial contributions received from CAEES/ACGPS are greatly appreciated.

## Introduction

Two earthquakes occurred in southeastern Türkiye on February 6, 2023, causing major devastation, and affecting eleven provinces. The earthquakes occurred along the East-Anatolian fault and caused over 50,000 casualties and over 110,000 injuries. More than 100,000 buildings were either collapsed or heavily damaged. The shallow nature of the earthquakes coupled with strong shakings, as well as the proximity to urban areas, unfavourable soil conditions and poorly designed and detailed structures resulted in a widespread disaster. According to the World Bank rapid assessment report released on February 27, 2023 [1] the earthquakes caused an estimated \$34.2 billion in direct physical damages, the equivalent of 4% of Türkiye's 2021 GDP. The Turkish Government declared, on March 17, 2023, that the total loss was \$103.6 billion [2]. The Canadian Association for Earthquake Engineering and Seismology/L'Association Canadienne du Genie Parasismique et de la Sismologie (CAEES/ACGPS) sent a reconnaissance team on May 6, 2023 to investigate the performance of engineering infrastructure. The team consisted of technical experts in seismology, geology, and ground motions, as well as geotechnical, structural, and hydraulic engineering. The reconnaissance took place between May 6, 2023 and May 13, 2023 and covered a large segment of the disaster area, as indicated in the observations contained herein. A second team was also organized by CAEES/ACGPS to visit the disaster area between June 5, 2023 and June 9, 2023 forming part of an international team of investigators. This report provides findings of the first reconnaissance team in the following areas:

- Seismology, geology, and tectonic setting of the region.
- Ground motions, ground rupture, and surface faulting.
- Geotechnical observations of the earthquake effects.
- Performance of building structures.
- Performance of historic masonry and cultural heritage structures.
- Performance lifelines and bridge infrastructure.
- Emergency response and temporary shelters.

A separate section is presented on each of the above topics, while addressing overlapping areas between ground motions, soil conditions, design and construction practices, and infrastructure performance. A pictorial presentation of seismic damage is provided with explanations on potential reasons as observed by the authors.

# 1. Earthquake Sequence Summary

**Tuna Onur**

A sequence of two damaging earthquakes happened within nine hours of each other on February 6<sup>th</sup>, 2023 in southeastern Türkiye. The first (Pazarcık) earthquake (Mw7.8, USGS; Mw7.7, AFAD) occurred at 04:17 local time (01:17 UTC/GMT) near Pazarcık, in the province of Kahramanmaraş (epicentral location: 37.226N 37.014E from USGS; 37.288N 37.043E from AFAD). The Pazarcık earthquake ruptured multiple segments of the southwestern portion of the East Anatolian Fault (roughly 300km of rupture length), which is a major left-lateral strike-slip fault forming the boundary between the Anatolian Plate and the Arabian Plate. The East Anatolian Fault connects with the Dead Sea Fault to the southwest and meets up with the North Anatolian Fault at the Karliova triple junction (between the Anatolian, Arabian, and Eurasian Plates) to the northeast (Figure 1.1). The rupture initiated on an adjacent fault called Narlı Fault (near the middle of the ruptured portion of the East Anatolian Fault) and propagated bilaterally towards southwest and northeast (Figure 1.2). Surface rupture from this earthquake can be traced from the northern outskirts of Antakya in the southwest, to the east of Çelikhhan in the northeast (see Section 3).



**Figure 1.1:** General Tectonic Setting, Plate Movements and Major Active Faults

The second (Elbistan) earthquake (Mw7.5, USGS; Mw7.6, AFAD) occurred at 13:24 local time (10:24 UTC/GMT) near Elbistan, Kahramanmaraş (epicentral location: 38.011N 37.196E from USGS; 38.089N 37.239E from AFAD), and ruptured the smaller east-west trending Sürgü-Çardak Fault (roughly 170km of rupture length), a left-lateral strike-slip fault near the northern end of

the first earthquake's rupture zone (Figure 1.2). The rupture initiated near Elbistan and propagated bilaterally towards east and west. Surface rupture from this earthquake extends from Göksun in the west to Doğanşehir in the east (see Section 3).

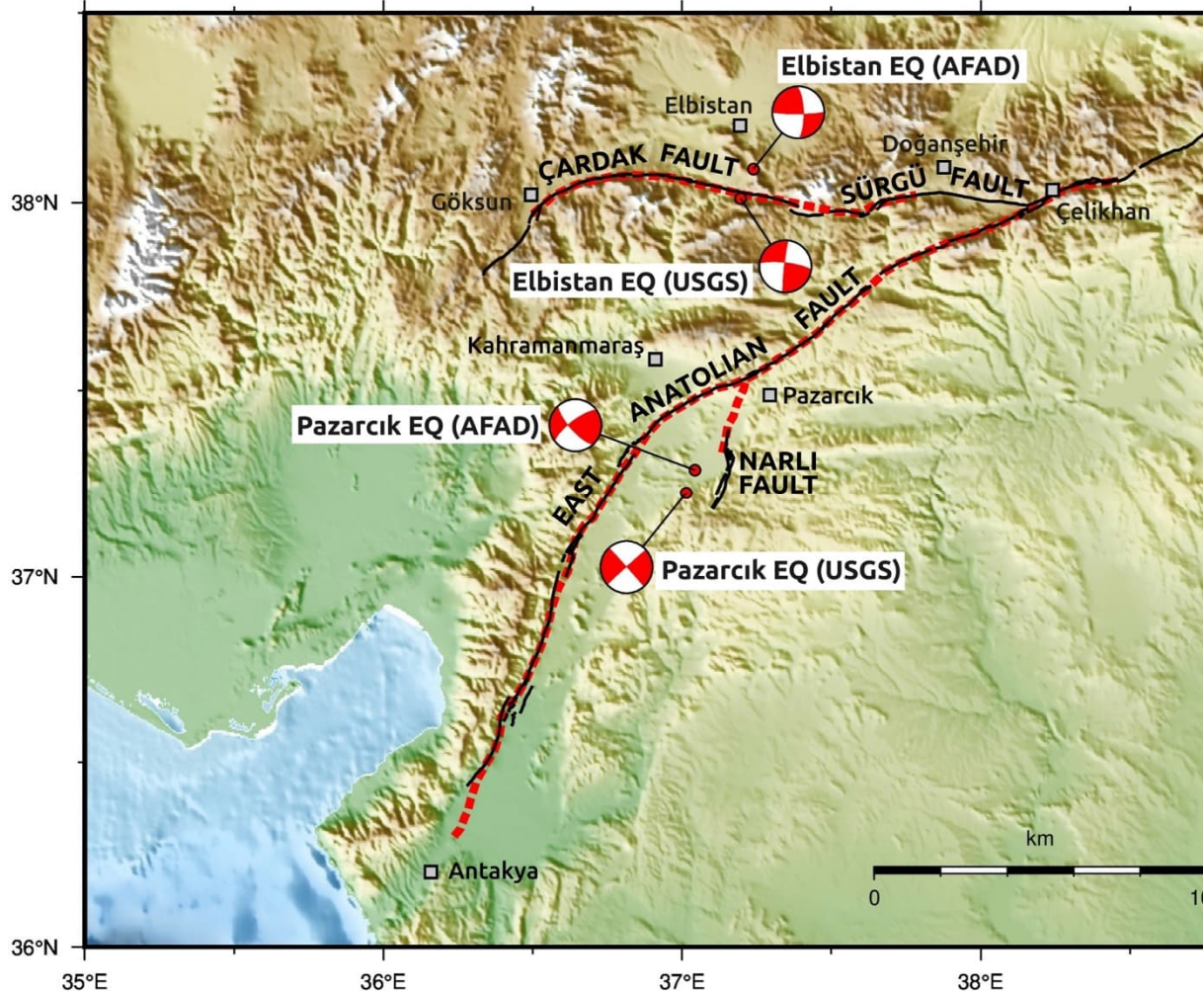


**Figure 1.2: Pazarlık and Elbistan Earthquakes** (thick red dashes indicate the ruptured segments of the faults)

The two earthquakes were followed by numerous aftershocks, the largest of which was a Mw6.8 (USGS) earthquake that occurred 11 minutes after the Pazarlık earthquake to the northeast of the Pazarlık earthquake's epicenter (Figure 1.3).

The Pazarlık earthquake ruptured the three southernmost segments of the East Anatolian Fault (Karabulut et al., 2023), from south to north: the Amanos segment (previous major rupture: M7.2 in 1872), the Pazarlık segment (previous major rupture: M7.0 in 1795), and the Erkenek segment (previous major rupture: M7.1 in 1893). A relatively recent earthquake near Elazığ (Mw6.8 in 2020) ruptured the adjacent segment to the north, raising concern about increasing the stress to the south, which indeed ended up being released three years later, in the 2023 earthquakes.

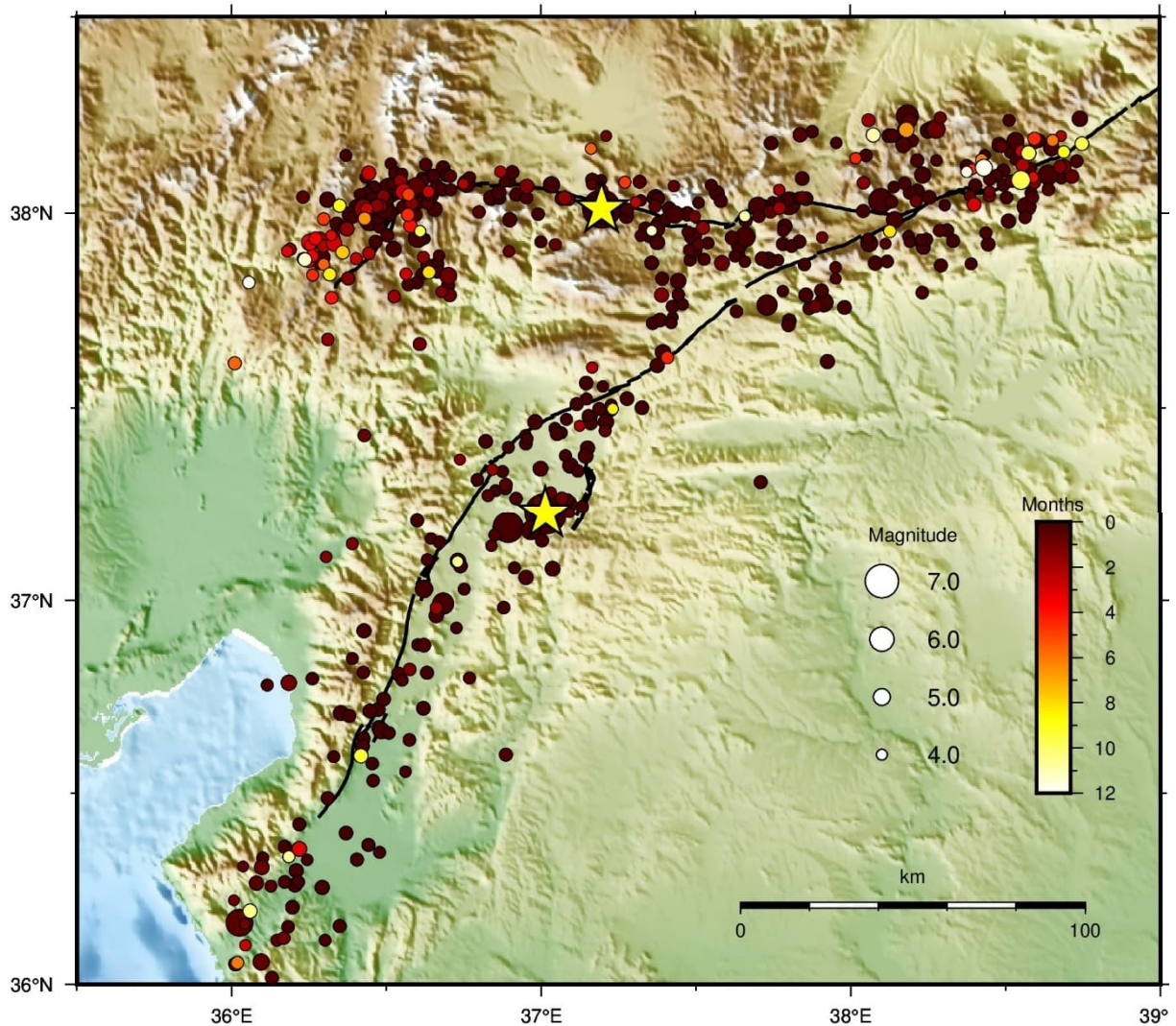


**Figure 1.3: Aftershock distribution of the earthquake sequence by month**

## 2. Geology and Tectonic Setting

Tuna Onur and Martin Zaleski

Türkiye geologically belongs to the Alpine-Himalayan orogenic belt that was formed in the Cenozoic era. It lies in a tectonically active region, geologically young and complex, consisting of several terranes with sedimentary rocks of varying ages, many intrusions, and areas of volcanic material.

The North Anatolian fault (right lateral strike-slip) forms the northern boundary and the East Anatolian fault (left lateral strike slip) forms the southern boundary of the westward moving Anatolian Block, which makes up most of the territory of Türkiye (Figure 1.1). The Anatolian

block is squeezed westward in a counterclockwise rotation by the northward motion of the Arabian Plate relative to Eurasian Plate. At its northern terminus, the East Anatolian Fault connects with the North Anatolian fault at the Karlıova triple junction, and at its southern terminus it connects with the Dead Sea fault, which forms the plate boundary between the Arabian and African Plates (Figure 1.1).

This complex tectonic setting causes a high rate of seismic activity in eastern Turkey. The two main faults, the North Anatolian fault and the East Anatolian fault, are capable of generating very large earthquakes ( $M_w > 7.5$ ), though they rupture at different rates. The North Anatolian Fault has a slip rate of about 25 mm/year, significantly higher than the East Anatolian Fault, which has a slip rate of about 10 mm/year [3].

### 3. Ground Rupture and Surface Faulting

**Martin Zaleski, Tuna Onur, and Tyler Southam**

Both earthquakes produced extensive surface fault rupture along the traces of the East Anatolian, Narlı, and Sürgü-Çardak faults. Observed offsets were left-lateral strike-slip with limited vertical separation along faults.

Along straight sections of the fault, observable ground-surface deformation was typically confined to within five metres of the main trace. Surface faulting was expressed as some combination of the following:

- Sharp linear scarps and mole tracks aligned with fault strike.
- Right-stepping, en-echelon tension cracks, often coupled with orthogonal thrust ridges connecting the cracks. Tension crack long axes were typically oriented about 30° counterclockwise with respect to fault strike.

At restraining and releasing bends, deformation zone widths increased to several tens to hundreds of metres. Surface faulting and ground rupture orientations were more variable and discontinuous. Restraining and releasing bends were typically located in mountainous areas, where it was difficult to distinguish between surface faulting, sackungen, ridge-top spreading, and coseismic-landslide-related fractures.

The CAEES/ACGPS team visited select locations along the East Anatolian fault between Kirikhan, Hatay Province, and Çelikhan, Adıyaman province; the Narlı fault between Bahçelievler and Tetirlik in Kahramanmaraş province; and the Sürgü-Çardak fault from Barış, Kahramanmaraş Province, to Polatdere, Doğanşehir Province. Observations from visited sites are summarized in the following subsections.

#### 3.1. East Anatolian Fault

The East Anatolian fault ruptured for a length of about 300 km from Antakya to Çelikhan. Observed surface ruptures extend as far south as the village of Akçaova, 13 km north of Antakya. Surface rupture was generally continuous for the southernmost 10 km from Akçaova

through Hatay Airport, and then was discontinuous for 23 km between the airport and the village of Karaçağıl, 10 km northeast of Kırıkhan in Hatay Province. A 44 km gap in observed surface faulting lies between Karaçağıl and Altınüzüm, Gaziantep Province, where the fault is within the Nur Mountains, to Çelikhan, Adıyaman Province. Discontinuous, distributed surface faulting resumed at Altınüzüm and extended northeast for 30 km to Nurdağı, Gaziantep Province, where the surface faulting became generally continuous and confined to a single trace for about 50 km to the village of Çiğli, Kahramanmaraş. Between Çiğli and Gölbaşı, Adıyaman Province, over a distance of about 70 km, the fault is continuous for straight segments through valleys, but becomes concealed at bends, through mountains, and at crossings of wetlands. The fault generally experienced limited observed surface rupture for the northeasternmost 60 km segment through the Nurhak Mountains, between Gölbaşı and Çelikhan; here, much of the observed ground rupture is related to coseismic landsliding and not unequivocally surface faulting.

The largest offsets observed by the CAEES/ACGPS team along surface ruptures of the East Anatolian fault occurred near the east end of the rupture zone, near Çelikhan, Adıyaman Province (4.9 m left-lateral offset), and near the junction of the East Anatolian and Sürgü-Çardak faults at Çiğli, Kahramanmaraş Province (4.8 m left-lateral offset). Near Türkoğlu, Kahramanmaraş Province, where 3.6 m of left-lateral offset was measured, post-earthquake orthophoto imagery reveals evidence for natural gas transmission pipeline ruptures. The East Anatolian fault crosses many towns and cities; extensive infrastructure damage and building collapse can be attributed directly to differential ground displacement along surface fault rupture.

### **3.1.1. Kırıkhan, Hatay**

The fault was observed as a 2.07 m left-lateral offset of a road ascending an alluvial fan Figure 3.1). Offset was distributed along two sharp strands 46 km apart. The road offset was in line with right-stepping en-echelon tension gashes and mole-track scarps extending north and south of the road crossing (Figure 3.2).



**Figure 3.1:** Facing west across fault offset of paved road, near Kırıkhan, Hatay Province (36.5284 N, 36.3711 E). Photo: M. Zaleski.



**Figure 3.2:** Facing north along right-stepping, en-echelon cracks that define surface fault rupture, near Kırıkhan, Hatay (36.5283 N, 36.3709 E). Photo: M. Zaleski.

About 650 m north of the road crossing, the fault splits into two strands where it leaves alluvial fans and ascends bedrock hills. Deformation was observed to be distributed across several strands over about 80 m width, each showing decimetre-scale left-lateral offset across paved and unpaved roads, and manifesting as scarps through orchards.

### 3.1.2. Altınüzüm, Gaziantep

At Altınüzüm, a cast-in-place concrete pad and attached concrete-block wall were damaged and offset by surface faulting directly through them. Up to 1.65 m left-lateral and 0.35 m west-side-up displacement occurred (Figure 3.3). To the immediate north, the scarp changes from west-side-up through alluvial fan deposits to east-side-up where it crosses a west-facing, bedrock-cored slope (Figure 3.4 and Figure 3.5).



**Figure 3.3:** Facing east across concrete pad cut by surface faulting at Altınüzüm (36.9550 N, 36.5839 E). 1.4 m left-lateral and 0.4 m east-side-up vertical offset were measured. Photo: M. Zaleski.



**Figure 3.4:** Facing south along fault strike, near Altınüzüm, showing right-stepping en-echelon surface rupture pattern (36.9576 N, 36.5840 E). Photo: M. Zaleski.



**Figure 3.5:** Facing east across left-lateral fault offset of an unpaved road near Altınüzüm (36.95856 N, 36.5843 E). Photo: M. Zaleski.

### 3.1.3. Ağabey, Gaziantep

At Ağabey, the main fault crossing becomes discontinuous as it enters the Nur Mountains, east of the main valley and D825 highway. The CAEES/ACGPS team found a 0.15 m left-lateral offset of the highway pavement, striking orthogonal to the fault and located about 1 km east of the fault's surface trace. This feature is interpreted as a flexural-slip fault accommodating elastic rebound strain release away from the fault.



**Figure 3.6:** Facing southwest along Highway D825, near Ağabey (36.9700 N, 36.5991 E), showing 0.15 m left-lateral offset of pavement along a structure orthogonal to the main fault trace. Photo: M. Zaleski.

### 3.1.4. Islahiye, Gaziantep

The main fault trace passes through the parking lot of the Islahiye hospital, north of the city (Figure 3.7). The fault is expressed as a 14 m wide graben, bounded by near-vertical scarps in agricultural fields south of the paved parking lot (Figure 3.8). 2.4 m left-lateral offset was measured at a concrete-block wall bounding the south side of the parking lot. The graben bottom was observed up to 1.6 m below the adjacent terrain. The overall vertical offset was observed up to 0.8 m, east side up.



**Figure 3.7: Facing south along fault trace, forming a graben at the Islahiye hospital parking lot (37.0450 N, 36.6295 E). Photo: M. Zaleski.**



**Figure 3.8: Facing south along fault graben, from Islahiye hospital parking lot (37.0443 N, 36.6294 E). Photo: M. Zaleski.**

### 3.1.5. Şekeroba, Kahramanmaraş

The main trace of the East Anatolian fault passes through the town of Şekeroba, where many structures sited across it experienced damage and collapse. At one home, the CAEES/ACGPS team was invited by a homeowner to view deformation of a backyard well. The well, located about 5 m off the fault trace, was originally round, but had become ovalized during the earthquake, with the long axis oriented about 30° counterclockwise from the strike of the fault trace (Figure 3.9). Offset walls and curbs along the fault trace record left-lateral slip of about 1.2 to 1.5 m with little discernible vertical separation.



**Figure 3.9: Ovalized well located 5 m from the East Anatolian fault trace in 3.1.5 Şekeroba (37.2587 N, 36.7742 E). Photo: M. Zaleski.**

### 3.1.6. Türkoğlu, Kahramanmaraş

Near Türkoğlu 3.6 m of left-lateral separation was measured at a road crossing of the fault (Figure 3.10) as well as in offsets of drainage ditches and furrows in adjacent farm fields. Surface rupture continues to the northeast and southwest of the road crossing, manifesting as a continuous array of moletracks, right-stepping en-echelon fractures oriented 20° counterclockwise from the main trace, and push-up ridges oriented 20° to 50° clockwise from the main trace (Figure 3.11 and Figure 3.12).



**Figure 3.10: Facing southeast across fault offset of a road near Türkoğlu (37.3706 N, 36.8693 E). Photo: M. Zaleski.**



**Figure 3.11: Facing northeast along fault strike near Türkoğlu, showing aligned moletracks and push-up ridges (37.3716 N, 36.8701 E). Photo: T. Southam.**



**Figure 3.12: Facing south toward push-up ridge along main fault trace near Türkoğlu (37.3716 N, 36.8703 E). Photo: T. Southam.**

Two known natural gas transmission pipeline crossings occur near Türkoğlu, both within about 3 km of the site at which the CAEES/ACGPS team measured 3.6 m left-lateral surface offset. Post-event orthophoto imagery available through Google Earth (dated March 1, 2023) depict charred craters and recent excavations, consistent with gas pipeline ruptures and exposures (Figure 3.13 and Figure 3.14). The crossings occur in floodplain deposits.

### **3.1.7. Çiğli, Kahramanmaraş**

The largest ground-surface offsets observed by the CAEES/ACGPS team along the East Anatolian fault were near the town of Çiğli. The main fault trace crosses the D835 highway about 3 km southwest of the town and a concrete-lined canal about 2 km southwest of the town. At both locations, the fault is confined to a width less than about 3 m, producing distinct offsets of these features. The CAEES/ACGPS team measured 3.5 m left-lateral offset at the highway crossing (Figure 3.15) and 4.8 m at the canal (Figure 3.16). At both sites, the infrastructure had been temporarily repaired before the CAEES/ACGPS reconnaissance: the highway pavement had been re-patched with new asphalt, and the canal had been re-lined with shotcrete.

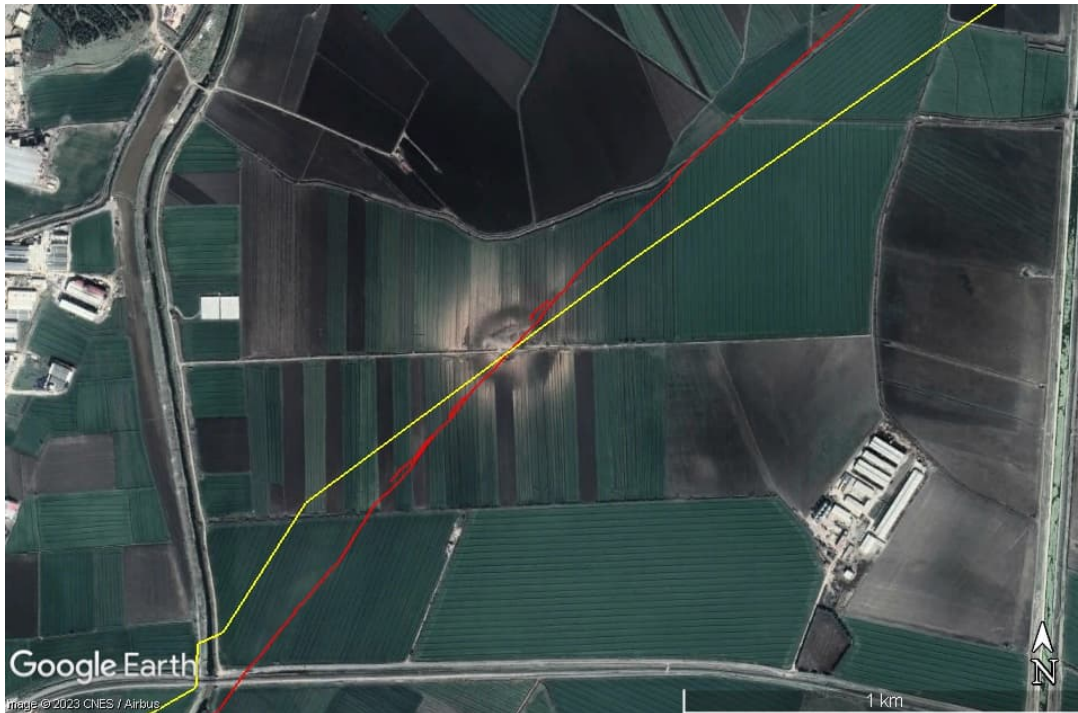


**Figure 3.13:** Google Earth imagery dated March 1, 2023, depicting a charred blast crater at a natural gas pipeline (yellow line) crossing of the surface fault trace mapped by USGS (red line). Site is located 3.4 km east of Türkoğlu, at 37.3880 N, 36.8852 E.

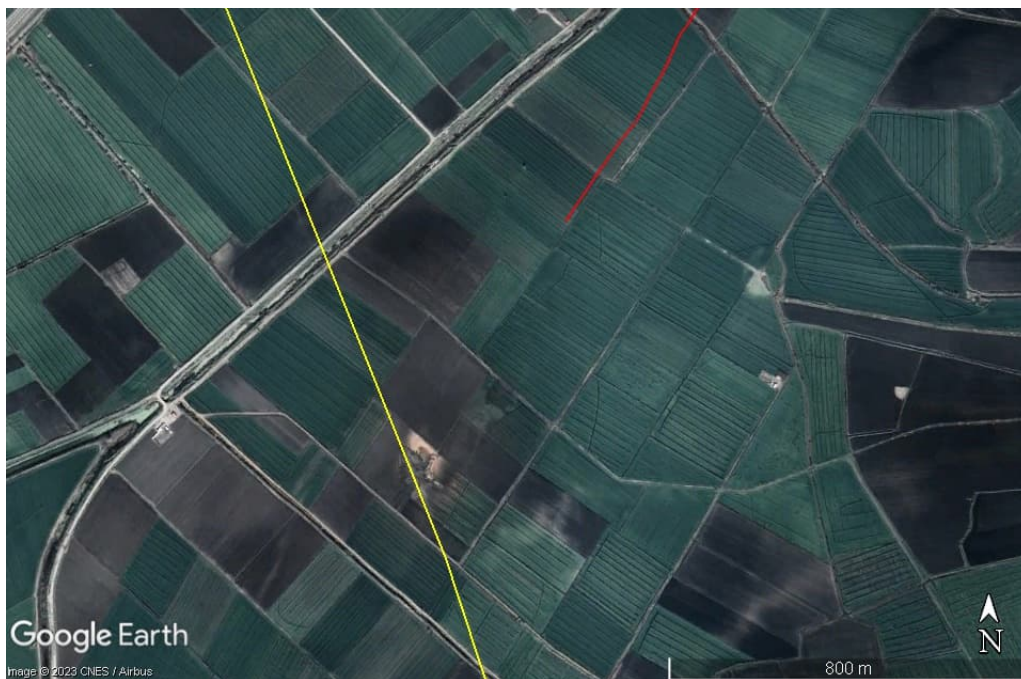


**Figure 3.14:** Google Earth imagery dated March 1, 2023, depicting a charred blast crater at a natural gas pipeline (yellow line), along strike of the surface fault trace mapped by USGS (red line). Site is located 3.8 km south of Türkoğlu, at 37.3880 N, 36.8852 E.



**Figure 3.15: Facing southeast at K835 highway crossing of the East Anatolian fault (37.4799 N, 37.0422 E), with 2.8 m left-lateral offset. Photo: M. Zaleski.**



**Figure 3.16: Facing southeast along canal offset by the East Anatolian fault (37.4850 N, 37.0540 E). Photo: T. Southam.**

The observable surface rupture terminates at Çiğli. The fault enters a restraining bend North of the town, and its surface expression became discontinuous and occupies a widely distributed zone of deformation. The residents described some scarps and grabens as faults, but upon review, some were interpreted by the CAEES/ACGPS team as coseismic landslide features. The CAEES/ACGPS team observed a home whose southeast corner was cut by the fault trace: this home was reportedly lifted off its foundation by the initial pulse of the earthquake and rotated 10° to 15° counterclockwise with respect to its pre-event foundation (Figure 3.17: ). The residents' reports and the observable ground-surface evidence is interpreted by the CAEES/ACGPS team as the home having been flung momentarily airborne by vertical accelerations in excess of 1 g, and rotated sideways by wrenching near-field ground movement while the southeast corner of the house was airborne. Left-lateral offset of a retaining wall next to the home was measured at 3.0 m (Figure 3.18).



**Figure 3.17: Gap between house foundation and adjacent patio in Çiğli, indicating counterclockwise rotation during the earthquake (37.4937 N, 37.0730 E). Photo: M. Zaleski.**



**Figure 3.18: 3.0 m left-lateral offset of a retaining wall in Çiğli (37.4936 N, 37.0278 E). Photo: M. Zaleski.**

### 3.1.8. Balkar, Adiyaman

The CAEES/ACGPS team measured 4.5 m horizontal separation and 0.4 m vertical separation on a northwest-facing, continuous scarp crossing the D-360 highway (Figure 3.19). Uncertainty introduced by the acute angle between the highway and fault is estimated at +/- 1.2 m.

### 3.1.9. Çelikhan, Adiyaman

The East Anatolian fault passes about 1 km south of the village of Çelikhan, following a well-defined lineament separating a steep, north-facing range front, from gentler-sloping alluvial fan deposits. The fan surfaces between the fault and the village are dissected by steep-walled gullies reporting to a linear, southwest-directed main drainage channel, suggesting relatively rapid tectonic uplift. Landslides are ubiquitous in the valley and on the range front, many of which have surface expressions consistent with coseismic landslides (e.g., fresh and unvegetated scarps and cracks; (Figure 3.20). Some lineaments mapped by USGS along the range front were re-interpreted as coseismic landslide scarps upon field examination by the CAEES/ACGPS team.

A clear, unequivocal surface rupture of the East Anatolian fault was observed on an elevated terrace, about 6 km east of Çelikhan (Figure 3.21). Here, the fault was expressed as a series of right-stepping en-echelon fractures. The features' location, set back from the terrace riser, and their linear form were inconsistent with coseismic landsliding.



**Figure 3.19:** Facing northeast along fault strike at the D-360 highway crossing in Balkar (37.7346 N, 37.5659 E). Photo: M. Zaleski.



**Figure 3.20:** Facing southeast across the trace of the East Anatolian fault, near Çelikhan (38.0368 N, 38.2621 E). Slope-scale coseismic landslides occur on the range front, collocated with the fault trace. Photo: M. Zaleski.



**Figure 3.21:** Facing southwest along East Anatolian fault trace, east of Çelikhan (38.0413 N, 38.3073 E). Right-stepping en-echelon crack array crosses the middle of an elevated terrace surface. Photo: M. Zaleski.

Horizontal separation of 4.9 m and vertical separation of 0.3 m (north side up) were measured at a highway crossing west of Çelikhan; however, the measurement assumes the road was straight before the earthquake and is therefore subject to an estimated +/- 1.5 m uncertainty (Figure 3.22). The scarp is confined to 1 to 2 m width across the hills on either side of the road crossing.



**Figure 3.22:** Facing north across East Anatolian fault crossing of a highway southwest of Çelikhan (38.0104 N, 38.2246 E). Photo: M. Zaleski.

### 3.2. Narlı Fault

The Narlı fault displays discontinuous surface rupture along its trace. The southern end, near Bahçelievler, is characterized by broad extensional deformation, producing locally downdropped terrain. As the fault leaves the lowland around Bahçelievler and proceeds northeastward into the hills toward its intersection with the East Anatolian fault, it displays intermittent rupture of relatively small left-lateral offset (typically 1 m or less), but confined to a trace width of less than 3 m. The fault was observed by the CAEES/ACGPS team at two locations.

#### 3.2.1. Bahçelievler, Kahramanmaraş

The Narlı fault passes through agricultural land along the east side of the town of Bahçelievler. Distributed faulting bounds an approximately 200 m wide graben, downdropped about 0.3 to 0.5 m with respect to the surrounding terrain (Figure 3.23). Soil within the downdropped block is anomalously wet. The fields are planted with garlic, which fares better in well-drained soil; accordingly, the downdropping is interpreted as tectonic and having occurred after the fields were seeded. Slip displacement could not be reliably measured using available piercing points.



**Figure 3.23: Facing south along a 0.4 m high fault bounding a downdropped graben along the Narlı fault near Bahçelievler (37.3908 N, 37.1511 E). Photo: M. Zaleski.**

### 3.2.2. Tetirlik, Kahramanmaraş

Near its junction with the East Anatolian fault, the Narlı fault passes through the village of Tetirlik. Surface rupture is discontinuous on a scale of tens of metres. Near the centre of the village, 0.9 m of left-lateral displacement has split a tree trunk (Figure 3.24) and pulled the base of a column at the corner of an adjacent house out of its original position (Figure 3.25).



**Figure 3.24.** Facing north toward a tree split by surface faulting, on strike with a displaced corner column at the east (photo right) side of the home in the background, in Tetirlik (37.5368 N, 37.2733 E). Photo: M. Zaleski.

### 3.3. Sürgü-Çardak Fault

The largest observed surface fault displacements are on the Sürgü-Çardak fault, with up to 8.2 m of left-lateral displacement measured near Barış. The CAEES/ACGPS team performed only a limited reconnaissance of this fault; accordingly, only two locations are described herein.

#### 3.3.1. Barış, Kahramanmaraş

The Sürgü-Çardak fault is near linear for about 8 km from Around Barış to the east; accordingly, fault deformation is confined to a sharp scarp, with little evidence for distributed deformation and en-echelon cracking (Figure 3.26 and Figure 3.27: ). The largest left-lateral displacement

measured by the CAEES/ACGPS team was 7.75 m across a linear creek channel about 2.25 km east of Barış.



**Figure 3.25:** Column separated from remainder of house by left-lateral offset along the Narlı fault in Tetirlik (37.5368 N, 37.2733 E). Photo: M. Zaleski.

### 3.3.2. Polatdere, Doğanşehir

Polatdere is near the easternmost limit of observed surface rupture along the Sürgü-Çardak fault. A releasing bend occurs at the fault's crossing of the D-850 (Gölbaşı to Malatya) highway, producing discontinuous, open tension gashes up to 0.5 m wide and 2.3 m deep, distributed over a zone up to 20 m wide (Figure 3.28). Left-lateral displacement of up to 1.4 m was measured across one of the fault segments, though this is interpreted as an underestimate, given the distributed nature of the faulting (Figure 3.29).



**Figure 3.26:** Facing east along Sürgü-Çardak surface rupture near Barış (38.0017 N, 37.3460 E). Continuous surface rupture is visible across the range front in the photo background.  
**Photo:** M. Zaleski.



**Figure 3.27:** Facing north at 6.9 m left-lateral offset of a field drain near Barış (38.0018 N, 37.3452 E). Photo: M. Zaleski.



**Figure 3.28: Open tension gashes in a releasing bend near Polatdere (38.1456 N, 37.9625 E). Photo: M. Zaleski.**



**Figure 3.29: Facing northeast along distributed surface rupture near Polatdere (38.1433 N, 37.9610 E). Zone of surface faulting is about 8 m wide. Photo: M. Zaleski.**

## 4. Ground Motions

Tuna Onur

The Disaster and Emergency Management Authority (Afet ve Acil Durum Yönetimi Başkanlığı, AFAD) runs a nationwide strong motion network in Türkiye. Currently, there are over 700 accelerometers in this network (Figure 4.1) and many of them recorded the February 2023 earthquakes (Figure 4.2). The data from these stations can be found at the AFAD web site: <https://tadas.afad.gov.tr/>

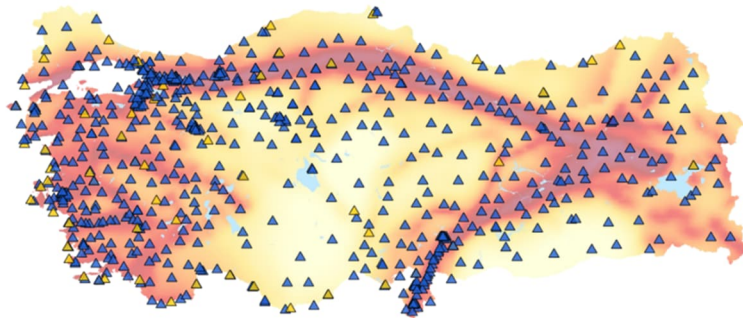
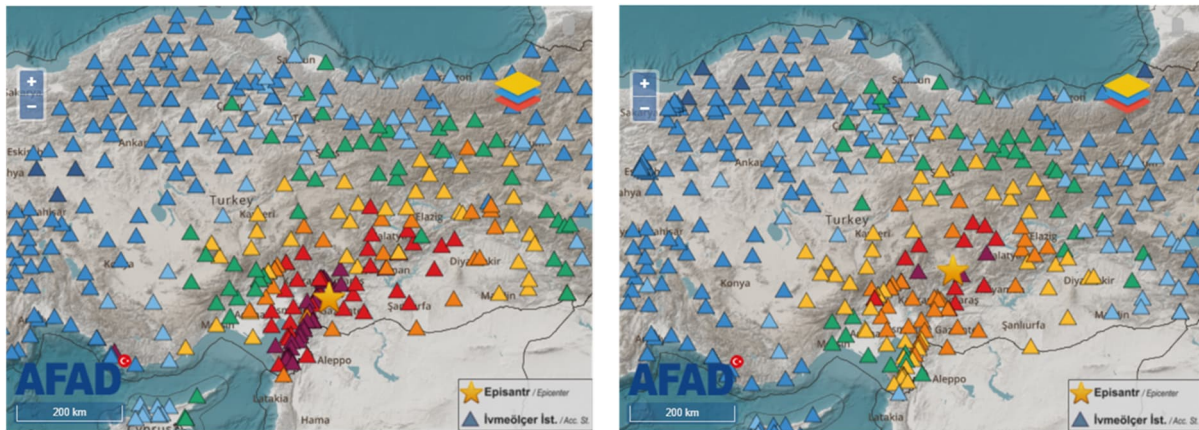


**Figure 4.1: Accelerometers in the AFAD strong motion network. The background colours indicate the seismic hazard levels in the current national seismic hazard map (from low hazard in yellow to high hazard in dark red and purple). Blue triangles indicate a stand-alone strong motion station. Yellow triangles indicate hybrid or multiple sensors, which include strong motion. Image credit: AFAD.**



(a)

(b)



**Figure 4.2: Peak ground accelerations (PGA) recorded by AFAD strong motion stations in (a) Pazarcik earthquake, (b) Elbistan earthquake. Image credit: AFAD.**

Shortly after the earthquakes, AFAD removed data from some of the strong motion stations due to problems in the instruments and/or recordings. In this report, those data are not used. In addition, the processed data from the AFAD web site uses an unconventional filter. Therefore, all the data shown in this Section was downloaded as raw (unprocessed) data and processed by the CAEES/ACGPS team using a bandpass Butterworth order 4 filter. Before filtering, a linear baseline correction was applied. The sampling rate for the instruments used in this report is 100 samples per second, i.e. the Nyquist frequency is 50Hz. Accordingly, the filter corners of 0.1Hz and 40Hz are used in processing the data.

The amplitudes of the ground motions generally attenuate by distance from the rupture ( $R_{rup}$ ). However, the stations are on varying ground conditions, which also influences the ground motions. The ground conditions vary from recent alluvial soft sediments, for which the average shear wave velocity in the upper 30m,  $V_{s30}$ , is generally lower than 400m/s; to rock (mostly limestone or basalt), for which the  $V_{s30}$  is generally higher than 700m/s. The region is also rich in weathered carbonate rocks with various degrees of weathering. The  $V_{s30}$  for these formations is generally between 400m/s and 700m/s. The  $V_{s30}$  for the strong motion stations is provided by AFAD for most of the stations, which are primarily calculated from shear wave velocities directly measured at the strong motion instrument sites.

The effect of ground conditions is clearly evident in the strong motion recordings. For example, the cities of Antakya (in the Hatay province) and Kahramanmaraş (in the Kahramanmaraş province) both have multiple strong motion stations on varying ground conditions. When the recording station is on softer sediments, the ground motions are higher in amplitude and the peaks of the response spectra are consistently at longer periods. Figure 4.3 shows two examples of the effect of ground conditions, (a) for Antakya, and (b) for Kahramanmaraş using a few select stations. The stations on rock are indicated by green (no rock recordings available at the appropriate distance range in Antakya), the stations on weathered carbonates by yellow/orange, and the stations on recent alluvial sediments by red triangles.

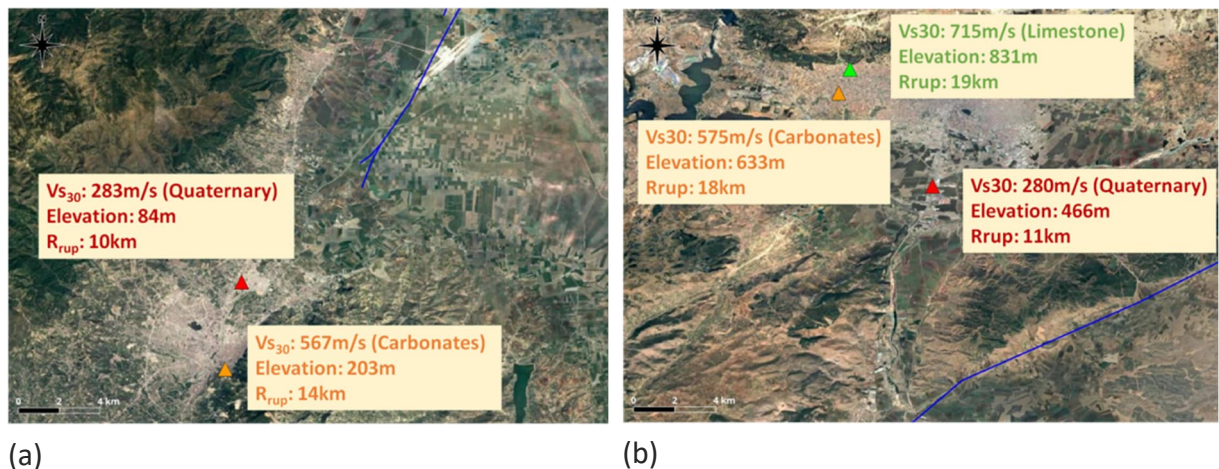


**Figure 4.3: Selected stations in the cities of (a) Antakya, (b) Kahramanmaraş. Green indicates  $V_{s30} > 700\text{m/s}$ , orange indicates  $400\text{m/s} < V_{s30} < 700\text{m/s}$ , and red indicates  $V_{s30} < 400\text{m/s}$ .**

In both figures, altitudes of the stations as well as  $V_{s30}$  from measured shear wave velocities are indicated. In general, the higher altitude stations are on stiffer ground in these cities. The response spectra for these stations are presented in Figure 4.4.

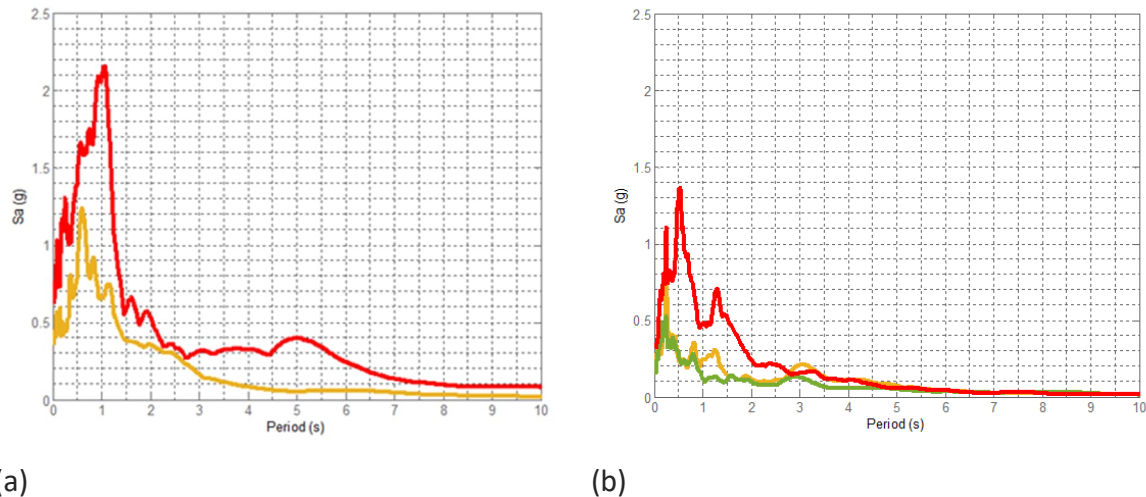


**Figure 4.4: Response spectra of the records from (a) Antakya, (b) Kahramanmaraş. The colours are consistent with the station markings in Figure 4.3.**

## 5. Geotechnical Observations

Tyler Southam, Thava Thavaraj

The team aimed to conduct reconnaissance to review the performance of geotechnical structures, ground conditions, and natural slopes as a result of the earthquake sequence. The geo-seismic impacts of the earthquakes included ground motion amplification (Section 4), ground rupture (Section 3), liquefaction-induced lateral spreading and settlements, rockfalls, and landslides. These impacts caused widespread damage to the infrastructure including buildings, bridges, earth dams, port structures, and lifelines. In general, the damage to buildings was much greater than those to the other infrastructure. Buildings built on liquefiable soils experienced significant settlement, tilting or foundation failure in both Iskenderun and Gölbaşı. Bridge abutments and approach embankments experienced failure due to slope instability and lateral spreading caused by liquefaction or strain softening. Evidence of a bridge span failure caused by rockfall was observed in northern Adiyaman. Minor to severe cracking on earth dams caused apparently by seismic compression or liquefaction was observed; however, none of the dams breached or experienced an uncontrolled release of the reservoir. Flooding near the seafront in Iskenderun was observed apparently caused by seismic compression and liquefaction-induced ground settlement.

## **5.1. Liquefaction and Lateral Spreading**

### **5.1.1. İskenderun, Hatay**

İskenderun is a coastal city within the Hatay province that is home to an estimated 250,000 people and is the second most populated district within Hatay [4]. İskenderun also is home to the second largest port in Türkiye [5].

The surficial soils are generally composed of Quaternary-aged alluvium with additional areas of reclaimed fill near the shoreline [5, 6]. In the Çay District, particularly along Atatürk Boulevard which runs parallel to the waterfront, there was extensive evidence of surface manifestations of liquefaction in the form of ejecta, lateral spreading, liquefaction induced settlements of buildings and infrastructure, and potential free-field settlements at the shoreline resulting in tidal water inflow.

As part of the work conducted by the Earthquake Engineering Research Institute (EERI) joint report with the Geotechnical Extreme Events Reconnaissance (GEER) the authors estimated ground motions for the area. At the closest estimated location (36.5756, 36.1732) to the Çay District, about 1.5km away, the estimated PGAs were 0.26g and 0.02 g for the M7.8 and M7.5 events, respectively, with PGV estimates of 46 cm/s and 11 cm/s respectively [5].

#### **5.1.1.1. Liquefaction Settlements**

The waterfront park is largely reclaimed land and constructed by placing fill along the shoreline in the 1980s [5]. Most of the liquefaction induced settlement was with about 150 m of the shoreline, with the highest concentration of observations in the waterfront park area and along Atatürk Blvd and Bahçeli Sahil Evler Cd.

The pedestrian pier on the waterfront adject to the İskenderun monument square displayed settlement of the area surrounding the pier of about 35 to 40 cm relative to the surrounding ground as shown in Figure 5.1.



**Figure 5.1: İskenderun Pedestrian Pier Settlement (36.5927,36.1727)**

Along the waterfront, there was widespread flooding and ponding of water along Atatürk Blvd and Bahçeli Sahil Evler Cd. While undertaking the reconnaissance tidal waters were observed to be flowing towards the city. From conversations with local residents they believed the ground level of the area had settled approximately 70 cm which has resulted in the water inflow. Images collected during the reconnaissance in the area on May 7, 2023 are shown in Figure 5.2.



**Figure 5.2: Top Left - İskenderun Shoreline Water Level on May 7, 2023 (36.5927,36.1727). Top Right – Water flowing from shoreline towards Atatürk Blvd (36.5907, 36.1754). Bottom Left – Water ponding along Atatürk Blvd (36.5907, 36.1747) Bottom Right – Water ponding along Bahçeli Sahil Evler Cd (36.5906, 36.1797).**

Typically the buildings located on Atatürk Blvd and Bahçeli Sahil Evler Cd experienced settlements up to about 70 cm. Limited differential settlements were observed in the structures, however due to the settlements positive drainage from the foundations was no longer present and in many cases ponding water was observed adjacent to the foundations as shown in Figure 5.3.



**Figure 5.3: Examples of Building Settlement and Water ponding typical along Atatürk Blvd and Bahçeli Sahil Evler Cd. Top Left 36.5908, 36.1782, Top Right 36.5907, 36.1789, Bottom Left 36.5907, 36.1789, Bottom Right 36.5911, 36.1795.**

A notable building in the area was the 7-storey Çivisöken Apartment building which did not display structural damage congruent with the surrounding areas which experienced a high level of damage and structural collapse. The report published by the Türkiye Earthquake Reconnaissance and Research Alliance notes that the foundation of the building included diaphragm walls and ground improvement [6]. The sidewalks adjacent to the building displayed approximately 15 to 20 cm of settlement, the observations of the building are shown in Figure 5.4.

To the west, the İskenderun Nihal Atakaş Mosque which is adjacent to the waterfront displays evidence of liquefaction induced settlements around the structure. The structure which appears to have been constructed on piles was observed to be approximately 30 to 50 cm above the surrounding ground as shown in Figure 5.5. At the time of the reconnaissance the area around the mosque was closed for repairs which limited detailed measurements from being obtained, surface ejecta was also observed within tiled area surrounding the mosque and is discussed further in Section 5.1.1.3.



**Figure 5.4: Çivisöken Apartment (36.5905,36.1757)**

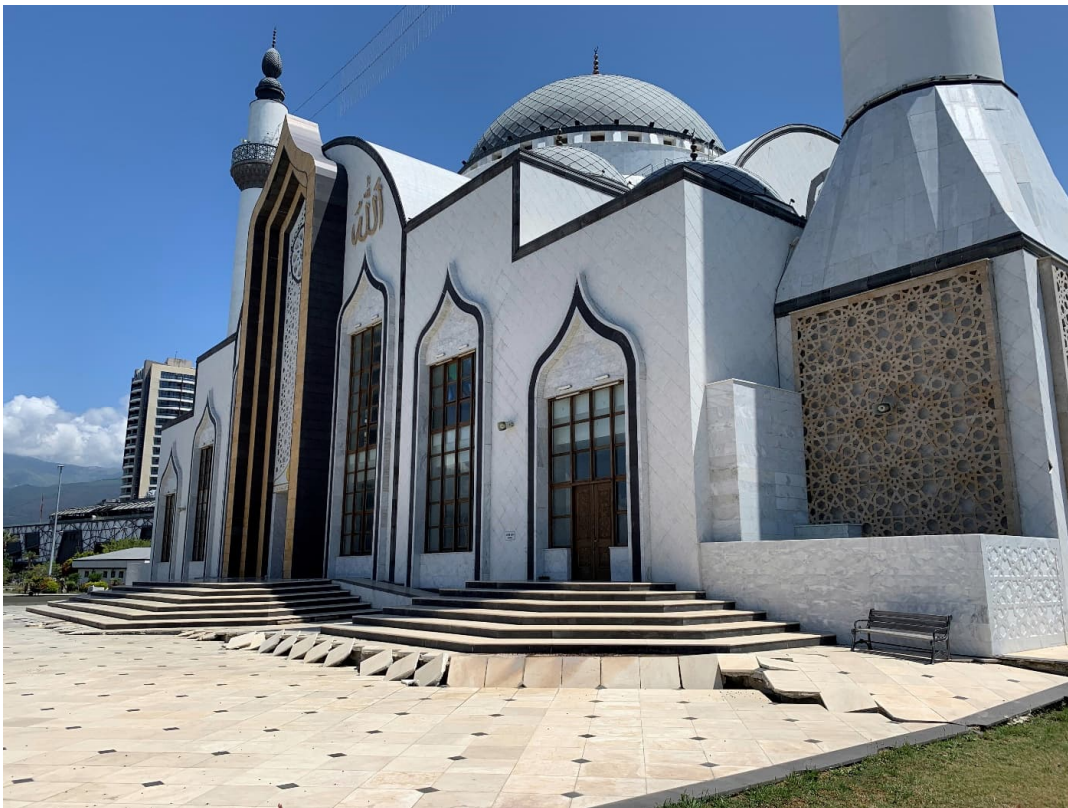


**Figure 5.5: İskenderun Nihal Atakaş Mosque (36.5927, 36.1572)**

### 5.1.1.2. Lateral Spreading

Along the waterfront of the Çay District there were comparatively minor observations of lateral spreading. At the Çay District Evlendirme Dairesi building, the structure generally appeared to have moved towards the shoreline. Several tension cracks were present surrounding the structure up to about 15 cm, indications of lateral spreading at the Evlendirme Dairesi building are shown in Figure 5.6.



**Figure 5.6: Lateral Spreading at Evlendirme Dairesi building (36.5915, 36.1743). Top Google Earth Aerial Imagery Dated Feb. 16, 2023 [7], Bottom left-right indications of movement.**

Other earlier reconnaissance observations noted more pronounced liquefaction induced lateral spreading within the port areas of İskenderun [5, 6]. These areas were not reviewed as part of the reconnaissance described herein. From conversations with security at the port facilities it was understood these areas had been repaired at the time of the reconnaissance. Examples of the lateral spreading from available aerial imagery are shown in Figure 5.7 below.

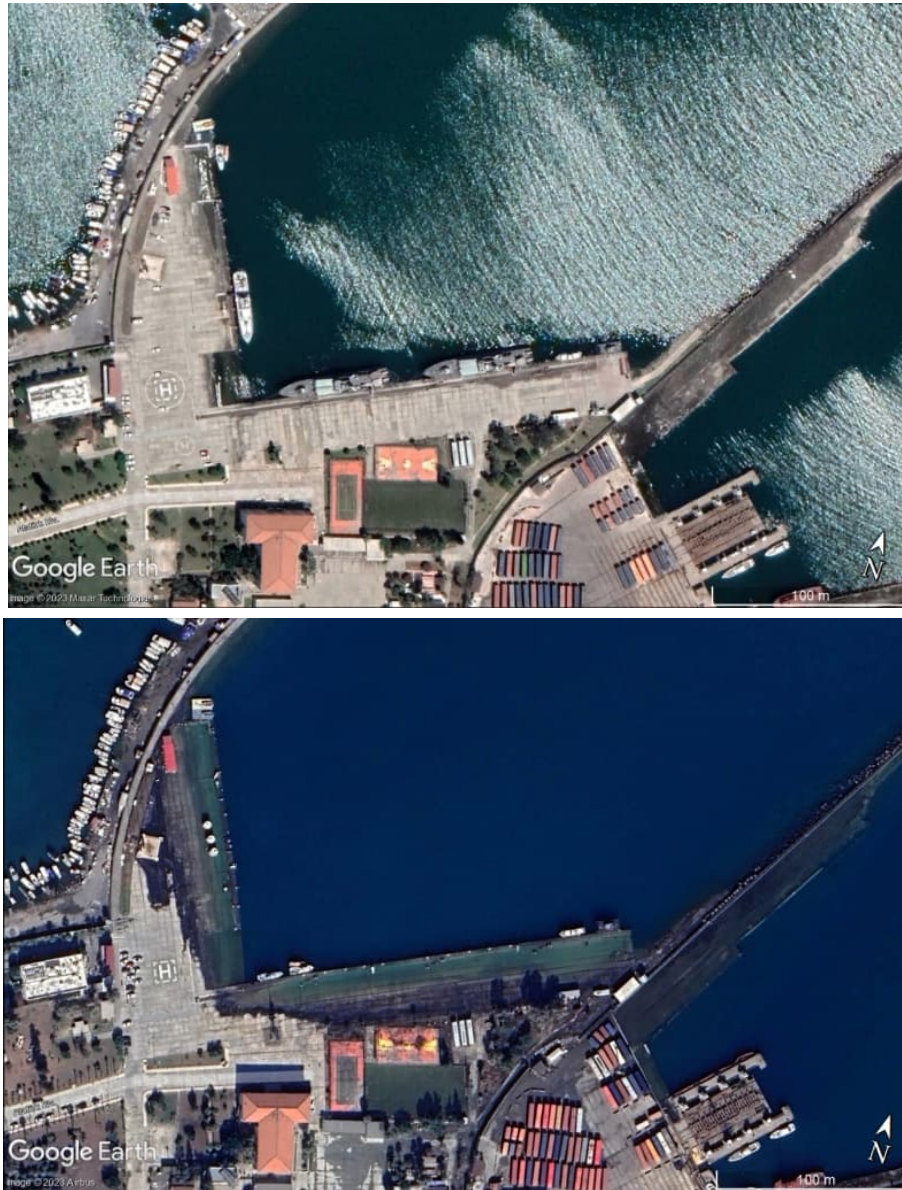


**Figure 5.7: Lateral Spreading within port area adjacent Atatürk Blvd (36.5928, 36.1806). Top Google Earth Aerial Imagery Dated Jul. 2022, Bottom Google Earth Aerial Imagery Dated Feb. 16, 2023. [7]**

### **5.1.1.3. Ejecta**

The remnants of liquefaction ejecta were observed throughout the waterfront of the Çay District. The ejecta generally appeared to be composed of grey fine sand with trace non-plastic fines (<10%), however subsequent laboratory testing will be required to substantiate field observations. Examples of the ejecta are shown in Figure 5.8.

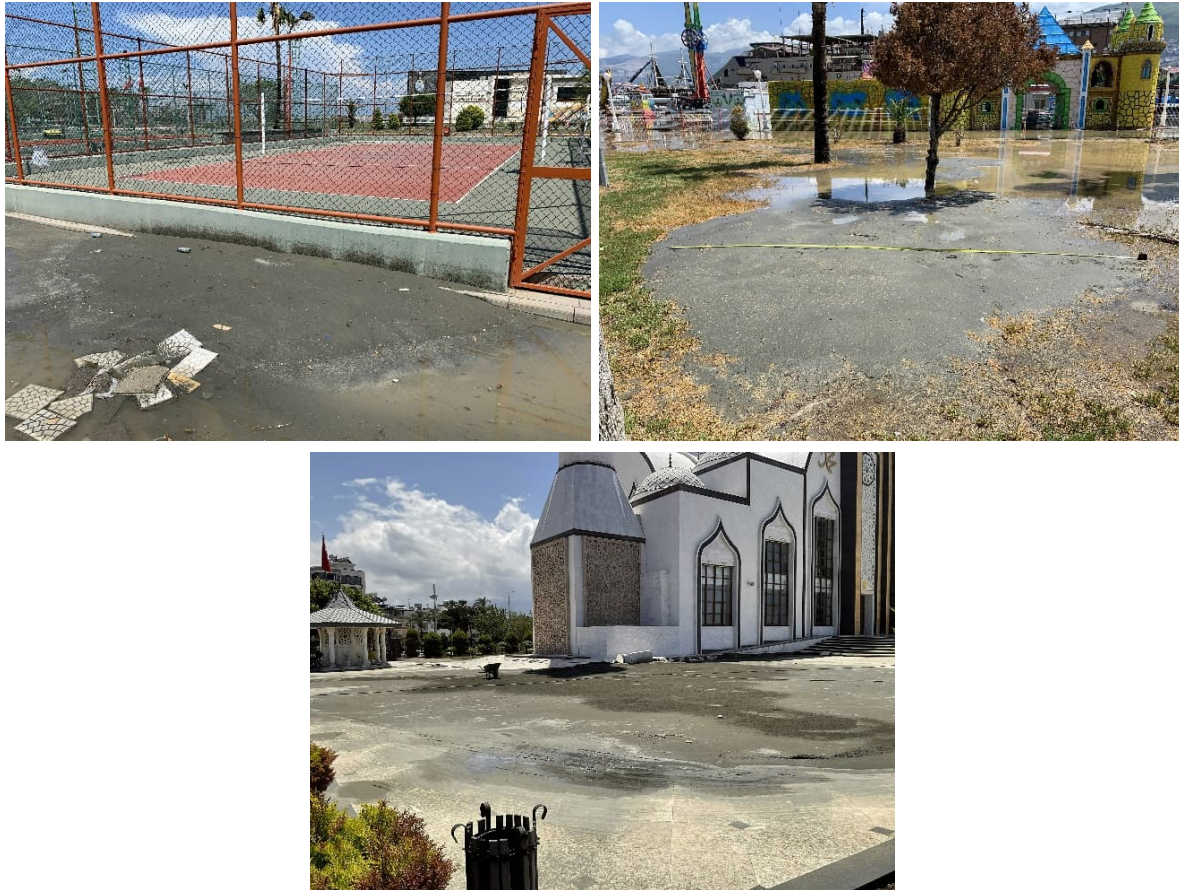


**Figure 5.8: Liquefaction Ejecta. Top Left - 36.5907, 36.1748, Top Right - 36.5914, 36.175, Bottom 36.5927, 36.1572.**

In addition to the areas of identified ejecta, large amounts of sand was observed along Atatürk Blvd and Bahçeli Sahil Evler Cd. It was not clear if these sands were ejecta or flood transported sediments. Earlier reconnaissance noted widespread ejecta along Atatürk Blvd which had been removed at the time of the reconnaissance described herein [6].

### **5.1.2. Orontes River Bridges, Demirköprü, Hatay**

In Demirköprü, Hatay on the Antakya Cilvegözü road there was failure of a pair of bridges that resulted from liquefaction induced lateral spreading. The bridges are three span structures with two piers within the river and abutments located about 10 m back from the riverbank. The abutments formed by four piles and a pile cap. As a result of the liquefaction induced lateral spreading the approaches to both bridges on both sides failed as shown for the northeast approach in Figure 5.9. At each of the four abutments, the abutments were observed to have rotated inwards approximately 23 degrees towards the free face of the Orontes River, as shown in Figure 5.9. In addition, the west pier on the north bridge appeared to have rotated in counter-clockwise when viewed from above as shown in Figure 8.10. At the time of the reconnaissance the south bridge approaches had been filled and repaved and was open to traffic. The bridges are further described within Section 8.2.3.



**Figure 5.9: Condition of Orontes River Bridges in Demirköprü (36.2456, 36.3573). Left - North East Approach Slab Failure Right - South East Abutment Rotation.**

Lateral spreading was evident both to the northeast and southwest of the bridges, with parallel tension cracks and back scarps present at both locations, as shown in Figure 5.10. An area of widespread sand boils and ejecta was present to the southwest. The sand boils were concentrated at the back scarps of the lateral spread features and were up to about 1.5 m in diameter. The ejecta was a light brown fine sand with trace (<10%) fines; subsequent laboratory testing will be required to substantiate field characterization. The sand boils and their ejecta are shown Figure 5.11.



**Figure 5.10: Lateral Spreading of the Orontes River Bridges in Demirköprü (36.2456, 36.3573) Left-Northeast, Right Southwest.**



**Figure 5.11: Sand boils adjacent to the Orontes River Bridges in Demirköprü (36.2456, 36.3573).**

### 5.1.3. Gölbaşı, Adiyaman

Gölbaşı is a lakeside city within the Adiyaman province that is home to an estimated 34,000 people [8]. The surficial soils are generally composed of Quaternary gravelly sandy soils with clay-silt intercalations [6]. The city is located on the south side of lake Gölbaşı with isolated buildings and infrastructure on the north side of the lake. Widespread evidence of surface manifestations of liquefaction was observed throughout the waterfront region on both the north and south sides of the lake. Similar to Iskenderun the EERI-GEER team provided preliminary estimates of the PGA within the city (37.7888, 37.6497); the estimates for the M7.8 and M7.5 events were 0.51g and 0.27g respectively, with PGV estimates of 122 cm/s and 70 cm/s, respectively [5].

#### 5.1.3.1. Liquefaction Settlements

The downtown lakeside area of Gölbaşı experienced widespread settlement of buildings which was inferred to be a result of liquefaction induced bearing capacity loss. Buildings above 3-4 stories typically experienced settlement, whereas buildings under this height generally showed less signs of settlement. Of the buildings that experienced settlements the settlements were generally relatively uniform; however, there were instances differential settlement caused buildings to develop excessive tilt and in extreme cases overturning of the buildings. Examples of relatively uniform settlements are shown in Figure 5.12, examples of differential settlements are shown in Figure 5.13.

#### 5.1.3.2. Lateral Spreading

Examples of lateral spreading were observed on both the north and south side of lake Gölbaşı. In both instances the slope of the ground was shallow, and material moved towards the free face of the lake. Examples of the lateral spreading around lake Gölbaşı are shown in Figure 5.14 through Figure 5.16.

### 5.1.3.3. Ejecta

Liquefaction ejecta was observed in isolated locations throughout Gölbaşı as shown in Figure 5.17. The ejecta generally appeared to be composed of red-brown fine sand with some low plastic fines (10%-20%), however subsequent laboratory testing will be required to substantiate field observations.

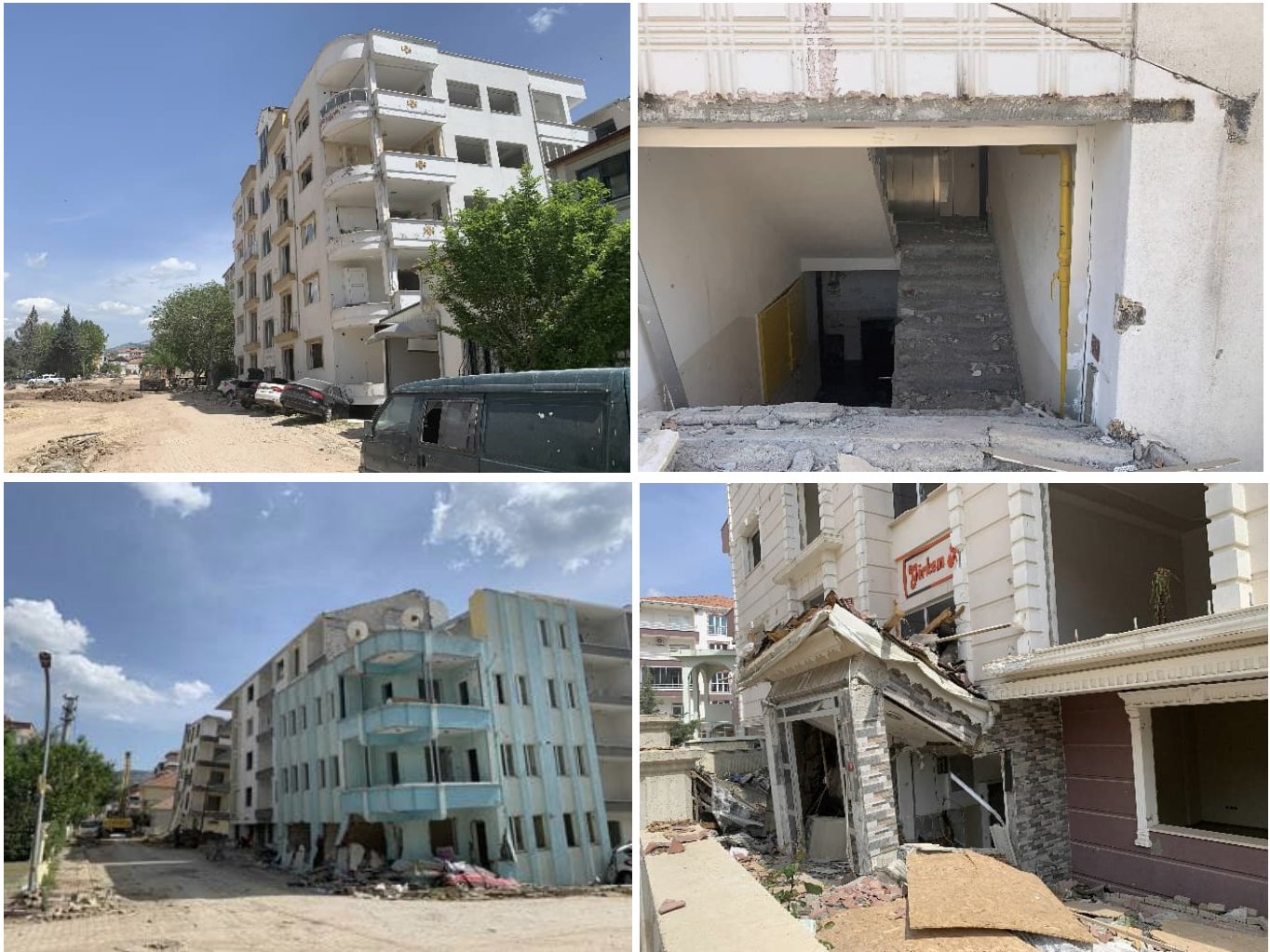


**Figure 5.12: Excessive building settlements. Top left and right - 37.7879, 37.6432, Bottom left - 37.7878,37.6427, Bottom right - 37.7887, 37.6453.**



**Figure 5.13: Examples of differential settlement. Top left - 37.7876, 37.6432, Top right - 37.7886, 37.6449, Bottom left 37.7888, 37.6454, Bottom right 37.7872, 37.6431.**



**Figure 5.14: Lateral Spreading on south bank of Lake Gölbaşı (37.7947, 37.6486). Top Google Earth Aerial Imagery Dated Jun. 10, 2021, Bottom Google Earth Aerial Imagery Dated Mar. 6, 2023. [9]**



**Figure 5.15: Lateral Spreading on north bank of Lake Gölbaşı (37.8059, 37.6550). Top Google Earth Aerial Imagery Dated Jun. 10, 2021, Bottom Google Earth Aerial Imagery Dated Mar. 6, 2023. [9]**



**Figure 5.16: Lateral Spreading on north bank of Lake Gölbaşı. Left – 37.8062, 37.6525 Right - 37.8001, 37.6363.**



**Figure 5.17: Liquefaction Ejecta observed within Gölbaşı. Left – 37.7886, 37.6418 Right - 37.7863, 37.6449.**

#### **5.1.4. Roadway Lateral Spreading, Malatya-Kahramanmaraş Road**

Liquefaction induced lateral spreading was observed on the D850 Malatya-Kahramanmaraş Road adjacent to the Göksu Stream in northern Adiyaman. The closest ground motion estimate location at 37.8666, 37.7744, about 350 m northwest from the damaged area, estimated a PGA during the M7.8 earthquake of 0.40 g and 0.26 g for the M7.5 earthquake [5]. Estimates of PGV were 83 cm/s and 56 cm/s for the M7.8 and M7.5 earthquakes, respectively [5].

At the time of the reconnaissance the roadway had been partially repaired to open to allow two lanes traffic to pass, prior to the damage the roadway had four traffic lanes. The water level of the stream also appeared to be lower than typical levels as assessed by the presence of wetland vegetation and streambed settlements on the banks of the stream which were approximately 3 m above the water surface. The stream is part of the impoundment for a run of river hydroelectric facility about 350 m east of the site.

The lateral spreading generally moved towards the Göksu stream to the south with damage extending along the length of the roadway for approximately 350 m. Photographs of the lateral spreading along the D850 Malatya-Kahramanmaraş Road are shown in Figure 5.18 below.

On the banks of the Göksu Stream on the southside of the roadway and in the flat area to the north of the embankment there was remnants of liquefaction ejecta. The ejecta was typically light grey fine sand with trace fines (<10%). Some of liquefaction ejecta appeared to contain some gravel to gravelly (10-35% gravel), it was unclear if the composition of this ejecta had been significantly altered since the event due to exposure to weather washing the sand fraction away or if the ejecta entrained or contained larger clasts. Photographs of the ejecta observed along the banks of Göksu Stream are shown in Figure 5.20 below.



**Figure 5.18: Lateral Spreading Observations on Malatya-Kahramanmaraş Road -37.8645, 37.7698.**



**Figure 5.19: Liquefaction Ejecta along banks of Göksu Stream - 37.8643, 37.7703.**



**Figure 5.20 (Cont'd): Liquefaction Ejecta along banks of Göksu Stream - 37.8643, 37.7703.**

## **5.2. Performance of Earth Dams**

### **5.2.1. Büyük Karacay Dam, Hatay**

The Büyük Karacay Dam is concrete face rockfill dam located in Samandağı region within Hatay about 20 km southwest of Antakya [10]. The dam is approximately 110 m high with a crest length of 260 m and was completed in 2019 [10, 11]. The upstream and downstream faces of the dam are 1.5H:1V. The spillway is located on the left abutment and is composed of a concrete open channel. The maximum estimated PGA at the dam was 0.46 g during the M6.3 aftershock with a PGA of 0.31 g during the M7.8 earthquake [5].

At the time of the review, the water level of the dam appeared to be at a typical operating water level and no damage was observed to the spillway or dam faces. Along the crest of the dam a 66 m tension crack was observed with maximum widths of 12 cm with up to 50 cm depth. This is illustrated in Figure 5.21.



**Figure 5.21: Condition photographs of Büyük Karacay Dam - 36.1877, 35.987**



**Figure 5.21 Cont'd: Condition photographs of Büyük Karacay Dam - 36.1877, 35.987.**

### 5.2.2. Karamanli Göleti Dam, Hatay

The Karamanli Göleti Dam is an embankment dam in the Yaylica region within Hatay about 11 km southwest of Antakya. The dam has a rockfill upstream face and vegetated downstream face which are both constructed at about 3H:1V. The crest of the dam is used as a local roadway and is paved with asphalt. The spillway was located on the right side of the dam and was a rip rap lined open channel. The closest EERI-GEER ground motion estimate location which was conducted at a nearby water treatment plant approximately 670 m south (36.1638, 36.0287) [5]. The estimated maximum PGA at the location was 0.42 g during the M7.8 earthquake and 0.65g during the M6.8 aftershock, the PGV was 83 cm/s and 61 cm/s for the events, respectively [5].



**Figure 5.22: Condition photographs of Karamanli Göleti Dam - 36.1693, 36.0329.**

At the time of the review, the water level of the dam appeared to be at a typical operating water level and no damage was observed to dam faces. Along the crest of the dam a 130 m tension crack with a maximum width of about 20 cm (Figure 5.21). The tension crack had been partially infilled with granular material to reinstate the driving surface.

### 5.2.3. Kartalkaya Dam, Kahramanmaraş

The Kartalkaya Dam located in Kahramanmaraş, shown in Figure 5.22, is a zoned embankment dam that was completed in 1972 and was developed for irrigation, drinking water supply, and flood control [6]. The dam is about 57 m high with a crest length of 205 m, which forms part of the roadway network [6]. The dam is located about 5 km away from Pazarcik which was the epicenter of the M7.8 earthquake. At the time of the earthquake sequence the dam was noted to be at a low operational level due to ongoing drought [6]. The EERI-GEER estimated PGA for the M7.8 and M7.5 earthquakes were 1.16 g and 0.12 g, respectively, with estimated PGV values of 102 cm/s and 27 cm/s, respectively [5].

The dam had a paved running surface but due to extensive cracking at the crest the running surface on the crest of the dam has been covered in granular material to reinstate the roadway. It appears the crest of the dam slumped at the center about 0.5 m and granular material has been placed to level the running surface nearly covering the steel road barriers on the upstream side. The spillway is a concrete lined open channel on the left side of the dam. The spillway has two radial gates which appeared to be operational and allowing water down the spillway at the time of the review. The dam appeared to be operating at a lowered water level at the time of the review. The left wingwall of the inlet gate appeared to have undergone repair at the concrete joint compared to earlier observations made by the Türkiye Earthquake Reconnaissance and Research Alliance (TERRA) [6].



**Figure 5.23: Condition photographs of Kartalkaya Dam - 37.4684, 37.2390.**



**Figure 5.23 (Cont'd): Condition photographs of Kartalkaya Dam - 37.4684, 37.2390.**

#### 5.2.4. Sürgü Dam, Malatya

The Sürgü Dam, shown in Figure 5.23, is an earth core rock fill dam in Malatya that was commissioned in 1969 [6]. The dam is 57 m high with a crest length of 736 m. The crest is paved with asphalt and forms part of the Hudutköy Köyü road. As a result of the earthquake sequence surface cracking was reported on the crest of the dam with surficial tension cracks 14-20 cm wide [5, 6]. The cracks have been paved over with asphalt since the event, however distress was observed within the asphalt. Minor bulging was observed in the upstream face. Additionally, the rockfill on the downstream face appeared to have undergone surficial movements with some of the rockfill having rolled beyond the downstream toe of the dam. The estimated PGA values for the M7.8 and M7.5 earthquakes was 0.19 and 0.50 g, respectively, with PGV values of 44 cm/s and 125 cm/s, respectively [5].

The dam has a concrete lined open channel spillway which has five sluice gates. The spillway is not attached to the dam and is separated from the dam about 500 m to the south on the left side of the dam. At the time of the review the central three gates were partially open. The south spillway wingwall had partially failed with debris still present within the spillway channel near the southmost gate. The reservoir appeared to at a normal operating level at the time of the review.



**Figure 5.24: Condition photographs of Sürgü Dam - 38.0350, 37.8795.**



**Figure 5.24 (Cont'd): Condition photographs of Sürgü Dam - 38.0350, 37.8795.**

### **5.2.5. Sultansuyu Dam, Malatya**

The Sultansuyu Dam is an approximately 60 m high earth core sand-gravel dam for irrigation purposes in Malatya that was commissioned in 1992 [6]. The dam crest is about 720 m and has a gravel running surface which is gated and inferred to be used for operational and maintenance activities. The spillway is a concrete lined open channel located on the right side of the dam which incorporates four radial gates. The dam also has a secondary outlet which drains into a concrete lined open channel on the left side of the dam.

As a result of the earthquake sequence, extensive cracking was observed along the crest of the dam. Tension cracks ran approximately 400 m along the central part of the crest and were up to about 2.5 m wide and 3 m deep. On the upstream face back tilted scarps up to 1 m high were observed along with budging along the face. Earlier reconnaissance reports reported observations of sand boils near the toe indicating liquefaction of the foundation soils likely resulted destabilization of the upstream face [5, 6]. PGA estimates at the dam were 0.19 g and 0.36 g for the M7.8 and M7.5 earthquakes, respectively, with PGV estimates of 53 cm/s and 76 cm/s respectively [5].

At the time of the review the dam was operating at a reduced water level due to the extensive damage. The radial gates appeared to be functioning and no damage was observed to the inlet or outlet of the spillway. Water was flowing out of the secondary outlet on the left side of the dam. The observed damage of Sultansuyu Dam is depicted in Figure 5.24.



**Figure 5.25: Condition photographs of Sultansuyu Dam - 38.3186, 38.0525.**

### **5.3. Performance of Retaining Structures**

The typical retaining structures observed throughout the region reviewed were gravity type stone walls, anchored/soil nailed walls with shotcrete facing, and Mechanically Stabilized Earth (MSE) walls. Additionally, there were several stone walls that did not appear to be an engineered type system which appeared too slender to constitute a gravity wall and often appeared to be more of a facing element on erodible cohesive soils or weathered rock. As a whole, the retaining structures performed very well, and failures were typically limited to stone

gravity walls or to non-engineered type systems. No damage was observed to MSE walls or anchored type walls during the field reconnaissance and these systems appeared to perform exceptionally well. Damage to the stone type gravity walls could be attributed to a variety of factors including and not limited to: being struck from rock fall, overloading due to sliding of material upslope of the wall, differential settlement and loss of bearing capacity due to liquefaction, and possible irregularities or defects in the stone wall construction. The typical wall types and observed failure modes are shown in Figure 5.26.

#### **5.4. Landslides, Rockfall, and Slope Stability**

Landslides, rockfall, and slope stability impacts were observed throughout the reconnaissance. Overall landslides, rockfall and slope stability failures resulted in relatively minor damage and interruption to the built environment in comparison to other failure modes such as liquefaction induced failure modes or structural deficits. At the time of the reconnaissance landslides, rockfall, and slope stability failures that interacted with the roadway network and other infrastructure had been partially cleaned; however, several locations were still in the process of being cleaned.

##### **5.4.1. D420 Transmission Tower Block Slide, Hancağız, Hatay**

In the Hancağız region of Hatay a translational block slide occurred on a rock outcrop adjacent to the D420 roadway. Atop the outcrop there was a high voltage transmission tower which failed as a result of the movement as shown in Figure 5.26. Two of the tower's four foundations had translated as a result of the block slide which caused the tower to collapse. The failure of the tower did not result in failure of the adjoining towers in the transmission line. The block slide had also caused bulging of the westbound roadway adjacent to the outcrop and at the time of the review two of the four lanes of the roadway were closed.

The block slide appeared to have been structurally controlled and translated upon shallow bedding planes; accurate determination of the bedding was not possible due to the translation of the outcropping faces but generally appeared to be 10-15 degrees from horizontal. The lithology of the rock outcrop comprised of interbedded claystone with fine grained sandstone interbeds. EERI-GEER estimates of the ground motions at the site for the M7.8 and M6.3 earthquakes for PGA were 0.49 g and 0.69 g, respectively, with PGV estimates of 78 cm/s and 60 cm/s, respectively [5].

##### **5.4.2. Olive Grove Block Slide, Tepehan, Hatay**

A notable landslide that occurred as part of the earthquake sequence was the olive grove block slide that occurred in Tepehan, Hatay. The block slide extents are about 500 m from back scarp to the toe, 200 m wide and 30 m deep. Fortunately, no infrastructure or buildings were within the limits of the slide mass.

The geology appeared to be comprised primarily of a weathered diatomaceous claystone with marl or shale interbeds. The geology consists of the Tepehan formation which comprises of sandstone, clayey limestone, claystone, and marl [5]. The bedding planes were dipping coplanar to the slope at about 7-10 degrees, with the slope angle varying between about 10 to 20 degrees. Locals noted the slide occurred following a period of wet weather. A small pond

had formed due to the accumulation of material at the toe of the landslide. Ground motions as a result of the M7.8 earthquake estimated the PGA as 0.40 g and the PGV as 48 cm/s [5]. Aerial imagery and observed conditions are shown in Figure 5.28 and Figure 5.29.



**Figure 5.26: Top left – Undamaged MSE wall along O-52 Adana Şanlıurfa Highway (37.1951, 36.7217). Top right – Undamaged anchored/soil nailed wall supporting O-52 Adana Şanlıurfa Highway Viaduct pier (37.1951, 36.7217). Middle left – Damaged stone gravity wall due to differential settlement (forefront) and surcharging from slide material (background) along Malatya-Kahramanmaraş Road (37.8634, 37.7669). Middle right – Failed gravity wall due to lateral spreading along Malatya-Kahramanmaraş Road (37.8634, 37.7681). Bottom left - Failed stone gravity wall inferred due to irregularities or construction defects (37.3909, 37.1533). Bottom-right Wall damage due to rockfall on Adiyaman Çelikhhan Road (37.9837, 38.2820).**



**Figure 5.27: D420 Transmission Tower Block Slide - 36.1483, 36.0832.**



**Figure 5.28: Aerial Imagery of the Olive Grove Block Slide, Tepehan, Hatay - 36.1618, 36.2195. Left - Google Earth Aerial Imagery Dated Sept. 26 2021, Right - Google Earth Aerial Imagery Dated Feb. 11, 2023.**



**Figure 5.29: Olive Grove Block Slide, Tepehan, Hatay - 36.1618, 36.2195.**

### **5.4.3. Tektuğ Erkenek hes Hydroelectric Facility, Adıyaman**

The Tektuğ Erkenek hes Hydroelectric Facility near Cankara Village in northern Adıyaman experienced heavy damage due to the earthquake sequence. The hydroelectric facility is a diversion type structure which diverts water from a nearby river through an intake tunnel to a forebay where it passes down a single penstock to the powerhouse before being released into Göksu Stream.

The powerhouse was destroyed during the earthquake sequence and in the process of being rebuilt at the time of the review. The simple fault model published by the USGS shows the fault crossing immediately north of the powerhouse building [12]. The reconstruction manager noted surface expression of faulting was initially present behind the powerhouse; however, at the time of the review, surface expression was no longer visible due to disturbance as part of the reconstruction work.

The forebay to the penstocks, which was comprised of three open channel concrete segments, underwent significant displacements at the joints and was no longer functional. Curvilinear

tension cracks and scarps were present around the forebay suggesting seismic slope stability as a probable cause of the observed displacements to the forebay. Additionally, significant damage was observed to the penstock foundation elements which had typically failed with the footings being observed downslope of the adjoining pipe connections. Furthermore, the penstock had buckled at one of the thrust blocks which appeared to be coinciding with the general trend of observed movement downslope. No damage was observed to the thrust blocks at the joints of the penstocks. The intake tunnel was not reviewed.



**Figure 5.30:** Comparison of Pre- and Post-event Satellite Imagery of Tektuğ Erkenek Hydroelectric Facility - 37.8694, 37.8201. Left - Bing Aerial Imagery Undated, Centre - Google Earth Aerial Imagery Dated Mar. 20, 2023, Right - Google Earth Aerial Imagery Dated Mar. 20, 2023 with overlay of original location (red) and surficial cracking (green).



**Figure 5.31** Error! Reference source not found. : **Damage to the Tektuğ Erkenek hes H ydroelectric Facility - 37.8694, 37.8201**

#### **5.4.4. O-52 Underpass Embankment Failure, Çöçelli, Kahramanmaraş**

Along the O-52 Adana Şanlıurfa Highway there was a failure of the approach embankments to an underpass near Çöçelli, Kahramanmaraş (Figure 5.32). The underpass is formed by a two-span bridge that passes over the O-52 Adana Şanlıurfa Highway. The approach embankments connect a local roadway to the north and south of the highway, which runs east-west. The embankments were initially constructed to about 2H:1V and were about 8 m high. The north embankment had a concrete box culvert passing through it perpendicularly to allow for a ditch conveyance of water from the nearby farm fields. As a result of the earthquake sequence both embankments failed, the underpass bridge appeared relatively undamaged with damage limited to the shear keys between the bridge girders. Estimated ground motions for a nearby water source pump about 1.2 km south (37.2711, 37.1146) of the embankment estimated the PGA and PGV the M7.8 earthquake were 0.46 g and 76 cm/s, respectively [5].

At the time of the review the north embankment had been removed and it appeared as though the joints of the box culvert had failed due to movement of the embankment. The south embankment did not appear to have undergone rehabilitation work. The south embankment failed on the outside bend of the approach embankment in what appeared to be a generally translational mechanism. The embankment showed bulging at the toe consistent with translational sliding on or near the original ground surface. The roadway had dropped by approximately 1.25 m forming a dropped graben like feature. On the inside bend of the roadway curvilinear backscarps were observed displaying movement to the outside bend. Slumping was also observed on the slopes adjacent to the bridge abutment. The material within the embankment appeared to be compacted sandy gravel with trace fines.

No signs of liquefaction were observed within the farm fields surrounding the south embankment. The general appearance of the failure modes suggests the embankment likely failed due to seismic slope instability due to the high ground motions. The southern termination of the Pazarcik segment USGS simple fault model is approximately 5.5 km away and roughly perpendicular to the embankment which may have resulted in directivity effects affecting the embankment [12].

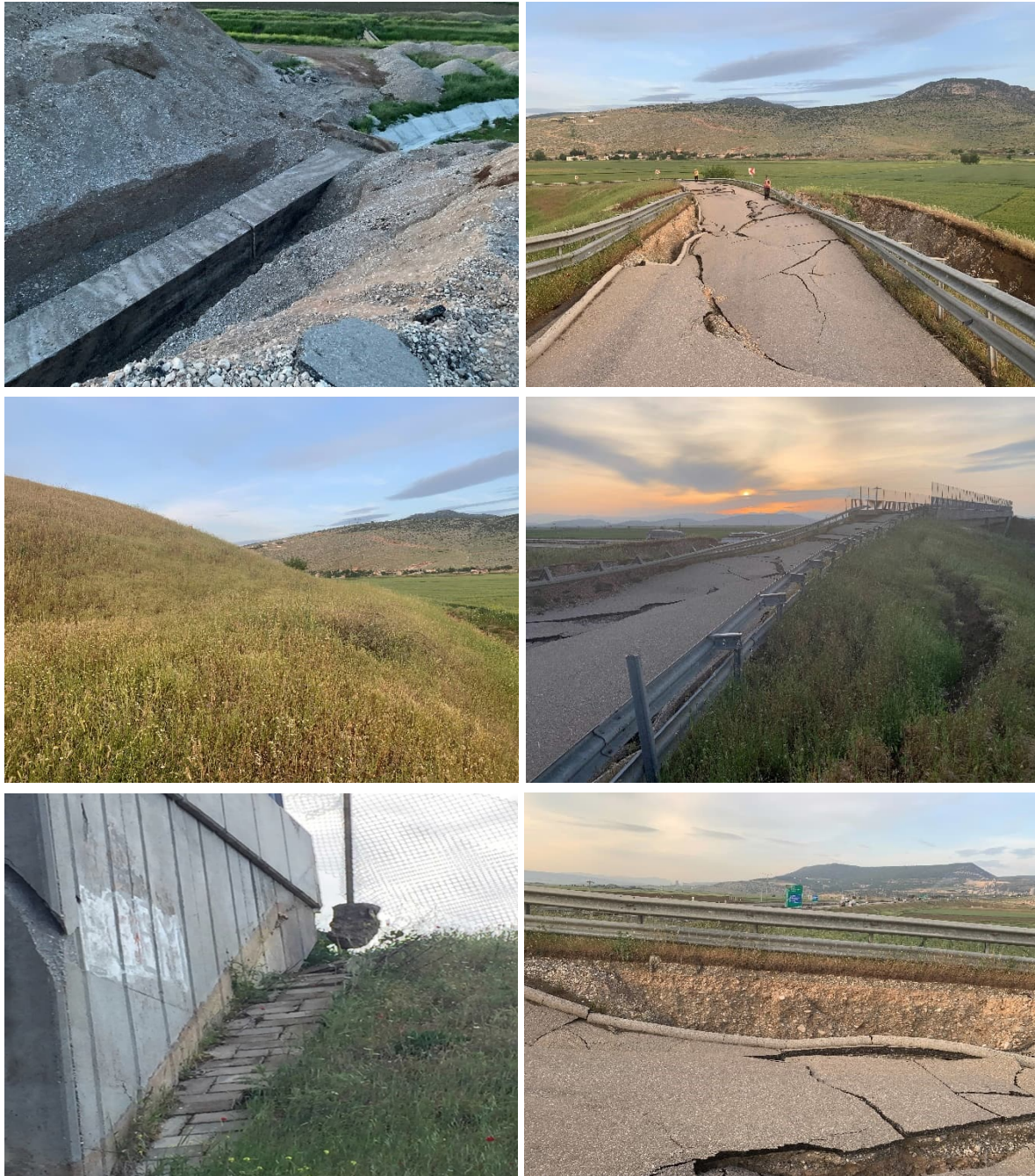


**Figure 5.32: O-52 Adana Şanlıurfa Highway Underpass Embankment Failure - 37.2824, 37.1158.**

#### **5.4.5. Rockfall outside of Nurhak, Kahramanmaraş**

Rockfall was noticed throughout the region with material deposited at the base of natural cliffs and rock cuts adjacent to roadways. One notable group of rockfalls occurred in the region outside of Nurhak in northeastern Kahramanmaraş. At this location two grouping of rockfall were observed at the base of a hillside. Clear runout paths and impact craters were visible in both cases. The western rockfall grouping included boulders up to about 30 m<sup>3</sup>. The eastern

grouping had one exceptionally large boulder which was approximately 150 m<sup>3</sup> and had left impact craters down its entire path length. The source to deposition lengths were about 275 m and 225 m for the west and east rockfalls, respectively. In both instances the runout angle for the boulders was about 22-24 degrees. The rockfall may have had increased mobility due to the spherical nature of the boulders, limited material in the fall path, and consistent slope gradient allowing them to roll relatively unobstructed.



**Figure 5.33: Rockfall outside of Nurhak - 37.9744, 37.4862.**

#### **5.4.6. Bulam 2 Bridge, Adiyaman-Çelikhan Road, Adiyaman**

The Bulam 2 bridge on the Adiyaman-Çelikhan road outside of Mestan village in Adiyaman failed due to rockfall during the earthquake sequence. The bridge was a three-span bridge with two piers within a creek channel. The bridge had an initial total span length of about 45 m between the two abutments. As a result of the rockfall the eastern most span was destroyed.

The rockfall appears to have originated about 100 m above the roadway and travelled down the 50 to 60-degree slope to where it struck the bridge. The rockfall material included limestone boulders up to approximately 80 m<sup>3</sup>, which were observed in the creek channel at the time of the review. Following the rockfall, the bridge was reinstated to allow for traffic to pass by infilling the failed first span with large rockfill to the eastern pier. The surface of the rockfill was paved to allow for traffic to pass. At the time of the review, holes were observed in the asphalt pavement which was attributed to material redistributing into the voids of the rockfill which appeared to be placed uncompacted and with an open gradation. Additional damage was observed to the stone retaining structures that appeared to be due to strikes from rockfall at the crests of the wall. Figure 5.34 below shows the condition of the Bulam 2 Bridge at the time of the review.

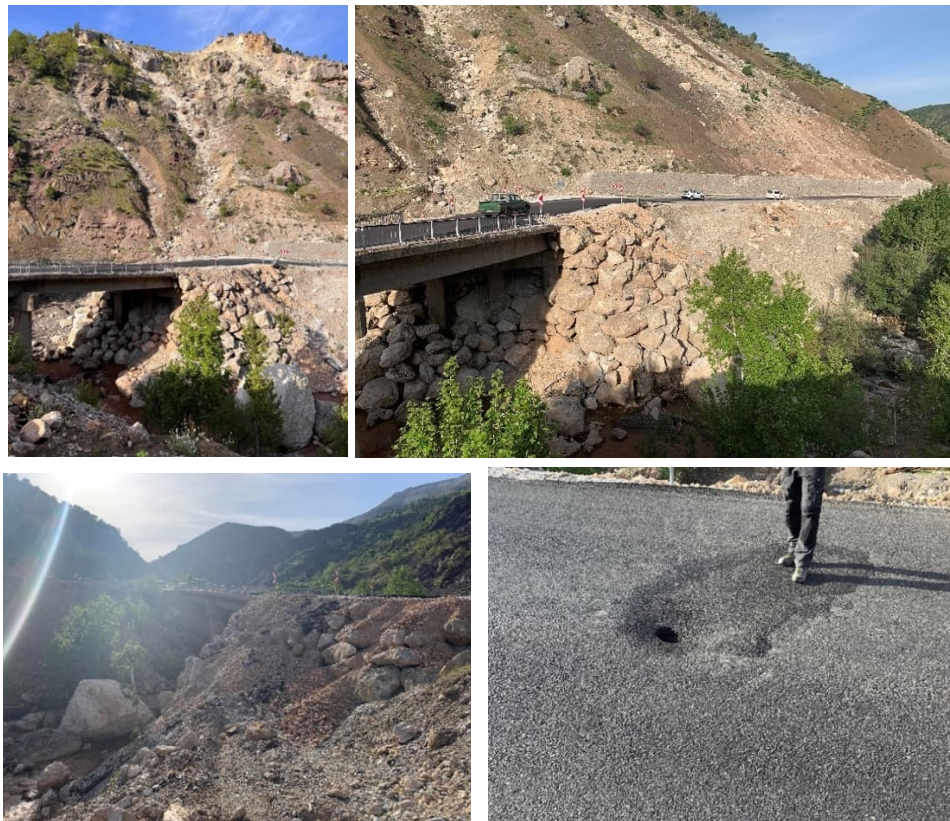


**Figure 5.34: Bulam 2 Bridge, Adiyman-Çelikhan Road- 37.9835, 38.2821.**

### 5.5. Karst Failures

In addition to the landslides, rockfall and slope stability there were two failures identified related to karst geology. The first was on the D360 Gaziantep-Malatya Highway where the road appeared to have experienced differential settlement due to infilled limestone dolines. At the time of the review, the north two lanes, the previous westbound lanes, of the four laned roadway were open allowing for a single traffic lane in each direction. The north lanes had been repaved and lowered relative to southern two lanes, the previous eastbound lanes. Review of the temporary soil cuts showed multiple layers of asphalt and road base suggesting this site had experienced problems with differential settlement in the past. The infilled dolines were

visible within the existing rock cuts and temporary excavations. It is uncertain if as a result of the earthquake sequence additional settlement occurred which resulted in the extensive repairs observed during the reconnaissance or if the repairs predated the earthquake sequence. Figure 5.35 shows the infilled dolines in the rock cuts and temporary excavations, and the multiple asphalt surfaces within one of the temporary soil cuts.



**Figure 5.35: 37.5104, 37.3876.**

A second area where karst geology resulted in a failure was within Gaziantep on a pedestrian path located at the end of Derin Çukur road. A large sinkhole developed on the path that was about 40 m long, 25 m wide and 10 to 20 m deep. Smaller sinkholes were observed further north along the pathway.



**Figure 5.36: Gaziantep Derin Çukur Road Sinkhole 37.0543, 37.3854.**

## 6. Performance of Building Structures

Murat Saatcioglu, Cheryl Sewell, Helene Tischer, Emre Insel

### 6.1. Overview

The CAEES/ACGPS Structural Team visited many of the main urban centres in 8 of the 11 earthquake affected provinces, including Antakya, İskenderun, Kırıkhan, Kahramanmaraş, İslahiye, Nurdağı, Gaziantep, Osmaniye, Pazarcık, Gölbaşı, Adıyaman, Çiğli, Malatya, Elbistan, and Şanlıurfa. The locations visited are shown on the map in Figure 6.1 below.

Field observations of building damage were made at each location. The team focused on understanding the main construction architypes, common building materials and construction practices, construction quality, and the relationship of the building performance in correlation to the type of construction, intensity of shaking, proximity to the earthquake epicenter, and impact of foundation bearing strata.

The team documented the performance of residential and commercial buildings, masonry religious and cultural buildings, industrial facilities, hospitals, and schools. Historic masonry structures are covered in Section 7. Approximately 75% of the buildings investigated were residential midrise structures ranging in height from 5 to 18 stories.

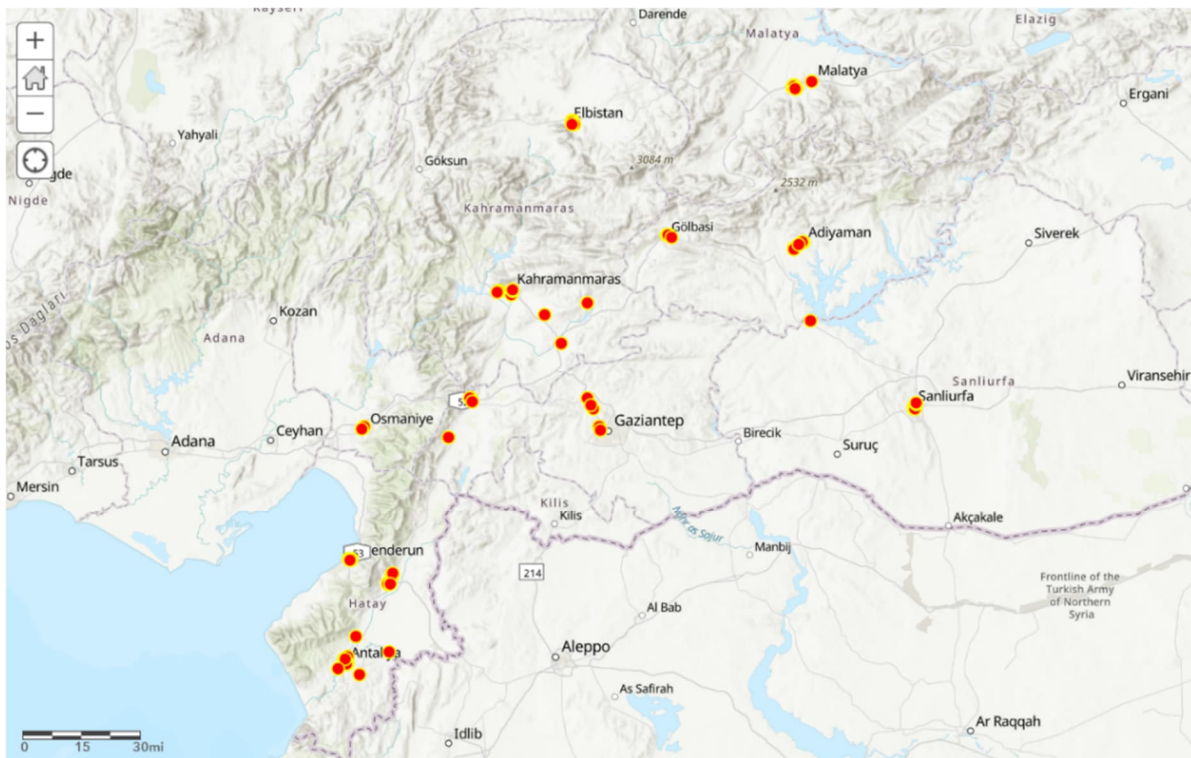


**Figure 6.1: Locations visited by the CAEES/ACGPS Structural Team.**

### 6.1.1. Typical Structural Systems in Türkiye

Most of the buildings in Türkiye are of cast-in-place reinforced concrete (RC) construction. Concrete is the preferred construction material since it is produced locally, and is more economical than other options like steel. Concrete ready mix batch plants are increasingly common near urban centres and provide improved material quality control.

Industrial buildings are predominantly constructed with precast concrete. Precast is viewed as more economical due to the speed of fabrication and erection. There is also an increased quality assurance with fabrication in a controlled environment and avoiding on-site mixed concrete. Industrial regions such as those in Kahramanmaraş and Gaziantep have many precast concrete buildings.

Despite Türkiye being a steel producer, structural steel construction is less common due to the high material costs, however, some construction of this type was observed. Steel is more commonly used for large span industrial structures and, as a hybrid system, for penthouse or podium roof structures supported on a RC main structure. Some smaller industrial buildings are also framed with pre-engineered lightweight steel systems.

Unreinforced load bearing masonry is permitted for low rise one and two storey structures, but it is not very common in new construction. They are restricted up to a building height of 7 m for higher Seismic Design Categories and up to 10.5 m for lower Seismic Design Categories.

With the introduction of modern seismic code provisions in 1998 and a new reinforced concrete design code (TS 500) in 2000, the building inventory can be divided into two groups based on their date of construction: pre-2000 and post-2000.

Prior to 2000, the predominant seismic force resisting system (SFRS) consisted of RC moment frames with unreinforced masonry infill. Since the 2000 seismic code provision update the predominant SFRS is a dual system of RC shear walls combined with traditional moment frames. The shear walls are typically quite short with a storey aspect ratio ( $h/L$ ) greater than 1.0. As such, many could be classified as elongated columns rather than shear walls.

Residential buildings in Türkiye are typically mid-rise RC structures of 5 to 18 storeys in height. Most of them have a greater first storey height to accommodate street level commercial occupancy. Single family houses are found mainly in rural areas and very small towns, mid-rise structures being common even in low-density or rural settings where these would not be found in Canada.

A common feature observed in midrise RC buildings is that the floor plates are supported on cantilevered beams extending 1.2 to 1.5 m from the building perimeter column lines on all levels above the ground floor. Local officials advised that this is done as a means avoiding local zoning bylaws which restrict the foundation footprint size by imposing setbacks from the plot line on the ground level.

### 6.1.2. Evolution of Turkish Seismic Design Codes for Buildings

Reinforced concrete is the predominant construction material used in Türkiye for building structures. Therefore, the emphasis is placed in this section on design and detailing requirements for RC buildings. These buildings are designed based on TS-500, *Building Code*

*Requirements for Reinforced Concrete*, except for seismic design, provisions of which are covered in *the Specifications for Structures to be Built in Disaster Areas*, referred to as the “seismic code” in this section. TS-500 is developed by the Turkish Standards Institute. The seismic code was developed by the Ministry of Public Works and Settlement until 2018. Thereafter, it was developed by the Disaster and Emergency Management Authority of Türkiye, known as AFAD, with the implementation and supervision responsibilities resting with the Ministry of Environment and Urbanization.

The first Turkish seismic code was developed in 1940 following the devastating M7.9 Erzincan Earthquake. The seismic base shear in this first code was defined as the product of seismic coefficient,  $C = 0.10$ , and the building weight,  $W$ , irrespective of the location, as seismic zonation had not been developed at that time. The first seismic map was developed in 1942, dividing the country into three zones: i) first-degree, ii) second-degree, and iii) no hazard seismic zones. The zonal boundaries primarily followed the provincial boundaries. The seismic zones were incorporated in the revised seismic code of 1947 with seismic coefficients of 0.10 and 0.05 for the first- and second-degree zones, respectively. The code was then revised once again in 1949 with more refined seismic coefficients that varied between 0.02 and 0.04 for the first-degree zone and between 0.01 and 0.03 for the second-degree zone depending on the soil condition and the construction type (to be established by the design engineer). The seismic coefficient was further refined in the 1961 edition of the code, and it was expressed as the product of three coefficients that accounted for building height, building type (structural steel or reinforced concrete) and soil type (Type I: hard and monolithic rock; Type II: sand, gravel and compact soil; and Type III: weaker soil not included in other soil types). The seismic zonation map was then revised in 1963 to include four zones based on the Modified Mercalli Intensity Scale.

Some of the modern concepts for calculating seismic base shear were introduced in 1968. Accordingly, the seismic coefficient was expressed as the product of four terms, incorporating the effects of seismic zonation, soil type, building importance and design spectral shape. The code provided expressions for building period and the distribution of seismic forces along the height of the building. It further specified minimum dimensions for beams, columns, and shear walls, as well as the maximum spacing for stirrups and ties. A change of significance was the addendum to the 1968 code that made the use of shear walls mandatory beyond a certain building height. Specifically, the requirement stated that buildings taller than 12 m, 15 m, and 18 m in the first-degree, second-degree, and third-degree seismic zones, respectively, must have shear walls along the height of the building to transfer lateral seismic forces to the foundations.

The seismic hazard map was updated once again in 1972 to include an additional seismic zone (bringing the number of seismic zones to 5), where each zone corresponded to different levels of earthquake intensity based on the Modified Mercalli Scale. The hazard values reflected earthquake data obtained during the previous 70 years. The new hazard map was adopted by the 1975 seismic code, which was significantly enhanced by incorporating seismic design concepts employed by modern seismic codes of the era. The seismic base shear was defined as the product of four terms, reflecting the effects of seismic zonation, type of lateral force resisting system, building importance, and design spectral shape for different soil types. The

soil types were classified based on soil shear wave velocity. Irregularities in buildings were introduced for the first time, albeit without many details. Minimum member dimensions were specified for beam, columns, and shear walls, with limits for longitudinal and transverse reinforcement ratios defined for ductile performance. Concrete confinement regions at the ends of members were identified with maximum transverse reinforcement spacing limits. Minimum bar sizes and reinforcement details were specified, including 135-degree hook details for confinement reinforcement.

The seismic code was revised once again in 1998 and included an updated seismic zonation map, which was developed in 1996 based on the peak ground acceleration with a return period of 475 years. Figure 6.2 shows the 1996 seismic zonation map. This edition included dynamic analysis (mode superposition method, linear and nonlinear time history analyses) for building design in addition to the equivalent static force method. A new base shear expression was developed for the equivalent static force approach for elastic force demands to be modified by a force reduction factor  $R$  to reflect non-linear response based on member detailing and associated ductility capacity as high or nominal level ductility. The  $R$  factor varied between 3 and 8. The seismic coefficient was replaced by the spectral acceleration coefficient, calculated by the product of the effective ground acceleration coefficient defined for each seismic zone, building importance factor, and seismic spectrum coefficient  $S$ . The coefficient  $S$  was calculated using three equations for the three regions of design spectrum, corresponding to short-period, constant acceleration, and constant velocity regions. The design spectrum varied with soil types and had a maximum soil amplification factor of 2.5. Seismic detailing requirements were expanded and became more stringent for high ductility buildings. Transverse reinforcement requirements were specified for both high and normal ductility buildings with closer spacing required near the ends of members. All hoops were required to have 135-degree hooks at both ends with cross ties permitted to have a 90-degree hook at one end. Strong column–weak beam concept was implemented with the summation of column strengths at each joint exceeding the summation of beam strengths by at least 20%. Brittle shear failure was prevented by providing higher shear strengths than shear forces associated with the formation of plastic hinges at the ends of members.

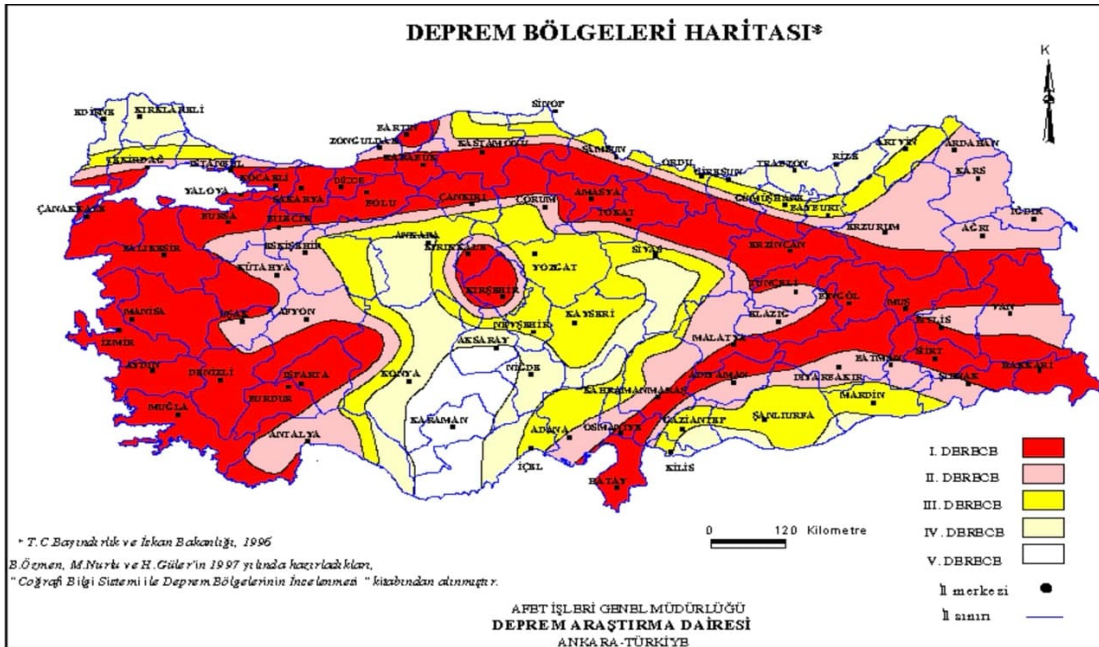


**Figure 6.2: 1996 Seismic Zoning Map.**

The devastating 1999 M7.4 Kocaeli Earthquake provided impetus for an improved new edition of the code in 2007. The 2007 seismic code introduced some improvements over the 1998 edition in terms of expanded description of irregularities and updated force reduction factors, while also increasing the volumetric ratio of confinement reinforcement, but otherwise remained similar to the 1998 edition. Equivalent static force procedure as well as dynamic analysis procedures were specified for use in design. As a result of the poor performance of non-ductile buildings observed during the 1999 Kocaeli Earthquake, an extensive section was added to the code on seismic safety assessment and retrofit of existing buildings, including the details of push-over analysis for vulnerability assessment.

The current Turkish seismic code was developed in 2018 and implemented in 2019 incorporating a new seismic hazard map and performance-based assessment and design procedures. Unlike the previous seismic zonation map, dividing the country into 5 seismic zones, the new seismic hazard map contains contours of spectral accelerations based on geographic coordinates. They were developed for a stiff soil condition (as a reference soil type) at return periods of 2475, 475, 72 and 43 years to enable performance-based assessment and design. Figure 6.3 illustrates the 2018 seismic hazard map for a very stiff soil based on 475-year return period. The design spectrum for a given site is obtained using spectral accelerations at periods of 0.2 and 1.0 seconds, amplified for the site soil condition. This is illustrated in Figure 6.4. The code species either Force-Based Design or Performance-Based Design. The latter is implemented through design, assessment, and re-design, when necessary. The Force Based Design procedure is similar to that of the 2007 code with the appropriate capacity design principles implemented. Perhaps the most important difference in the static base shear expression is the definition of the response reduction factor,  $R$ , which included overstrength in members (factor  $D$ ). The overstrength factor is defined for different structural systems. Factor

D alone may be used to reduce elastic force demands for brittle elements. The code also permits engineers to compute ductility related force reduction factor as R/D.

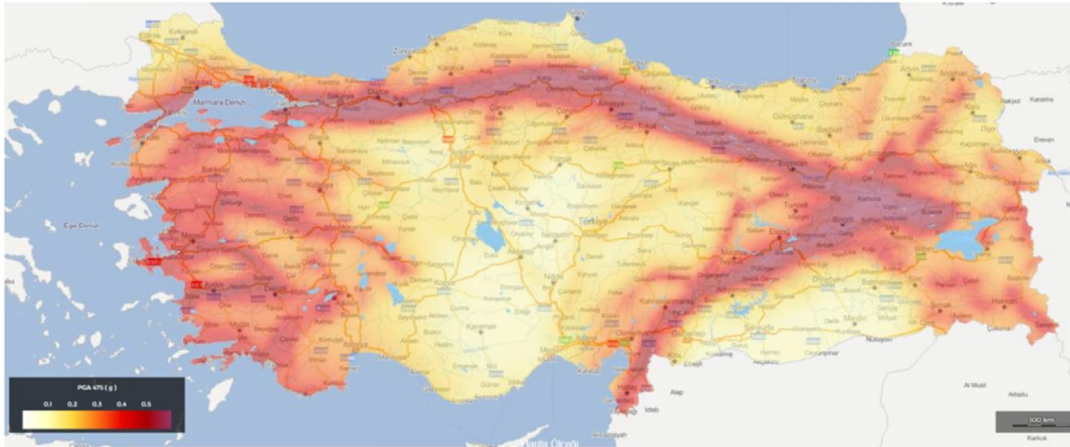
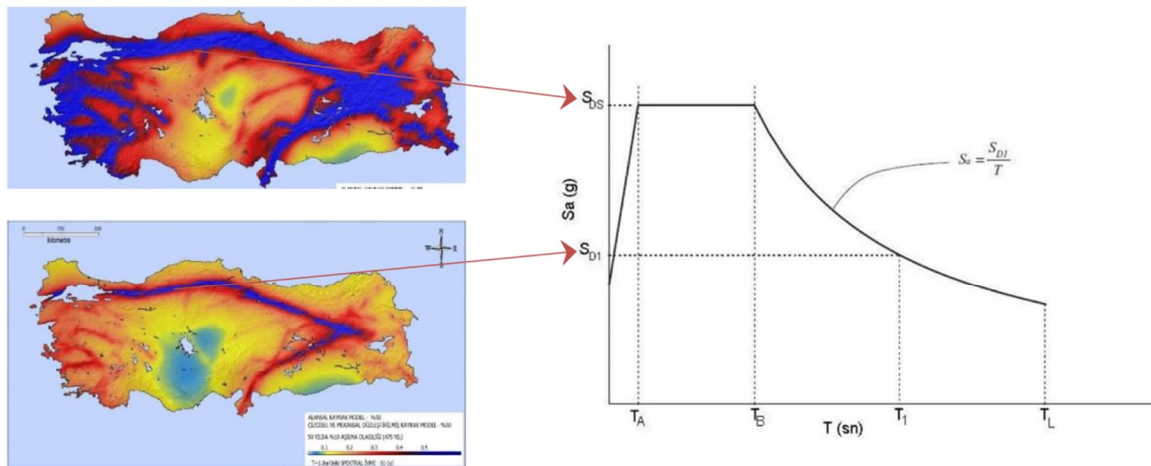


**Figure 6.3: 2018 Seismic Hazard Map.**



Contour maps for  $T=0.2\text{ s}$  and  $1.0\text{ s}$  ( $S_s$  and  $S_1$ , 475 years)

475-year design spectrum (5% damping)

**Figure 6.4: Design Spectrum based on 2018 Seismic Hazard Map for 475-year return period [1]**

Performance-based assessment and design is employed by using different hazard and building performance levels to achieve the desired building design targets. Four different Hazard Levels are specified in terms of probabilities of exceedance within a given time period as DD-1 with 2% in 50 years, DD-2 with 10% in 50 years, DD-3 with 50% in 50 years, and DD-4 with 50% in 30 years. Similarly, four different Building Performance Levels are specified as Continued Operation Performance (CO), Limited Damage Performance (LD), Controlled Damage Performance (CD), and Collapse Prevention Performance (CP). Two Design Performance Targets are specified under various combinations of hazard levels and building performance levels as Ordinary Performance Target, and Advanced Performance Target. Table 6.1 provides a summary of cases to be considered for different Seismic Design Categories. These design

categories depend on the level of seismicity (as governed by design spectral values) and are established based on building importance and building height. Despite these recent advancements in the seismic code, performance-based design and non-linear dynamic analysis have very limited use, if any, in the Turkish seismic design practice. None of the buildings assessed in the disaster area is believed to have benefited from such advanced concepts.

**Table 6.1: Design performance targets in the 2019 Turkish Seismic Code [14]**

**Buildings with less than 70 m to 105 m (Depending on the level of seismicity):**

Hazard (EQ)	Ordinary Performance Target	Advanced Performance Target
	All Buildings	Post Disaster Buildings*
72-Year EQ	-	Limited Damage
475-Year EQ	Controlled Damage	Controlled Damage
2475-Year EQ	-	Controlled Damage

**Tall buildings:**

Hazard (EQ)	Ordinary Performance Target	Advanced Performance Target
	All Buildings	Post Disaster Buildings*
43-Year EQ	Controlled Operation	-
72-Year EQ	-	Limited Damage
475-Year EQ	Controlled Damage	Controlled Damage
2475-Year EQ	Collapse Prevention	Controlled Damage

\* In medium to high seismic regions

### 6.1.3. Design Response Spectra for Selected Locations Visited

Design response spectra were plotted for selected locations that were visited by the team. The damage observed in these regions is discussed in subsequent sub-sections. Both 2007 code (based on 1996 hazard values) and the 2019 code (based on 2018 hazard values) were used to generate the spectra. The locations of cities are shown in Figure 6.1. The seismic zone for each city as per the 2007 code is identified and the spectra are plotted for different soil conditions in Figure 6.5. For the 2019 code, geographic coordinates are used to identify the seismic zone as per the 2018 hazard map. The spectra are plotted for two types of soil conditions, Soil Type ZB: Rock with shear wave velocities between 760 and 1500 m/sec and Soil Type ZD: Stiff Soil with shear velocities between 180 and 360 m/sec in Figure 6.6.

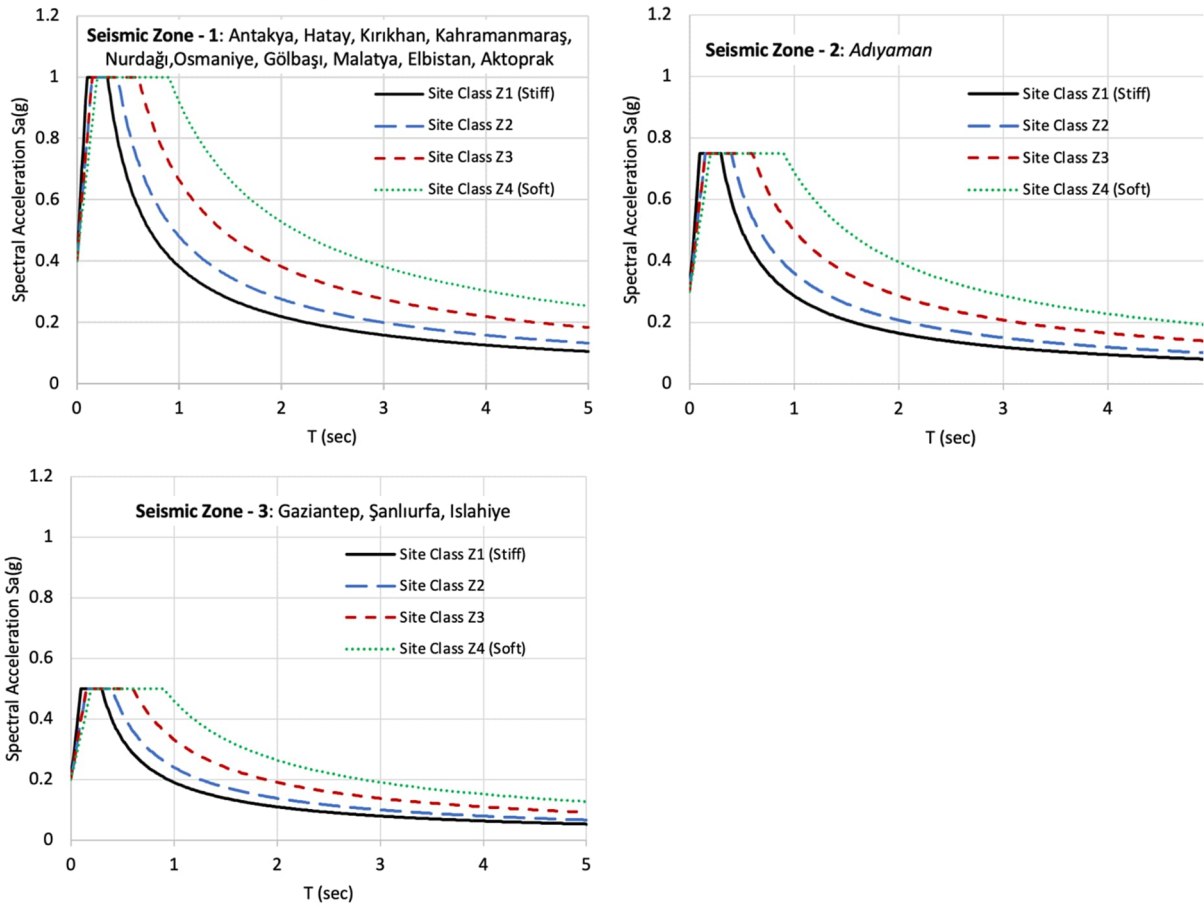


Figure 6.5: Design Response Spectra based on 2007 Seismic Code [15] for different sites and soil conditions.

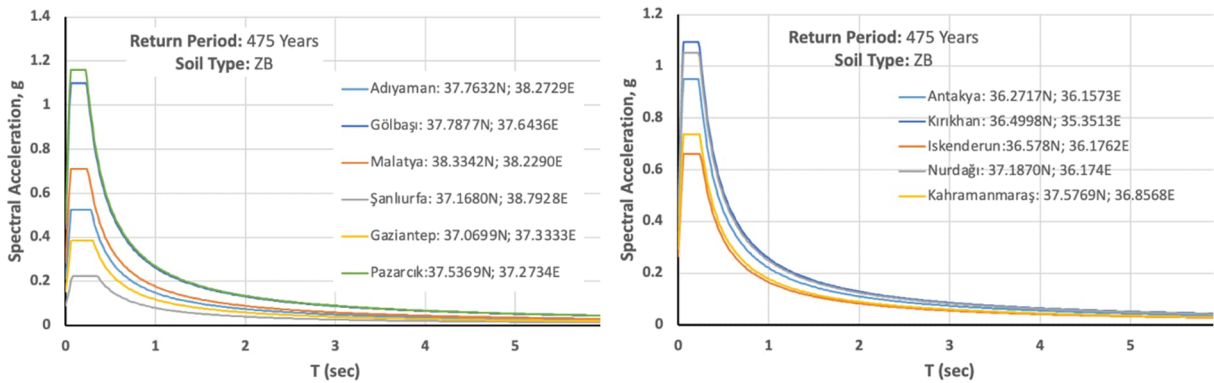
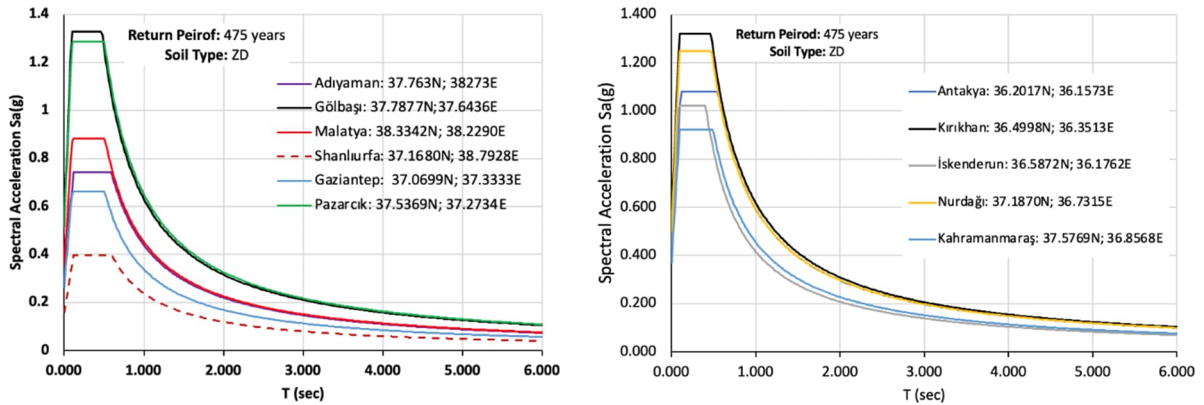
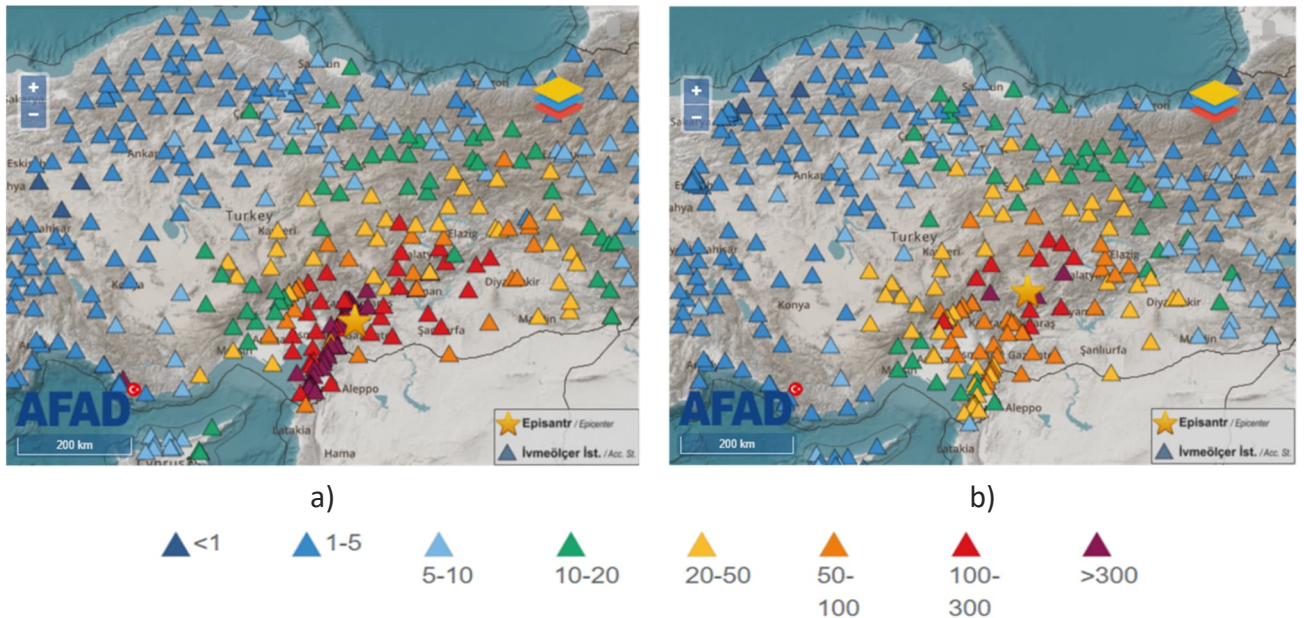


Figure 6.6: Design Response Spectra based on 2019 Seismic Code [14] for different sites and soil conditions (ZB: Rock with shear wave velocity 760 – 1500 m/sec).



**Figure 6.6 (Cont'd): Design Response Spectra based on 2019 Seismic Code [14] for different sites and soil conditions (ZD: Stiff Soil with shear wave velocity 180 - 360 m/sec).**

The details of the ground motions recorded are discussed in Section 4. Figure 4.1 shows peak ground accelerations recorded in the region during the two events that occurred on February 6, 2023. This figure is reproduced in Figure 6.7 to provide context for the ground motion magnitudes in regions for which design spectra are provided in this section. The response spectra for the N-S and E-W components of the ground motion recorded at Station No. 3139 at Kırıkhan, Hatay are illustrated in Figure 6.8, indicating higher spectral values than the design response spectra shown in Figure 6.5 and Figure 6.6 for the same location. Additional comparisons are presented in Figure 6.9 and Figure 6.10 for two sets of ground motions recorded in Kahramanmaraş. These comparisons indicate that the recorded ground motion exceed the design response spectra in many locations in different period regions of the spectra.



**Figure 6.7: Peak ground accelerations (PGA) recorded by AFAD strong motion stations in (a) Pazarcik earthquake, (b) Elbistan earthquake (accelerations are in cm/ecs2). Image credit: AFAD.**

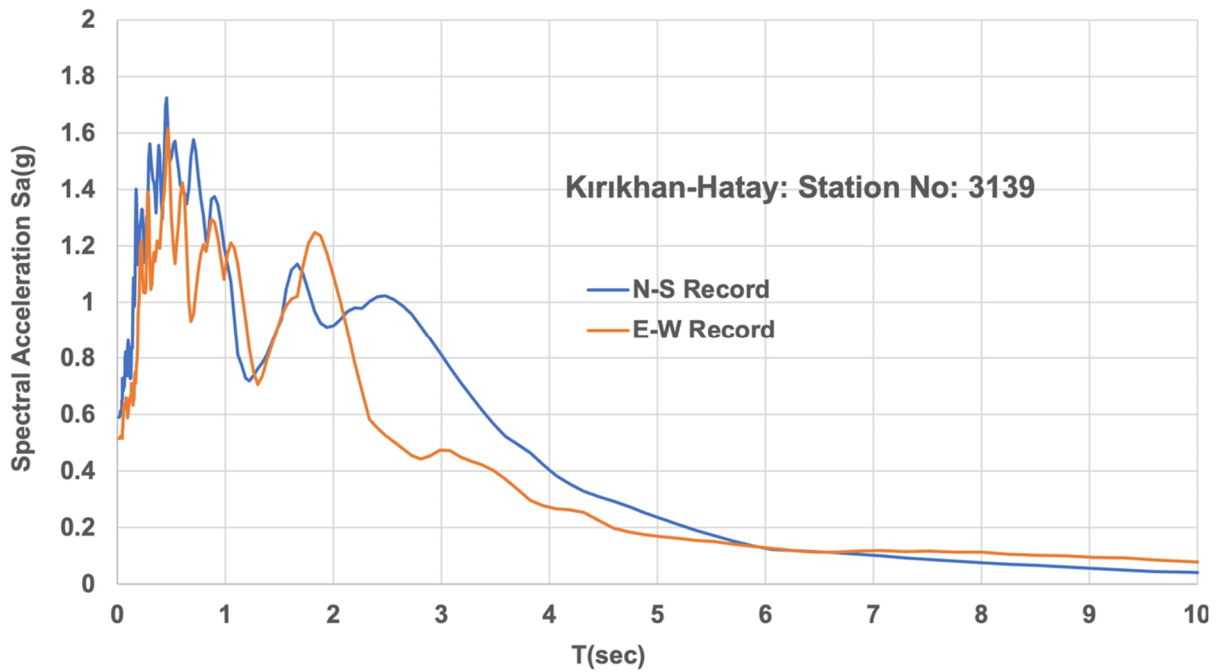


**Figure 6.8:** Acceleration response spectra for ground motions recorded at Station No: 3139 at Kırıkhan Hatay.

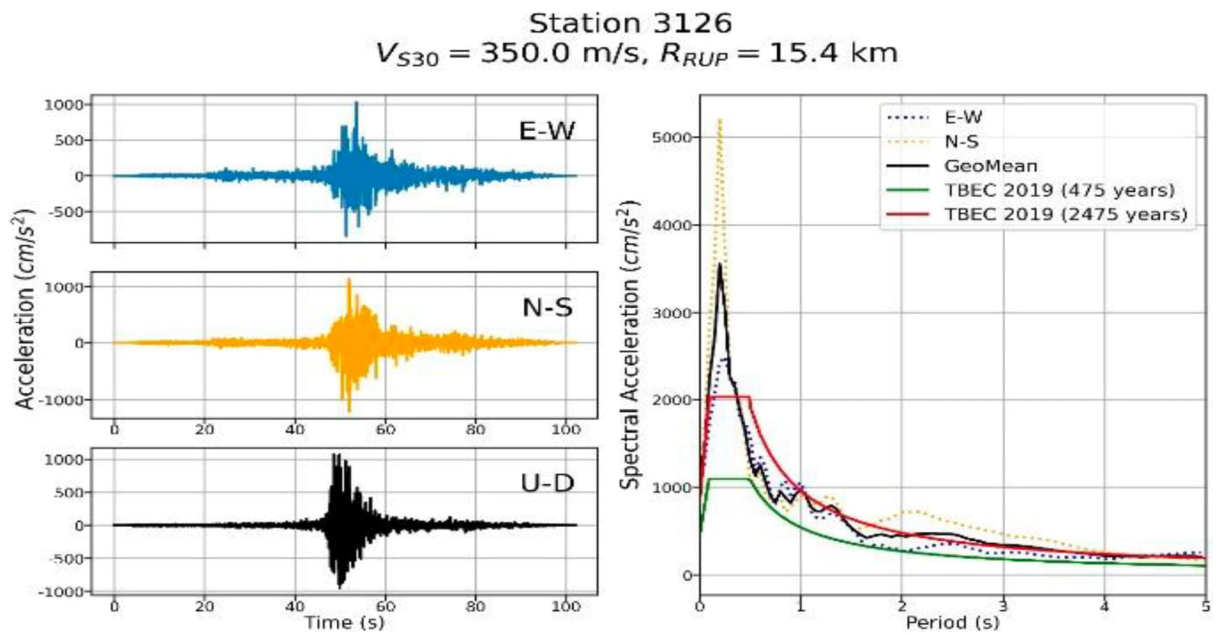


**Figure 6.9:** Ground motions recorded at Station 3126 in Kahramanmaraş-TBEC indicates Turkish Seismic Code Spectrum [17].

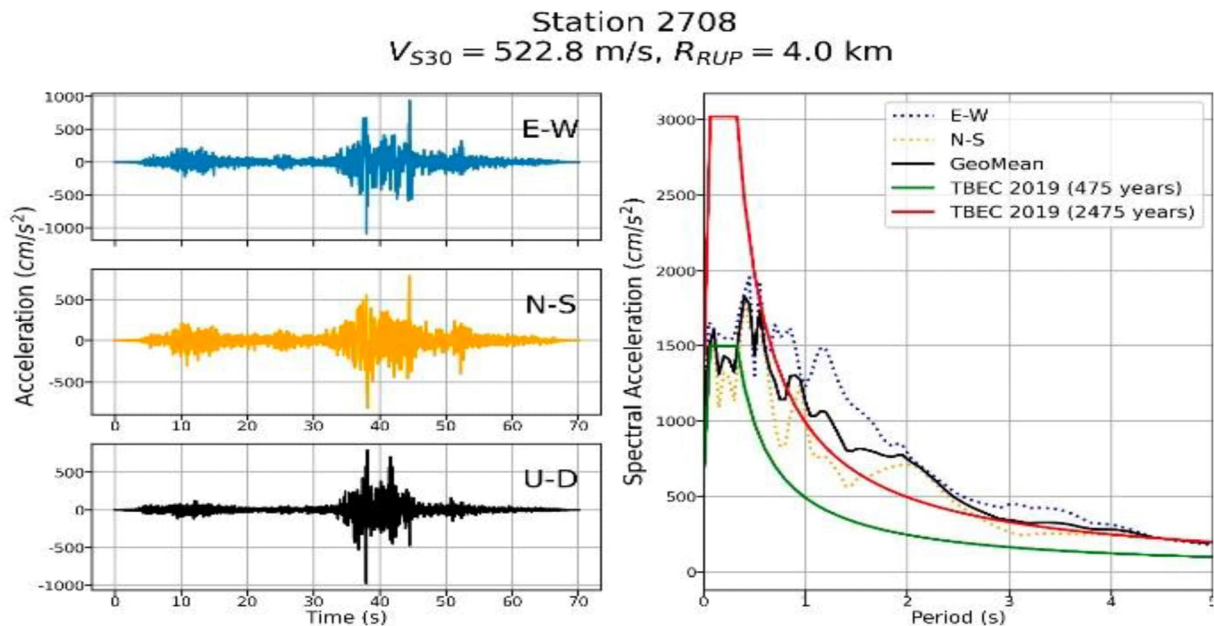


**Figure 6.10: Ground motions recorded at Station 2708 in Kahramanmaraş-TBEC indicates Turkish Seismic Code Spectrum [17].**

## 6.2. General Overview of Observed Damage

According to the Government of Türkiye Recovery and Reconstruction Assessment report [16] the total number of buildings in the earthquake affected area is around 2.6 million and comprises of approximately:

- 90% residential
- 3% public
- 6% offices

The CAEES/ACGPS Structural Team field observations were consistent with these ratios and found that the most damaging impact of the earthquakes was to residential buildings.

An example of the extent of building damage can be seen in Figure 6.11 where images are presented of Antakya, Hatay Province, city centre before and after of the earthquakes. The city centre is located where the roads converge at the central bridge crossing the Orontes River. The old city is located to the right of the river on the image. The damage observed in Antakya was the most extreme of all the locations visited.

Overall, several factors were identified as contributors to a given building performance:

- PGA intensity;
- soil conditions;
- building characteristics, including:
  - building age (pre- or post-2000);
  - type of seismic force resisting system;
  - construction quality and material properties;

- adherence to building code regulations;
- structural irregularities.



**Figure 6.11: Google Earth satellite images of Antakya: Top – historic image from 21-12-2022 before the earthquake, and Bottom – 4-25-2023, 2 months after the earthquake (accessed 23-07-2023).**

### 6.2.1. PGA Intensity

Ground motion recordings show that the structures close to the epicentre and fault rupture were subjected to very high horizontal and vertical accelerations. Figure 6.7 displays the peak ground acceleration intensity for both earthquakes. The highest accelerations were recorded in the first earthquake along the fault just north of the epicenter in and at the bottom end of the fault in the Antakya region. The areas where the greatest damage was observed correspond to the regions of highest recorded PGA. The recorded PGA exceeded the design spectral accelerations plotted in Figure 6.5 and Figure 6.6 in many locations.

Surprisingly, proximity to the epicentres and to fault surface ruptures appeared to be less significant factors in the performance of buildings for this earthquake scenario and fault type.

### 6.2.2. Soil Conditions

General observations of the team were that soil conditions were one of the most important factors contributing to building performance. Buildings on soft alluvial soils without site specific foundation design performed much worse than those on more competent soils or rock, and those with foundations adequately designed for the given soil type.

### 6.2.3. Building characteristics

It is generally recognized in Türkiye that there is poor regulatory control and lack of oversight over construction practices and quality control for buildings. Engineers also do not have professional licensing associations for governance over engineering practice standards. That being said, it was generally observed that buildings constructed before 2000 performed worse than those constructed after 2000, if the design and construction was compliant with the updated seismic provisions. Government buildings, which have an importance factor of 1.5, also performed better since they were designed for a higher seismic force level.

## 6.3. Observed Damage Based on Locations Visited

*Antakya*, the capital of the province of Hatay, is the southernmost province of Türkiye. Located in close vicinity to the Syrian border, this city was identified as that most damaged during the earthquakes. The main reason for the extensive damage is due to the fact that Antakya is founded on deep alluvial deposits. During the reconnaissance, the extent of damage was confirmed, in particular in the city center along the Orontes River. Entire neighborhoods appear to have been abandoned due to the catastrophic and extensive damage. The team focused on the severely affected historic center with many masonry and stone structures and a nearby neighborhood characterized by older concrete buildings. Typical damage observed in Antakya is illustrated in Figure 6.12. Better performance was observed for newer buildings founded at higher elevations which are inferred to have been constructed on more competent soil conditions.



**Figure 6.12: Typical observed damage in Antakya.**

*İskenderun*, a port city located in the province of Hatay, was also heavily affected by the events. The reconnaissance was focused on neighborhoods close to the waterfront. The team observed widespread damage associated with poor soil conditions and liquefaction in a well-defined area. See Section 5.1.1 for further details on the liquefaction observed. Buildings in other areas of the city also presented damage to historic buildings and non-structural damage to modern construction observed, although in a smaller proportion than the waterfront regions. Figure 6.13 shows typical damage observed in İskenderun.





**Figure 6.13: Typical damage observed in İskenderun**

**Kırıkhan** is a smaller town in Northern Hatay. Widespread damage was again observed throughout the town. Detailed observations were focused on historic structures. A monument of high religious and cultural significance, Türbe, in the vicinity was also visited. Figure 6.14 shows some of the damage observed in Kırıkhan.



**Figure 6.14: Typical damage observed in Kırıkhan**



**Figure 6.14 Cont.: Typical damage observed in Kırıkhan**

**Kahramanmaraş**, the administrative center of the province with the same name, and with a population of around 1 million people, was one of the larger cities visited. Widespread damage was observed in the alluvial plain, with a significant number of buildings already demolished with vacant sites cleared of debris. The team focused their attention on the historical neighborhood exhibiting significant damage to different types of masonry structures, as well as a zone on higher ground where modern high-rise buildings and tunnel form construction fared relatively well. These are shown in Figure 6.15.



**Figure 6.15: Typical damage observed in Kahramanmaraş**

**Nurdağı** is a small town in the Gaziantep province, located approximately 45 km west of the city of Gaziantep. Nurdağı is located only 6 km from the epicenter of the February 6 earthquake, and widespread damage was observed. The structural team focused their attention on two hospital buildings as well as some general observations of nearby buildings. One hospital, located south of the town, had a large surface rupture in close proximity to the building structure. Figure 6.16 shows buildings that suffered some damage in Nurdağı.



**Figure 6.16: Typical damage observed in Nurdağı**

**Osmaniye**, located in the district of the same name and roughly 100 km East of Adana, is a small city of with approximately 250,000 inhabitants. This town was specifically visited to try to assess tunnel form buildings. The building complex visited showed little to no damage. Again, widespread damage was observed to other types of buildings, in particular to those of the more common concrete construction systems.



**Figure 6.17: Typical observed damage in Osmaniye. Tunnel form buildings in right photo.**

Gaziantep, commonly known as Antep, is the capital of the province of Gaziantep with approximately two million inhabitants. The structural team focused primarily on industrial facilities in Gaziantep and were invited into some newer facilities which performed quite well and displayed little damage. Overall, the damage in the city appeared less widespread than in other locations.

Other building structures that suffered damage were visited with local structural engineers. The team was advised that 26 residential buildings collapsed during the event. No industrial buildings collapsed. Some residential buildings constructed in the mid 1990's collapsed within the first 10 seconds of the first earthquake excitation. The collapse was captured by surveillance cameras at a neighboring gas station. All collapsed buildings were demolished, and the sites cleared of debris at the time of the reconnaissance. Figure 6.18 shows some observed buildings in Gaziantep.



**Figure 6.18: Typical observed observations of damage in Gaziantep**

**Gölbaşı**, a town of approximately 30,000 inhabitants located in the Adıyaman Province, is located roughly equidistance between Malatya and Gaziantep. The damage observed in Gölbaşı was extreme and was primarily related to construction of buildings on ground conditions. In particular, damage to buildings was generally caused by excessive settlement due to loss of bearing capacity as a result of liquefaction. Refer to Section 5.1.3 for more details on the geotechnical discussion in Gölbaşı. In the worst affected areas building settlements of over half a storey were observed. These buildings were only about five years old. Many buildings were completely intact but had experienced differential settlements and rotated out of plumb up to approximately 30 degrees.

Many other buildings had collapsed due to severe rotations causing instability. The most damaged buildings were already demolished, and the sites cleared of debris at the time of the reconnaissance. Some buildings were in the process of being demolished and locals advised that all of the buildings in this area would be demolished, and no reconstruction was permitted due to the poor ground conditions. Examples of observed settlement and building rotation are shown in Figure 6.19.

A recently constructed building complex located on more competent soil was also visited and no damage was observed.



**Figure 6.19: Typical observed damage observed in Gölbaşı**

**Adıyaman**, a city of roughly 250,000 inhabitants, is the administrative center of the province of the same name, and is located roughly 150 km north-east of Gaziantep. Observed damage in Adıyaman was primarily limited to multi-storey residential construction. Damage was widespread, with structural damage and collapsed buildings observed near the town's center. There were many vacant sites of recently demolished buildings.

A neighborhood, of newer construction, located near the city boundary was also visited. Here damage was mostly non-structural in nature.

Figure 6.20 shows some of the damage observed in Adıyaman. Note the time that the clock stopped – 4:17 a.m. was the precise time that the first earthquake hit.



**Figure 6.20: Typical damage observed in Adiyaman**

**Malatya**, the capital of the province of the same name, was the most northern city visited. Two neighbourhoods were again visited: one of newer construction near the city limits, and the more densely populated city center with older construction. For buildings of newer construction, typically concrete high-rises, widespread non-structural damage and some structural damage was observed. The city center consisted of mainly older, mid-rise concrete frame structures with masonry infill walls constructed tight to adjacent buildings with little or no gaps. Damage was more serious in the city centre, with many sites with collapsed buildings already cleared of debris.

Structural and non-structural damage was observed in many buildings which survived the earthquakes. Figure 6.21: Typical observed damage in Malatya shows examples of damage of building damage in Malatya.



**Figure 6.21: Typical observed damage in Malatya**

**Elbistan**, with a population of around 150,000, is located in the Kahramanmaraş province, around 100 km north of Kahramanmaraş city. The epicenter of the second earthquake (Mw 7.5, USGS; Mw7.6, AFAD) was located approximately 20 km south of Elbistan. Significant structural and non-structural damage was observed mostly to mid-rise concrete buildings with infill masonry walls. Some high-rise buildings assumed to be of newer construction fared better, mostly with non-structural damage as shown in Figure 6.22.



**Figure 6.22: Typical observed damage in Elbistan**



Figure 6.23: Damage observed in RC moment frame structures.

**Şanlıurfa**, also known as Urfa, is the most eastern location visited, and the one situated furthest away from the epicenters of both earthquakes. Observed damage was modest. A plot of land where a building had recently been demolished, as well as a building with non-structural damage, were observed. Other buildings appeared to have fared well, including historic masonry construction. According to locals, some minarets collapsed, and cracks had formed in some of the historic buildings, but most damage was already repaired at the time of our visit. Figure 6.24 shows sample building damage seen in Şanlıurfa.



**Figure 6.24: Typical observed damage in Şanlıurfa**

Other than the main urban centers described above, small villages in rural areas were also visited. Damage varied from one to another, but overall, the damage was significant when a building site was closer to a fault line. Typically, construction was made from reinforced concrete and/or masonry, with buildings one or two storeys in height. Examples of these buildings are shown in Figure 6.25: Typical observed damage in small villages.



**Figure 6.25: Typical observed damage in small villages**

#### **6.4. Reinforced Concrete (RC) Structures**

Most of the building collapses observed were in RC residential structures. While many of the collapses could be attributed to poor performance of RC frame structures with masonry infill walls constructed prior to 2000, a surprising number of structures constructed since the 2000 seismic code provision update, collapsed or suffered severe damage. Since most of the collapsed buildings had been removed at the time of our site investigation, observations primarily pertain to the remaining damaged buildings.

The issue of stiffness imparted to the structure from masonry infill, soft storey failure, short column failure, diagonal shear cracking of elements, and building pounding were common to all buildings regardless of year of construction. Rebar buckling was overall the most frequently observed damage which is typically a result of inadequate tie/stirrup spacing, or failed ties/stirrups. Another commonly observed deficiency was inadequate anchorage of transverse reinforcement. In many damaged columns and beams 90 deg hooks as opposed to the more structurally accepted 135 hooks were observed in columns and beams and shear wall horizontal reinforcing. Once the concrete cover spalled off, transverse bars lost their capacity to confine the vertical bars and lap splices in the vulnerable hinge zones. No tied end zones were observed in concrete walls that suffered severe damage.

##### **6.4.1. RC Buildings constructed prior to 2000**

Damage to RC moment frame structures was widespread and significant. Repeated damage patterns observed in building constructed prior to the modern seismic design standards were

mostly due to known design and construction deficiencies as identified after the 1999 Kocaeli earthquake [18] such as:

- use of smooth reinforcing steel;
- insufficient reinforcement detailing:
  - inadequate tie spacing;
  - inadequate reinforcing splice length;
  - splices located in locations of highest stress / hinge zones;
  - lack of anchorage of ties, stirrups and horizontal reinforcing;
  - insufficient reinforcing area and element size;
- low concrete strength and quality control issues of on-site mixed concrete;
- inadequate SFRS for very high seismic and displacement demand;
- Stiff beam/floor weak column construction.

**Figure 6.23** and Figure 6.27 show examples of damage in pre-2000 buildings. Many of the above deficiencies have been addressed by the current seismic design code provisions.



**Figure 6.26: Damage in moment frame buildings due to soft storey effects**

#### 6.4.2. RC Buildings constructed since 2000

Buildings constructed after the 2000 seismic code provision update generally have a dual SFRS system of RC shear walls supported by traditional moment frames. The shear walls are typically quite short and are more like elongated columns or “wallums”. Documented issues with shear wall layout were that shear walls are often located within partition walls of residential buildings with masonry infill constructed tight to the walls, slabs, and beams, and shear walls are not always evenly distributed in both orthogonal directions, or across the floor plate.

The structural team observed many buildings with shear walls oriented mainly perpendicular to the street front or set back from the front to maximize window area for ground floor commercial spaces of multi-story buildings. Most buildings also have a greater first storey height for the street level commercial space. Some buildings had commercial occupancy on the first two storeys with both having a greater storey height than the residential storeys above.

The commercial storeys often exhibited increased drift due to the stiffness irregularity caused by the unintentional stiffening of building by the unreinforced masonry (URM) infill partition walls of the residential storeys above.

Buildings with shear walls showed improved performance over older RC moment frame structures but many were still heavily damaged in areas that experienced very high ground motions. Some examples of severe damage observed in shear walls are shown in Figure 6.27 in Antakya. This building was located a couple of blocks from the Orontes River. Despite that this building was constructed only 5 years ago, the team observed issues of inadequate reinforcing detailing and questionable concrete material quality. It should be noted that the earthquake ground motions in this area exceeded the design level forces and despite the high level of damage, the building could be deemed as meeting its performance objectives since it did not collapse. A significant number of new buildings, presumably of similar construction and with shear wall SFRS, collapsed in this area.

Observed damage to shear walls includes:

- plastic hinging at beam and column extremities;
- shear wall sliding shear, diagonal tension failure, and shear or bond failure along lap splices or anchorages;
- bar buckling failure – broken vertical bars;
- concrete crushing and breaking into large rocks within rebar cage – perhaps due to concrete material strength issues.

Similar damage patterns were repeated in locations which experienced high ground motions.



(a) vertical bars buckling



(b) diagonal tension failure



(c) vertical bars buckling failure, concrete crushing



(d) hinge in coupling beam and top of SW (left); shear or bond failure causing bar buckling and concrete crushing in SW (right)

**Figure 6.27: Damage to shear walls and coupling beams, Antakya**

Sliding shear failure was also documented in newer buildings a bit further distanced from the Orontes River in Antakya, see Figure 6.28. The team also observed examples of shear wall buildings in this same area which performed very well with only minor cracking evident in the shear wall elements. It was the opinion of neighboring building owners that the buildings which did not perform well had poor oversight during construction and were not constructed in conformance with the seismic code. Those documented had only minimal shear walls in relation to the height of the building. They also advised that, at the time of construction of their buildings, it was often difficult to get ready mixed batched concrete in Antakya since the nearest concrete plant was some distance away. There are currently ready-mix concrete suppliers in Antakya.



**Figure 6.28: Examples of shear wall sliding shear failure, Antakya**

- Common deficiencies observed include:
- Non-code compliant reinforcing detailing – ties spaced too far apart and of small diameter (8 mm typical).
- Inadequate SFRS for very high seismic and displacement demand.
- Horizontal reinforcing in shear walls not anchored within vertical tied end zones.
- No ties or stirrups in damaged buildings were observed to have 135° hooks.

### **6.4.3. Effects of Structural Irregularities**

A few deficiencies were observed which have not been addressed in the current seismic provisions and will be described in the next sections.

#### **6.4.3.1. Stiffness Irregularity**

##### **Short Column Effects**

Short column failures were observed in many buildings and in both those with RC moment frame and dual shear walls and moment frame SFRSs. Short columns were observed in cases where a building had a partial basement and the columns above the foundation wall to the first floor level were shorter and stiffer than for the typical storey height, see **Error! Reference source not found.** for examples. As a result of the increased stiffness in short columns they are prone to shear failure. Collapse of building with short columns was more common in frame buildings than shear wall buildings.



(a) short column hinging & partial collapse of ground floor level, frame structure



(b) classic diagonal shear cracking



(c) short column shear failure, shear wall SFRS



(d) ground floor collapse – column snapped off due to large drifts, frame structure

**Figure 6.29: Short column failures in buildings in Antakya**

### Soft Storey

A soft storey is the opposite stiffness irregularity to short columns. In a soft storey mechanism, the SFRS, usually of the lowest storey, is less stiff than for the storeys above.

In many of the buildings documented soft storey issues were due to two reasons: 1) the first storey was of greater height to accommodate commercial occupancy at the street level and 2) masonry infill partitions constructed tight to the columns and beams imparted significant stiffness to the structure in the storeys above the ground level which was not accounted for.

The combination of these two characteristics created a soft storey mechanism in a significant number of buildings.

Another observed scenario was a strong beam-weak column condition. In this case, a soft storey will occur and cause hinges to form on the columns. This was observed in buildings with URM infills at the top levels only. The stiffness imparted by the URM infill was so much greater than the inherent stiffness in the SFRS of the storey below without URM infill, that it resulted in a strong beam-weak column mechanism. The maximum displacement demand was concentrated in the first storey below the residential floors and resulted in complete building collapse, collapse of the first storey, or significant residual drift and concentrated damage in the lower storey lateral resisting elements (Figure 6.30 and Figure 6.31).



**Figure 6.30: Pancaked ground floor (top) and total building collapse (bottom), Kırıkhan.**



**Figure 6.31: Observed residual drift, Antakya.**

#### 6.4.3.2. Cantilevered floors

The slabs of the stories above the ground level were observed to typically cantilever out from the perimeter columns or shear walls. This was observed to have a detrimental effect on the building performance of both structural and nonstructural elements. Although not a defined irregularity, cantilevered elements are more vulnerable to the effects of vertical accelerations and there is a possibility of dynamic amplification of vertical ground motions resulting from the vertical flexibility of the cantilevers [19].

Figure 6.32 shows images of hinging in a cantilevered beam on the second floor level of a 9-storey residential building in Antakya (top left). The second image (bottom left) is of a collapsed façade and infill URM at the corner of the third floor in a shopping centre in Kahramanmaraş. There appears to be large cracks in the column supporting the cantilevered beam, but it was the team's opinion that these are cold joints in the concrete. The shopping centre suffered only non-structural damage in the earthquake and was under repair at the time of the reconnaissance. The third image (right) is of a failed cantilevered façade.



**Figure 6.32: Damage due to cantilevered floor beams**

#### **6.4.4. Damage to Stairs**

Of particular concern was the damage observed to exit stairs which were intended to be the main means of egress from the building as illustrated in Figure 6.33. Unrestrained URM infill walls collapsed onto the stairs and the stairs hinged at landings and storey levels, certainly making it difficult for inhabitants to exit the building as the falling blocks posed a life safety hazard. Detailing for stairs and egress routes needs to be addressed.



**Figure 6.33: Damage observed to exit stairs.**

### **6.5. Reinforced Concrete Tunnel Form Shear Wall Buildings**

Tunnel form (also known as box-type) buildings are a distinct form of reinforced concrete construction that utilizes custom made, tunnel-like formwork for progressive construction. The resulting structure is composed of concrete shear walls, used for all exterior and interior walls and thus avoiding columns and infill walls, and flat slab only [20]. Tunnel form construction can be recognized by its characteristic numerous, relatively thin shear walls, regular, small windows and absence of balconies, a popular feature in Turkish construction.

This type of structure has been used in Türkiye predominantly for multi-storey, relatively low-rise buildings, and was popularized by its adoption by the state for the construction of social housing. While the system's performance can be influenced by irregularities and poor detailing, between others, various references report a better seismic performance of this system when

compared to common concrete frames or hybrid shear wall buildings similar to those described above [20] [21] [22].

The team was able to observe several tunnel form buildings at two locations. In Kahramanmaraş, around 30 buildings of this type were observed on the same site, with little to no damage, as shown in Figure 6.34. Damage observed could likely have been caused by degradation and may not be a result of the earthquakes. For example the exposed, corroded bars may be due to lack of concrete cover, or cracks in cold joints as shown in the figure. While the buildings performed well, it is important to note that they were located in an area that overall suffered limited damage. Figure 6.35 shows a photo of the neighboring buildings for comparison.



**Figure 6.34: Tunnel form buildings in Kahramanmaraş [37.57628, 36.857665].**



***Figure 6.35: Performance of regular concrete buildings next to tunnel form buildings in Kahramanmaraş [37.57628, 36.857665].***

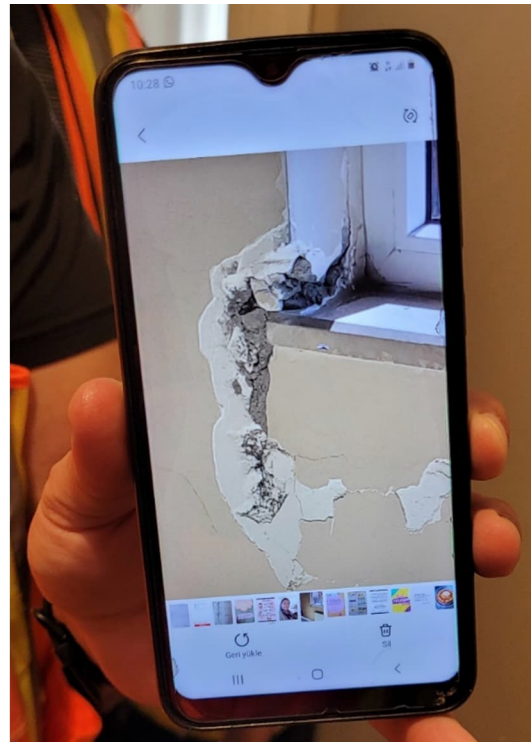
Another complex of tunnel form buildings (10 individual buildings) was visited in Osmaniye, where the team was granted access to one of the units (Figure 6.36) **Error! Reference source not found.** While no damage was observed, some small damages were reported by the inhabitants, but these had already been repaired (Figure 6.36 (c)).



(a) Exterior



(b) Interior



(c) Reported damage



(d) Building exterior

**Figure 6.36: (a), (b), & (d) Tunnel form buildings in Osmaniye [37.07506627, 36.2285699], (c) Only reported damage to tunnel form buildings.**

Figure 6.37 shows the generalized damage at the location of these buildings in Osmaniye (shown in the center of the image) for comparison. As can be seen, severe damage was observed to the buildings immediately to the north of the complex. However, these are low-

rise, non-engineered type structures, and as such, not directly comparable to the tunnel form buildings. Buildings to the south seem to have fared significantly better.

In conclusion, while observed tunnel form buildings performed well during the events, a direct comparison with more traditional engineering concrete buildings was not possible for the visited locations.

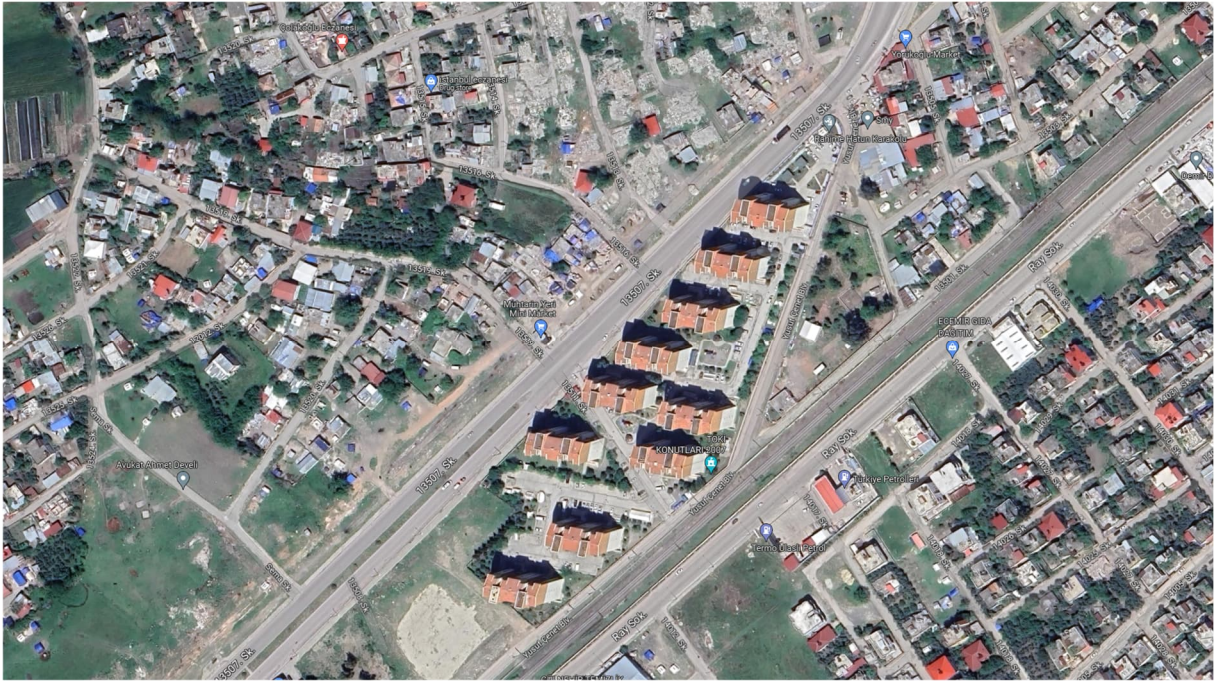


**Figure 6.37: Generalized damage around tunnel form buildings observed in Osmaniye, Google Maps (accessed on 2023.07.15).**

## 6.6. Precast Concrete Buildings

Precast concrete frame structures are commonly used in Türkiye for industrial facilities typically of one or two stories of rectangular plan. The most typical structural system observed consists of an assembly of fixed base cantilevered columns. The columns are anchored into precast socketed foundations, shimmed to plumb, and secured with shrinkage compensating grout. Columns are tied together at the top with double tapered I-section roof girders (triangular shaped) which bear on the column corbels. Girder to column corbel connections are typically simply supported pin connections with two anchors embedded into the corbels. The girder beams have cast-in sockets which are placed over the corbel dowels and are filled with shrinkage compensated grout. Gutter beams run perpendicular to the roof girders at the low ends. The long span girder beams are typically prestressed.

Another common precast configuration in Türkiye termed “Lambda Frames” consists of fixed base frames with pinned beam connections at locations of contraflexure under gravity loads. [23]. The structural team did not visit any precast lambda frame structures.

Single storey precast warehouse structures usually range from 7 to 10 m clear height and typically have internal mezzanines or platforms on the sides or ends of the building which are used for offices, storage, service spaces or open platforms for equipment access.

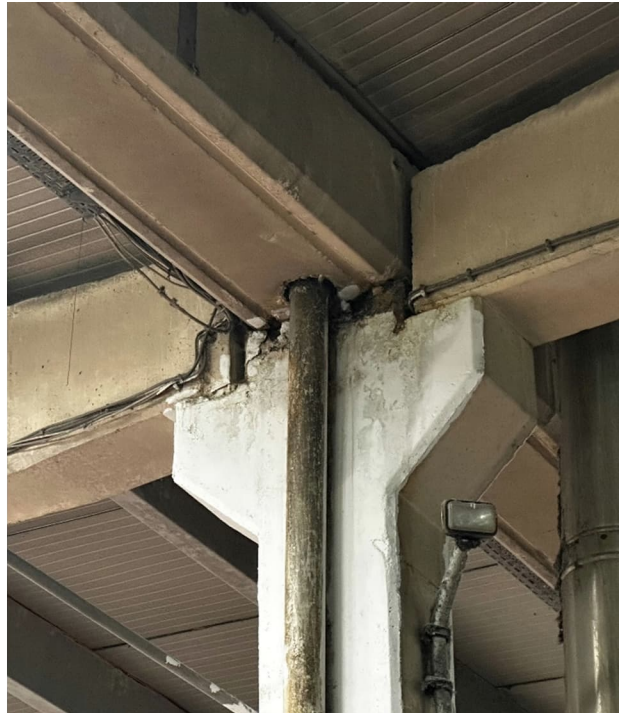
Precast structures were observed by the structural team at three locations. The first structure was an industrial yarn factory in Gaziantep, see Figure 6.38. This facility was a single-storey building, with roof girders spanning 22.5 m, spaced at approximately 8 meters. The roof height was raised in one bay to accommodate a double running girder crane. Equally spaced precast concrete purlins spanned between the roof girders. The roof purlins were tapered down at the supports and sheathed with insulated steel sandwich panels. Perimeter walls were framed with URM or insulated steel sandwich panels.

Figure 6.39 shows a close-up of the typical column-to-beam connections. **Error! Reference source not found.** shows the only damage observed at this location consisting of spalling of the concrete cover on the column corbel. The structure had already been retrofitted by the addition of a new steel column and shoe bracket to support the beam at the damaged corbel. The factory owners reported very little disruption due to the earthquake. The perceived shaking intensity was so low that work continued uninterrupted through the night shift.

According to the team's local engineering contact similar damage was reported to other facilities in the Gaziantep region. He also advised that no diaphragm action is assured by this system due to a lack of connection between the roof girders, gutter beams, and roof purlins. Gutter beams are also not connected to the columns or girder beams. The open warehouse configuration allows for no redundancy in the roof structure support. Although no industrial buildings were reported to have collapsed in Gaziantep, the local engineer advised that precast concrete buildings had performed poorly and collapsed in other locations.



**Figure 6.38: Precast concrete frame industrial facility, Gaziantep [37.16311557, 37.29198872].**



**Figure 6.39: Typical beam-to-column connections [37.16311557, 37.29198872].**

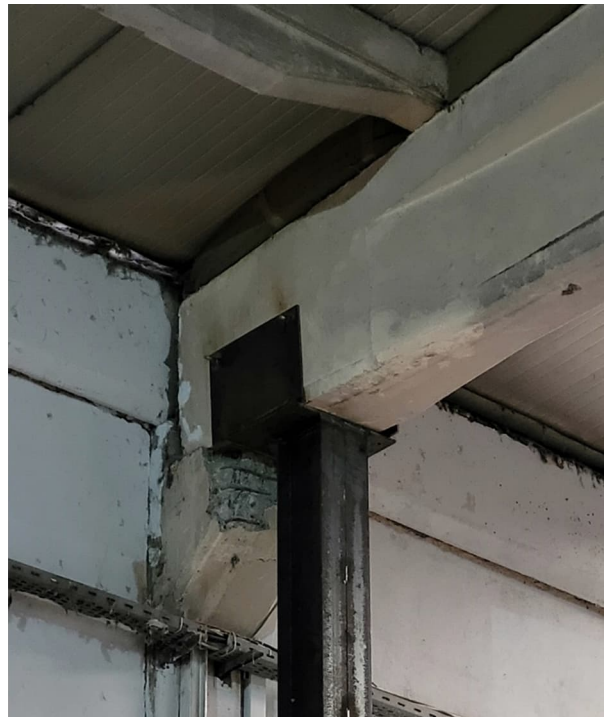


**Figure 6.40: Observed damage and repair at connection, precast frames [37.16311557, 37.29198872].**

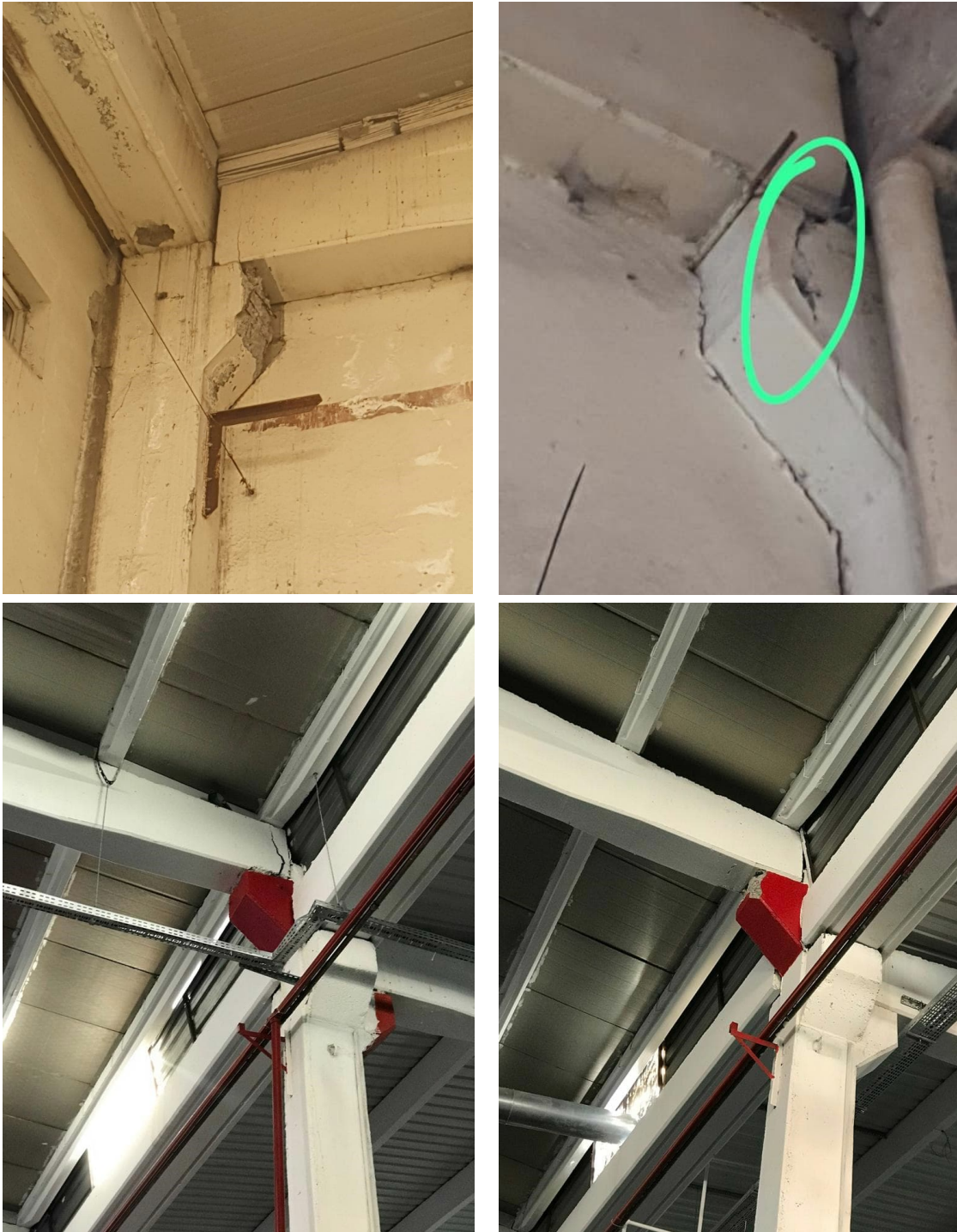


**Figure 6.41: Observed damage to connections of precast concrete frames, provided by the team's local engineering contact, Ali Kürşad Bozbaş.**

The second site visited was a much smaller rural industrial facility in Nurhak, 50km south-east of Elbistan). As can be seen in Figure 6.42, infill walls collapsed and some damage was observed

to the column corbels, although it appeared that the damage was limited to spalling of the concrete cover over the ties and did not penetrate into the corbel core.



**Figure 6.42: Precast concrete frame rural industrial facility [37.968578, 37.487122].**

Finally, the third site visited was a precast building under construction in Aktoprak, approximately 15 km northwest of Gaziantep, see Figure 6.43. This frame system deviated from the typical observed in that the precast columns were five-storeys tall for the front section of the building, and most of the beam-to-column connections were modified from the standard pin dowel detail. Pockets were formed in the columns at each beam level directly above the column corbels leaving the column reinforcing continued through the pockets. The pockets would presumably be filled with concrete once the beams were placed. Some of the corbels had the typical two pin dowels extending up to receive the beams. The floors consisted of double Tee sections which had a line of U-bar reinforcing extending above the beam webs, presumably to be anchored to a topping slab.

Note also, the base detail where the columns were anchored into precast foundation sockets, plumbed with thick wood shims, and the gap filled with grout. The socket foundations were tied by a continuous cast-in-place grade beam. No damage was observed at this site since its construction commenced after the earthquake.



**Figure 6.43: Pre-cast concrete frame under construction, Aktoprak [37.18609275, 37.2723584].**

Although the structural team did not observe collapsed precast concrete buildings directly, there were many large, cleared areas where industrial buildings previously stood in Kahramanmaraş and Kırıkhan. It was confirmed by Google Earth historic photos before and after the earthquake that many precast buildings had collapsed and were demolished.

The collapses were presumably due to beam girder to column connection failure or a combination of this with poor diaphragm connections. The structural team's observations agree with other independent findings that identify the connections as the most vulnerable element of this type of construction. References [24], [25] describe damage during the 2023 earthquakes, as well as the previous 1999 Kocaeli Earthquake, mainly correlated to beam to column connection failure and lack of stiffness of the structures. Reference [26] also observed column base spalling in damaged precast facilities in the Türkoğlu Organized Industrial Zone.

### **6.7. Steel Buildings**

Structural steel construction is not very common in Türkiye. The structural team documented only two completely structural steel industrial buildings. The first building shown in Figure 6.44 is a structural steel industrial carpet factory which performed very well despite that the connections are not detailed following capacity design principles. This structure consists of a system of welded W-shaped girder moment frames spanning 35 m. Columns are also W-sections anchored at the base. The lateral system in the direction perpendicular to the moment frames consists of steel rod bracing tensioned with turn buckles. The bracing terminates about 2.5 m – 3 m above the floor to minimize interference with factory operations. Similar in-plane roof bracing runs the width of the building between vertical bracing lines. Vertical bracing is located every second or third bay.

The only visible damage was buckling of some of the in-plane rod roof bracing, although the damage is not evident in the photos. The factory owner was fully aware of the damaged elements and intended to replace the yielded bracing.

A second warehouse storage building on the same site was a hybrid structural steel and RC structure, see Figure 6.45. Long span truss girders span 32 m across the width of the warehouse and are supported onto precast concrete columns. Evenly spaced steel channel purlins span between the truss girders and support an insulated metal panel roof deck. Steel channel girts with sag rods span between the columns and support insulated metal panel exterior cladding. A system of round HSS in-plane roof bracing forms the lateral resisting system for the roof. Given their size they are assumed to be tension/compression bracing. The roof bracing is anchored to upstand posts on top of the concrete columns.

The concrete columns are precast and are fixed at the base into socketed footings similar the precast concrete columns described in Section 6.5. A continuous cast-in-place upstand RC wall approximately 1.2 m high runs between the RC precast columns.

This building performed very well in the earthquake and showed no visible signs of damage to the structure. The factory was fully operational. The factory owner informed the team that both buildings were founded on a rock substrate.



**Figure 6.44: Structural steel industrial carpet factory in Gaziantep.**



**Figure 6.45: Hybrid Structural Steel and RC warehouse support structure for carpet factory, Gaziantep.**

Another industrial structure was investigated on the outskirts of Antakya which was constructed with a light steel framed roof consisting of a form of open web steel joists supporting very light purlins and corrugated metal decking (Figure 6.46). This structure was a support building for a cotton oil factory. The centre beam strut, providing lateral support for the center concrete columns, consisted of a triangular steel space frame. The roof girder layout was not well coordinated with the exterior masonry wall pilaster spacing and beam to wall connection locations were not located at pilasters. Significant damage was observed at the joist to wall connections. The bracing visible in the photos was not present prior to the earthquakes and was being added at the time of the reconnaissance. The structure adjacent to the open wall had collapsed and was being reconstructed at the time of the reconnaissance.



**Figure 6.46: Industrial steel roof structure outside Antakya.**

Steel is more commonly incorporated as components in residential and commercial buildings such as sandwich panel roof decking on precast concrete buildings or to frame penthouse or podium roof structures. Figure 6.47 shows observed examples of structural steel structure framing for a new podium roof under construction and a collapsed penthouse roof on a four-storey building. Many light framed roof structures observed had collapsed, presumably due to inadequate bracing or anchorage to the main structure.

Although the CAEES/ACGPS structures team did not investigate any residential buildings with structural steel as the main gravity and seismic force resisting system, the good performance of a multistorey three building residential complex in İskenderun was reported in a local publication named “Çelik Yapılar” published by the Turkish Structural Steel Association (TUCSA). This three-building complex named “Steel Towers” did not experience notable damage and continued to be occupied by residents without any interruption. The photograph of this complex is the courtesy of TUCSA (Figure 6.47 b)).



Structural steel podium (left) and roof (right)



Residential buildings with structural steel framing.

**Figure 6.47: Examples of structural steel in residential buildings (image courtesy of Celik Yapilar).**

## 6.8. Hospitals

The structural team visited two hospital sites. While more recent hospitals are required to be base isolated, these two were not.

The Islahiye hospital, a shear wall concrete structure with three storey above ground with one basement remarkable because of the little damage it presented to the building, while an important surface rupture was observed in the parking lot, as illustrated in Figure 6.50 and further discussed in Section 3.1.4. Exterior damage was limited to failure of limited portions of the façade cladding. Vertical displacement of exterior slabs on grade was also observed due to

the surface rupture. Hospital officials and staff indicated that the construction of this hospital dates from 2014, and that it was constructed on a mat foundation due to an underground waterway found on site. They reported no to limited structural damage, but damage to medical equipment. Service was continuously provided after the earthquake. To achieve this, power was supplied by a generator, and water and sewage, cut off due to the earthquake, was replaced by portable systems.



**Figure 6.48: Islahiye hospital [37.04449522, 36.62957175].**

The Nurdagi hospital, nonfunctional at the time of our reconnaissance, is a two storey and a basement concrete structure relying primary on frames as the lateral load resisting system. While no structural damage was observed, the building stood out for its extensive non-structural damage. Figure 6.49 shows the exterior damage to the building's cladding. It appears that the attachments to the supporting structure were not adequate. Figure 6.50 illustrates the interior damage, including failure of suspended ceilings and mechanical fixtures, as well as cracking of infill unreinforced concrete walls.

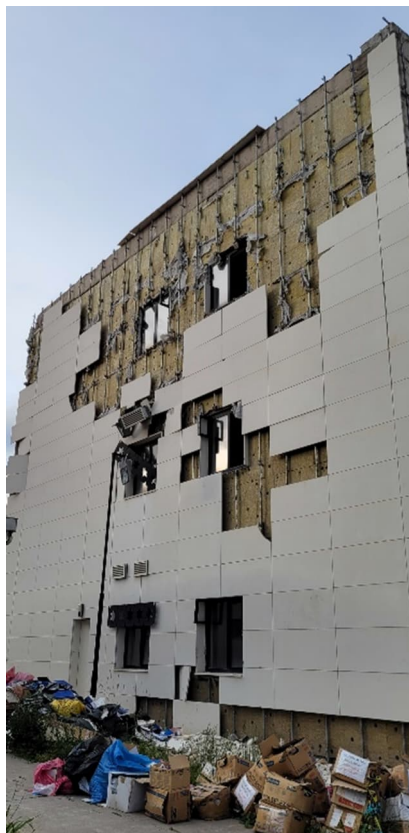


**Figure 6.49: Nurdagi hospital, exterior [37.18729225, 36.73195308].**



**Figure 6.50: Nurdağı hospital, interior damage [37.18729225, 36.73195308]**

## 6.9. Schools

The team visited six schools exhibiting different levels of damage. Two of these were located in Antakya, one in Kirikhan, one in Kahramanmaraş, one in Adiyaman and one in Malatya. Most of these schools were comprised of more than one independent structure. As evident below, the schools of modern construction performed well, while those predating the enforcement of modern codes fared poorly.

In Antakya, the first visited school was housed in two buildings of different structural characteristics. One building was a two-level historic stone masonry structure, the second was a three-level concrete frame building with masonry infill. Located in the historic neighborhood ravaged by the earthquake, the school buildings also presented severe damage and partial collapse for the historic building, Figure 6.51. The more modern concrete construction fared better, although several of the infill walls collapsed rendering the use of the school impossible as shown in Figure 6.54.



**Figure 6.51: Damage to the historic masonry building, school No.1 in Antakya [36.19927577, 36.15955117].**



**Figure 6.52: Damage to the concrete frame building, school number 1 in Antakya [36.19927577, 36.15955117].**

The second school visited in Antakya was also in a neighborhood that was severely damaged. This school was composed of several buildings of different characteristics and likely different construction dates. The older, single-storey buildings appeared to be non-engineered buildings

of a variety of construction materials, mostly concrete frames with light roofs, but also unreinforced rubble wall and some light structural steel. As can be seen in Figure 6.53, the damage was heavy, including concrete column collapse, infill wall failure, permanent displacement (leaning) and partial collapse of some buildings.



**Figure 6.53: Damage to various older buildings, school number 2 in Antakya [36.2022693, 36.15850883]**

The third visited school was located in Kirikhan with what appeared to be a two-level concrete frame building with a light wooden roof, see Figure 6.54. Observed damage was produced from an inadequate connection between the roof and the walls: the gable wall failed out of plane (potentially for lack of connection to the roof diaphragm). The entire roof also appeared to be displaced. No damage was observed to the building.



**Figure 6.54: Damage to school in Kirikhan [36.50216861, 36.35216615].**

A more modern construction school was visited in Kahramanmaraş, see Figure 6.55: Condition of school in Kahramanmaraş [37.5843718, 36.92947084].

This building, according to school staff, was constructed in 2005, and is a shear wall building with large columns and deep beams. According to staff, some clay roofing fell off, and the roof was scheduled to be replaced with corrugated steel sheets. Other than this, only some wall painting was needed.



**Figure 6.55: Condition of school in Kahramanmaraş [37.5843718, 36.92947084].**

At the school in Adiyaman, a 4 storey construction, damage to the gable walls and the roof was observed, as can be seen in Figure 6.56. It is assumed that the gable walls of the taller construction did not have a positive (tension) connection to the roof diaphragm, which made them fail out of plane. The impact would then have destroyed the lower roof. On the upper roof, displacement of the clay tile roofing can also be observed, similar to the damage described by locals for the school Karhramanmaras.



**Figure 6.56: Damage to school in Adiyaman [37.76252745, 38.26990334].**

The final school visited during the reconnaissance was a private institution located in Malatya. The school was composed of four individual buildings with different levels of damage (Figure 6.57). The school owner, who was present on site during the review, confirmed these buildings as being constructed in 2006, with concrete mixed on site.

Building 1, a 2-storey concrete frame building, showed the most damage of the four, as well as being an irregular building (see Figure 6.). Other than extensive damage to the unreinforced masonry infill walls, damage to columns was observed, where no or very highly spaced ties were observed. Additionally, pounding damage with the adjacent building was also apparent. This building was classified as heavily damaged by building inspectors.



**Figure 6.57: General overview, school in Malatya [38.3268974, 38.22168567]**



**Figure 6.58: Damage to building 1, school in Malatya.**



**Figure 6.59 (Cont'd): Damage to Building 1, school in Malatya**

Building 2, a 3-storey above ground structure with a single storey basement, with concrete shear wall as the lateral load resisting system, showed much less damage, indicating that the use of shear walls was beneficial (see Figure 6.59). Here, some damage to the infill walls was observed, but little damage was visible from the outside other than at the joint to building 1. Inside, as for the other buildings, extensive damage to the operational and functional components was observed. This building was classified as low damage by building inspectors.

Building 3 was also a concrete frame building, of 3 storeys, with a more regular shape than Building 1 (see Figure 6.60). Insufficient clearance to Building 4 resulted in pounding that damaged some beams and a column. Damage was not observed in the rest of the concrete structure. Additionally, the roof of this building collapsed, and damage to the infill walls was observed. It was classified as heavily damaged by building inspectors.

Finally, Building 4, a one level concrete frame building, did not exhibit any visible damages (see Figure 6.61).



**Figure 6.59: Damage to Building 2, school in Malatya.**



**Figure 6.60: Damage to Building 3, school in Malatya.**



**Figure 6.61: Damage to Building 4, school in Malatya.**

## 6.10. Performance of Non-Structural Components

Large spread damage to non-structural components was widely observed, even for buildings with moderate to no structural damage. These damages not only represent financial loss, but they can be a hazard for life safety during and after the event, as well as impacting the operation of the buildings.

Two other, less obvious consequences of these damages were also observed on the field. First, the team was approached by building owners wanting a second opinion on their buildings throughout the visit, which on several occasions, were observed to have no to little structural damage but were deemed unfit for repair by the rapid screening according to local sources. This conservative approach is understandable given the large number of buildings that needed to be evaluated within a short time span immediately after the event.

Second, conversations with locals also allowed us to understand the loss of confidence of many building inhabitants. An example of this was a private school scheduled to be demolished and reconstructed by the owner's decision, even for buildings with non-structural damage only, to ensure parents would enroll their children again once the new buildings were completed. Both scenarios result in unnecessary demolition of buildings, with the associated disruption, economic loss and environmental impacts, and demonstrate once more the importance of a robust seismic design of non-structural components.

The most common and impactful damage observed was to unreinforced masonry infill walls, constructed tight to surrounding structural elements (columns, shear walls, beams and slabs). These were commonly found at all visited locations and many instances of poor performance were observed. Various blocks types were observed being used for infill masonry. Figure 6.62 shows typical infill wall material seen frequently used in reinforced concrete frame construction. Terracotta hollow clay tile masonry was the most observed type overall.

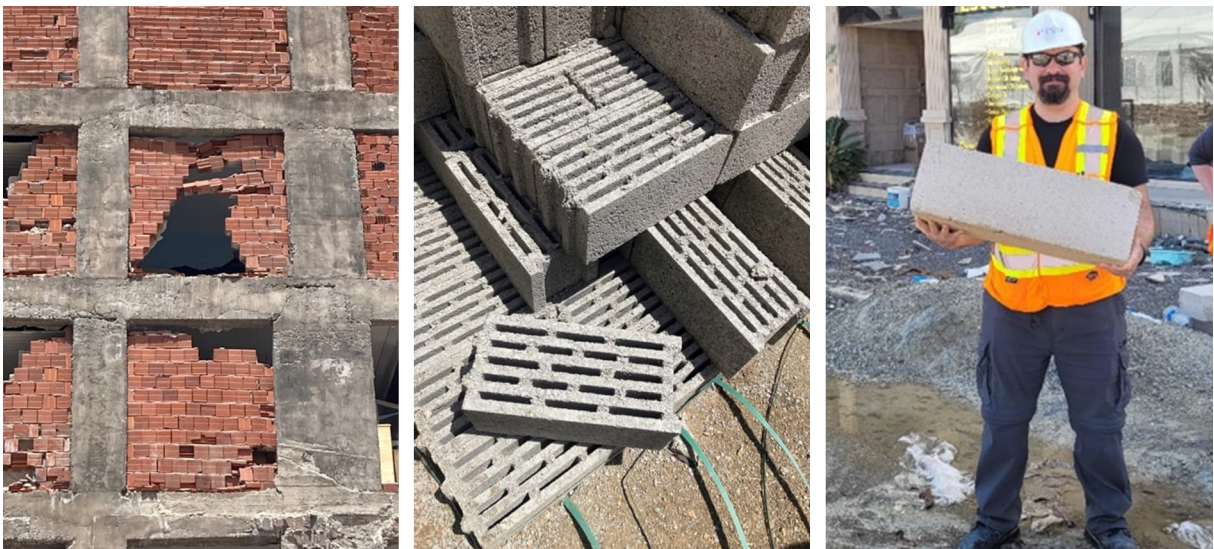


**Figure 6.62: Examples of block types commonly used: terracotta hollow clay tile, lightweight concrete masonry blocks, and autoclaved aerated concrete blocks.**

More recent construction appeared to be installing mostly light-weight alternatives, such as autoclaved aerated (AAR) concrete blocks. AAR is extremely light weight and has superior insulation characteristics.

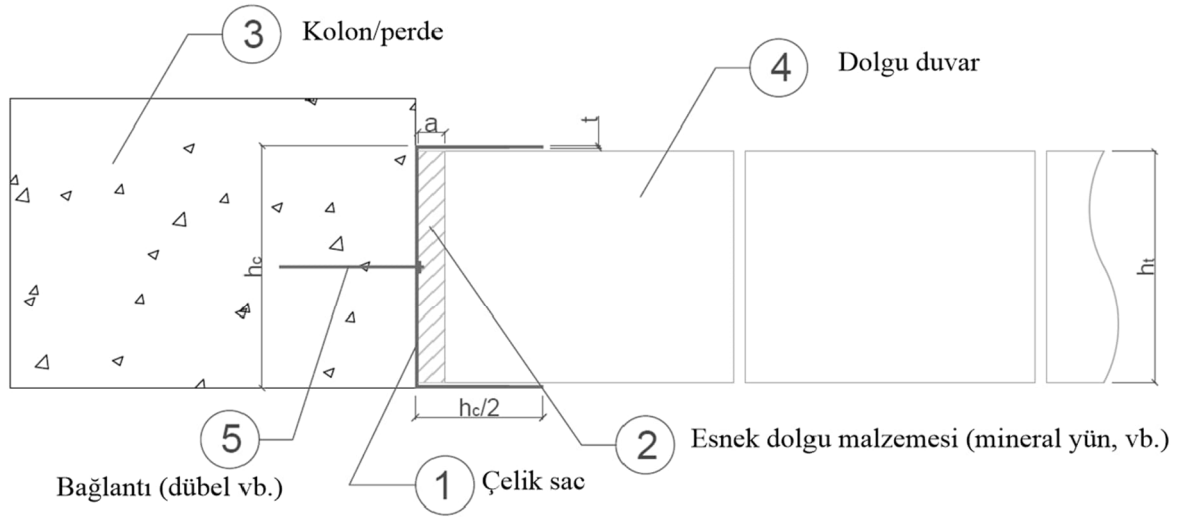
Figure 6.63 shows some examples of buildings that structurally fared well, but that had extensive damage to the infill walls. It is worth noting that these types of damage were found even in buildings of recent construction. In fact, the image on the right is of a building under construction at the time of the earthquake.



**Figure 6.63: Buildings with damage to unreinforced masonry infill walls.**

Two failure modes were commonly encountered: (1) in-plane diagonal cracking, and (2) out-of-plane failure. In-plane diagonal cracking (Figure 6.65) was observed mostly for wall piers between windows, and over the full height on infill panels. Some cases of damage to spandrels were observed (see first image in Figure 6.66). This appeared to occur where spandrels were shallow.

Since the 1975 edition, the seismic code in Türkiye has required that URM partitions be constructed to not carry gravity loads but be connected to framing for out-of-plane stability. The 1998 and 2007 codes require a minimum 10mm gap above the infill walls while keeping the same connection requirement at the ends. The 2019 seismic code was the first to include a figure showing the masonry restrained with a C-shaped bent plate (Figure 6.64). The structural team did not observe any form of restraint for masonry partitions or infill in the field. Even buildings currently under construction had no evidence of restraint angles or gaps to structural framing.



Şekil 4C.1

**Figure 6.64: Figure from the 2019 Seismic Code detailing required out of plane restraint for masonry infill walls.**

As can be seen throughout this section, other building components were severely affected by the earthquake. Some observed damage typologies are collapse of heavy façades due to inadequate attachment to the supporting structure (Figure 6.66), failure of suspended ceilings and related MEP equipment (Figure 6.67) and damage to ancillary light-weight steel structures (Figure 6.68).



**Figure 6.65: In-plane diagonal cracking of masonry infill walls.**



**Figure 6.66: Inadequate attachment of façade cladding.**



**Figure 6.67: Collapse of ceiling and mechanical, electrical, plumbing (MEP) fixtures.**

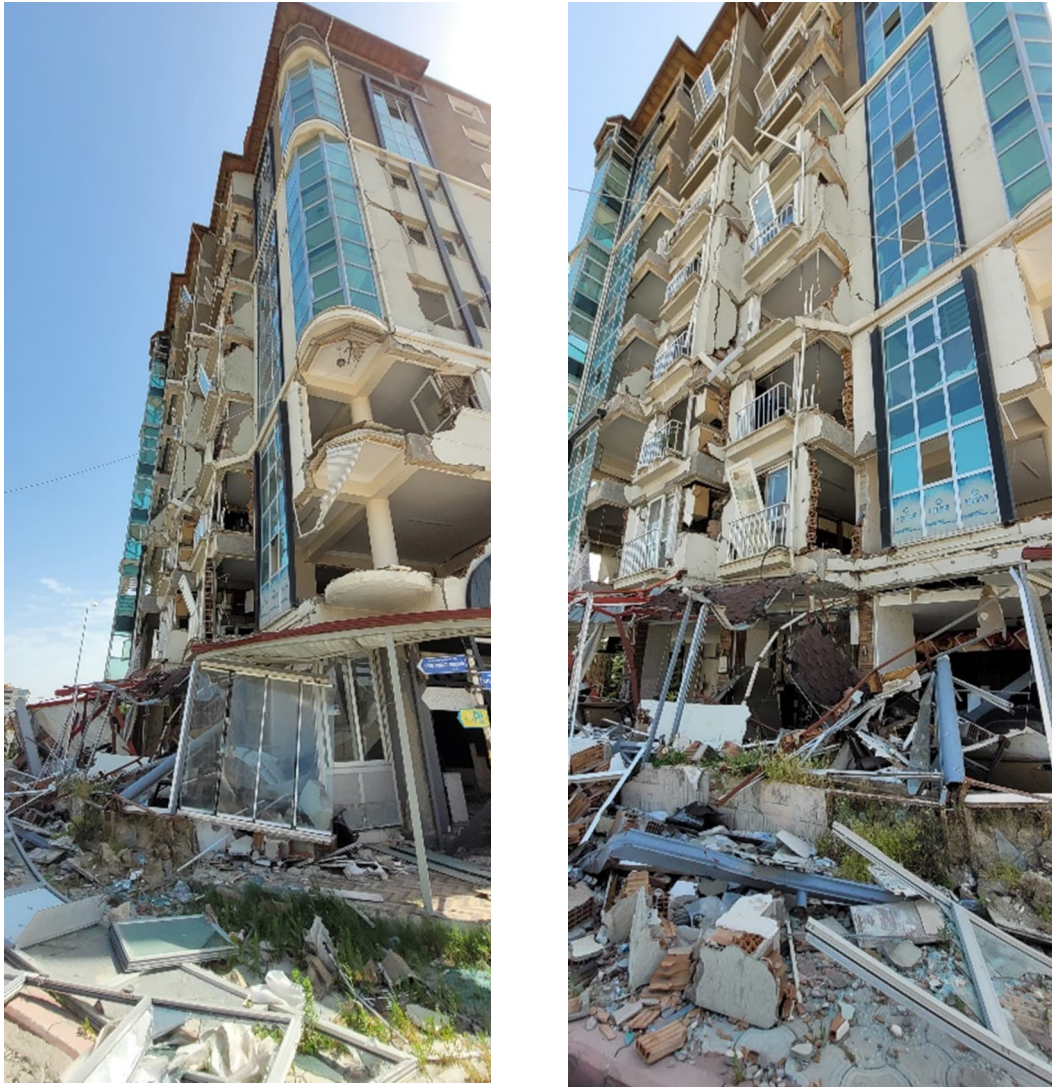


**Figure 6.68: Damage to entry canopy and windows.**

### **6.11. Pounding and Impact Damage**

While buildings, especially in densely populated areas, were observed to be constructed without any or with an insufficient seismic gap, damage was mostly seen for cases where the floors of the two structures were misaligned, and/or where structural characteristics of the two buildings were dissimilar.

In Gölbaşı, pounding was observed between a 4-storey and a 2-storey building with misaligned floor diaphragms, see Figure 6.69. The slab of the taller building impacted an infill wall causing its failure. Note that the lower building also presented significant structural damage that could not be attributed to pounding.



**Figure 6.69: Pounding damage in Gölbaşı [37.78972311, 37.65123458].**

Another example of pounding was observed in Adiyaman, where a 5-storey and 9-storey building, with misaligned floor diaphragms, exhibited damage produced by pounding, see left images (a) in Figure 6.70. In Kahramanmaraş, the façade of a shopping mall appeared to have been constructed without respecting the minimum spacing of the building's seismic joint, producing local failure of the cladding, see right image (b) in Figure 6.70.



(a) Adiyaman



(b) Kahramanmaraş

**Figure 6.70: (a) Pounding damage in Adiyaman [37.76320913, 38.27261233] and (b) Kahramanmaraş [37.56952171, 36.92154011].**

Another type of damage found frequently was due to impact of a building on the surrounding structures when collapsing. Some examples observed in Antakya are presented in Figure 6.71, where buildings have partially collapsed in the zone where impacted, over a height of several storeys. This type of damage is virtually impossible for building owners to foresee or avoid, given that it would require the distance to neighboring buildings to be equivalent to their height.



**Figure 6.71: Damage due to impact of adjacent building collapse in Antakya, (a) [36.22763627, 36.16370273] and (b) [36.22044677, 36.14869397] and (c) İskenderun [36.59072930, 36.17922080]**

## 6.12. Effects of Soft Soils and Liquefaction

The area affected by the two earthquakes have extensive regions of soft soils, some prone to liquefaction. Figure 6.72 illustrates the areas of liquefaction and soft soils.

İskenderun and Antakya suffered significantly from the effects of soft soil, resulting in settlement, tilting, and sinking of otherwise well-constructed buildings. The effects of liquefaction and lateral spreading are discussed in detail in Section 5.1 with examples of associated damage to buildings in İskenderun and Gölbaşı (Figures 5.2 to 5.8, 5.12 to 5.13, 5.17 and 6.20). The extent of damage sustained due to soft soils and liquefaction was observed to be very significant, resulting in the total destruction of a large area in downtown Antakya. This emphasizes the importance of geotechnical assessment prior to site selection for building construction.

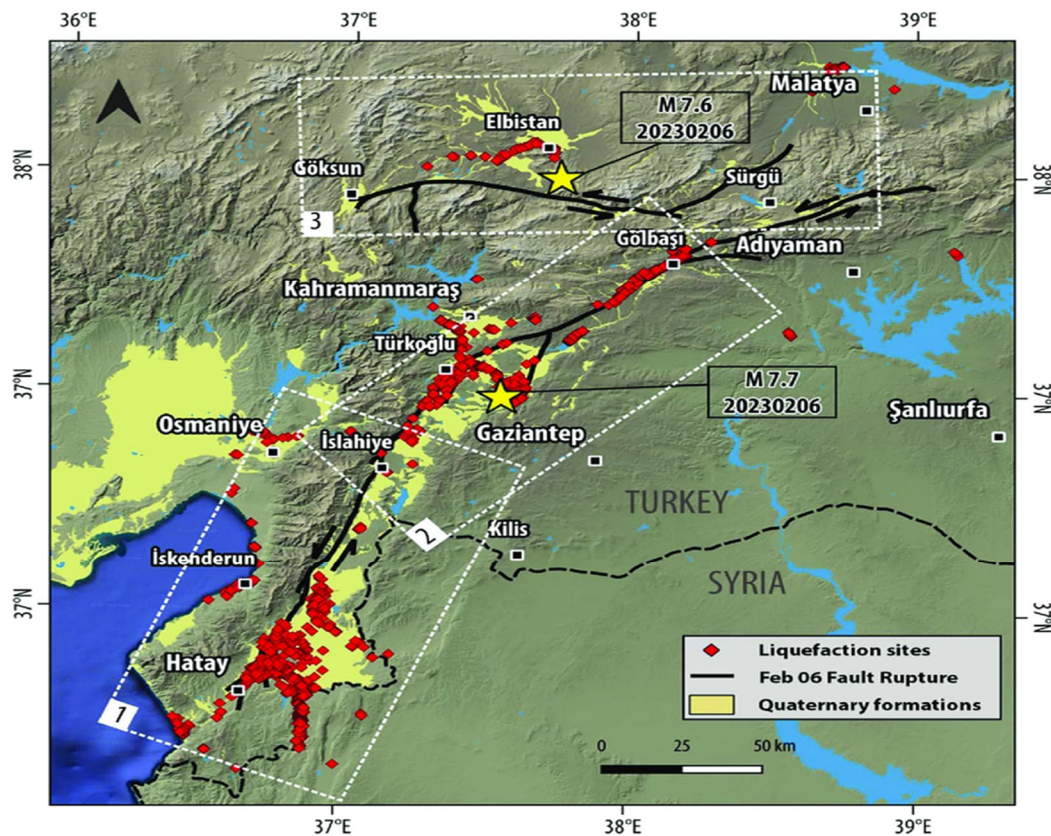


Figure 6.72: Areas of liquefaction and soft soils [27].

## 7. Traditional Residential Buildings and Cultural Heritage

Bora Pulatsu

### 7.1. Introduction

A remarkably diverse traditional residential and heritage building stock was observed during the reconnaissance visit of seven cities in the Southeastern part of Turkey severely affected by the Kahramanmaraş earthquakes. Among the wide range of construction techniques, unreinforced stone and brickwork masonry was the dominant construction morphology for the non-engineered residential buildings, together with timber-frame with infill masonry and timber-laced masonry wall constructions. Also, a wide range of traditional seismic strengthening techniques was noted, such as the implementation of tie rods and ring beams and large and regular cornerstones connecting orthogonal walls, significantly reducing the damage in the load-bearing components of the buildings by enhancing the structural integrity. It is worth highlighting that most of the failures noted during the reconnaissance were related to a lack of proper connections among the load-bearing transversal and longitudinal walls, incompatible interventions, and poorly constructed unreinforced masonry walls. On the other hand, a significant number of masonry buildings performed exceptionally well, which had good material and construction quality with necessary detailing ensuring the “box behaviour”. The

following sections discuss and provide an overview of the most common failure mechanisms and the significant aspects regarding the seismic response of unreinforced masonry (URM) and timber-reinforced masonry buildings.

## 7.2. Damage and Failure Mechanisms of Unreinforced Masonry Buildings

Masonry is a composite construction material consisting of units (*e.g.*, stone block, clay brick, or adobe) and mortar joints (*e.g.*, lime or cement-based mortar). Significant differences in stiffness and strength parameters between the masonry constituents typically yield localized cracks predominantly along the unit-mortar interfaces due to low bond strength in tension and shear at the mortar joints. This salient feature of URM structures leads to distinct crack patterns associated with specific failure mechanisms both in and out-of-plane directions. Also, it needs to be stressed that geometrical characteristics of the URM walls (*i.e.*, slenderness ratio (height/length), size and location of the openings), mechanical properties of masonry constituents, boundary conditions, pre-compression load, and the construction quality have an important role on the developed crack pattern and associated collapse mechanism.

The most observed in-plane (IP) structural failure modes for regular and irregular URM walls were diagonal shear cracking and flexural/rocking failure, among other mechanisms, including bed-joint sliding and toe crushing. The different failure mechanisms often occur subsequently or almost simultaneously in URM walls under seismic actions since the interaction between failure modes can happen under increasing lateral displacement. Figure 7.1 shows diagonal shear and flexural/rocking failures noted at the single and multi-storey residential unreinforced stone masonry buildings. Different failure mechanisms can be seen at the URM walls in the same structural system, as shown in Figure 7.1a, in which the inner URM panels show diagonal shear cracks, whereas a flexural/rocking mechanism was observed at the right (slender) pier (Figure 7.1a). Specifically, diagonal shear failures develop when the principle tensile stresses violate the tensile strength of the masonry material and are mainly depicted by diagonal or “X” shape cracks in URM panels (see Figure 7.1b). The size and position of the openings have a decisive role in the IP crack pattern (see Figure 7.1a) and the seismic capacity of URM walls, as discussed in [28].

If the structural integrity of a URM building is not ensured, out-of-plane (OOP) mechanisms become inevitable under strong ground motions. Depending on how well the URM walls were connected to longitudinal and transversal walls as well as the floor slabs, the URM walls may fail under one-way or two-way bending. A rocking failure (cantilever behaviour) is expected when the front façade is only constrained at the base and not properly connected to the roof. In Figure 7.2, several OOP failures of multi-storey unreinforced stone masonry buildings are shown. It is worth noting that the out-of-plane failures comprised the majority of collapse mechanisms observed throughout the reconnaissance visit, suggesting a lack of proper connections, rigid diaphragm and detailing among the load-bearing wall systems in the URM buildings and heritage structures.

The wall cross-section morphology (*i.e.*, size and shape of masonry units, mortar thickness, number and frequency of through stones, etc.) has a considerable influence on the local failure mechanisms of multi-wythe (or multi-layer) URM walls. Providing inner and outer wall leaf connections via through-stones (or diatons) is critical to obtaining acceptable seismic

performance and developing monolithic action (hence a predictable kinematic mechanism) in URM walls. All these aspects are related to the construction quality of masonry walls and can be collected within the masonry quality index framework used for preliminary seismic assessment [29]. Figure 7.3 shows several of the many local mechanisms observed throughout the reconnaissance caused by poor material and construction quality. The presented wall cross-sections comprised two or three layers, where the inner space was filled with irregular small stones and rubble. Typically, wall delamination (or disintegration) is the leading cause of failure for multi-layer low-bond rubble-infilled URM walls that must be eliminated by properly connecting the inner and outer wall layers. As depicted from the failure modes (see Figure 7.3), these local failures occur prematurely under seismic forces and yield quite vulnerable conditions for the load-bearing wall system of a URM building. The photos taken from partially or fully collapsed URM buildings reveal that most multi-level walls had no through stone, transversal interlocking masonry units or any connection between interior and exterior layers, as shown in Figure 7.4. This phenomenon highlights the importance of workmanship and the quality of masonry wall construction. The separation of masonry leaves can be seen in Figure 7.4.



(a)



(b)



(c)

**Figure 7.1: In-plane failure mechanisms of unreinforced masonry buildings: (a) diagonal shear failure and flexural/rocking behaviour at the right pier (Antakya), (b) diagonal shear failure of rubble (irregular) stone masonry wall (Antakya), (c) flexural/rocking failure at the URM panel between two openings (Osmaniye).**



(a)



(b)



(c)

**Figure 7.2: Out-of-plane failure of front façade:(a-b) stone masonry building (Antakya), (c) mixed timber-stone masonry house (Kahramanmaras)**

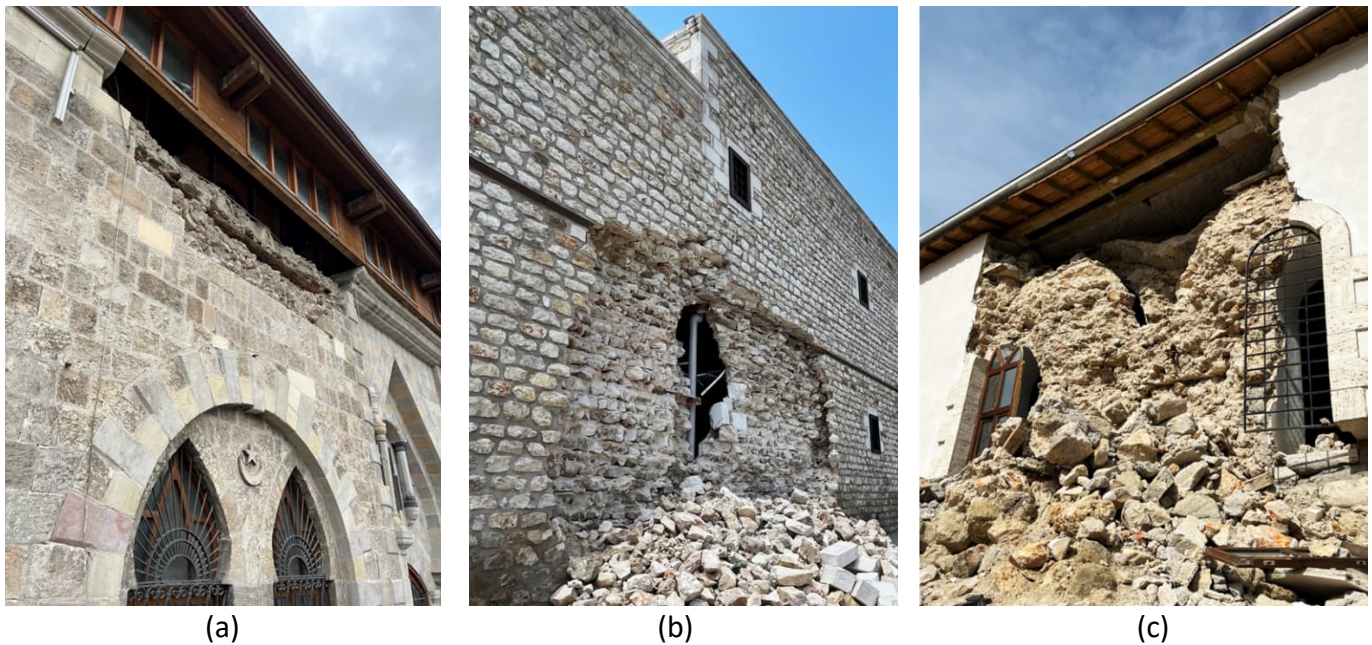


**Figure 7.3: Local failures due to wall disintegration: (a) Arasa Mosque (Kahramanmaraş), (b) stone masonry building (Adiyaman) and (c) Cami-i Kebir – Mosque (Malatya)**



**Figure 7.4: Typical multi-leave URM wall cross-sections taken from partial or total collapsed buildings**

Corner and combined IP-OOP failures were another local mechanism noted during the reconnaissance visit, shown in Figure 7.5a and Figure 7.5b, respectively. The former failure

mode generally happens when one corner of the building is free to displace (no adjacent structure), and the orthogonal URM walls are well-connected so that wedge shape cracks can develop (see Figure 7.5a). The openings closely positioned to the corner and the thrust force imposed by the roofs inclined in perpendicular directions are the primary factors initiating this mechanism. The latter, the combined IP-OOP mechanism, corresponds to failures stemming from the combined action of IP and OOP damages. As presented in Figure 7.5b, a URM wall initially suffered from IP damage that was later exposed to the OOP component of the ground motion leading to failure. It is worth noting that this kind of bidirectional interaction becomes very important considering the aftershocks for already damaged buildings. *Both* corner and combined IP-OOP failure modes are open for research and need further experimental and computational investigations.

### 7.3. Traditional Timber-Laced and Infill-Frame Masonry Buildings

The utilization of timber lacing in masonry structures constitutes a considerable portion of the existing residential building stock in non-metropolitan settlements of Türkiye. Although the timber frame typology and detailing may vary from one region to another based on the local building tradition and skill set of the craftsman, the braced timber frame with masonry infill has distinct features from a structural behaviour and seismic performance point of view when compared to modern and URM buildings. This traditional form of construction is called “*Hımiş*” in Turkish, shown in Figure 7.6a, and it is possible to notice similar construction morphologies in other European countries, including France (Colombage), Germany (Fachwerk), Portugal (Pombalino Gaiola), among others as well as in India (Dhajji-dewari). The masonry infill is single wythe (approximately 10-15 cm thick) and covered with plaster (see Figure 7.6c). While the upper floors are built using timber frames with masonry infill (either regular/irregular bricks or rubble stone with mud or lime mortar), the lower floors have stone masonry walls, including horizontal timbers (so called “*hatıl*”) embedded into the wall, presented in Figure 7.6c. These horizontal timber elements improve the structural integrity of the stone masonry walls, especially when they are appropriately connected via wooden tie rods according to the wall thickness, which can be seen in Figure 7.6c. Instead of masonry infill, short timber studs may also be used for infilling purposes of the timber frame (called “*Bağdadı*” in Turkish), making the upper storey even lighter, as seen in Figure 7.6d.



(a)



(b)

**Figure 7.5: (a) Corner and (b) combined IP-OOP failure mechanisms**



(a)

(b)



**Figure 7.6: Traditional building typologies (a) Timber frame with masonry infill, (b) Adobe building (Malatya) and (c) Timber laced masonry wall construction (Kahramanmaraş), (d) “Bagdadi” – short pieces of timber studs used for infill (Kahramanmaraş)**

The observed failure mechanisms in traditional timber frames with masonry infill buildings were primarily caused by the damage noted at the stone masonry walls serving as a supporting system to the upper storey. The failure can occur due to excessive cracks at the URM walls and/or connection failure between the timber frame and masonry walls. Note that timber frames limit crack propagation at the masonry; hence the overall structural system conserves its integrity and continues to resist seismic loads effectively. As shown in Figure 7.7a, the excessive displacement of the timber-laced masonry walls in the OOP direction and the lack of proper detailing of the wooden frame to the stone masonry wall yielded loss-of equilibrium of the upper storey, which ended up with the total collapse of the structure. In Figure 7.7b, a local failure can be noticed at the anchoring detail of the timber frame to the masonry wall. Moreover, the contribution of the timber lacing used in the stone masonry walls can be better understood in Figure 7.7c-d. In the presence of timber lacing, the sliding and cracking failures noted at the mortar joints were limited compared to one with no horizontal timber elements (see Figure 7.7c-d). The use of horizontal timbers in the masonry wall construction provided reasonable confinement since it was continuously used through the height of the wall.

Overall, it was noted that the ductile behavior of timber frames with regular or rubble masonry infill, consisting of soft mud or lime-based mortar, offered a reasonable energy dissipation during the seismic event. In most cases, the plaster cover was cracked; however, the structural system was not failed. In most of the examined traditional buildings, the light timber frame infilled with brick masonry infill performed acceptable. This phenomenon suggests the resiliency of traditional construction techniques, including necessary detailing and compatibility among the structural materials.



**Figure 7.7:** (a) Total collapse of a “Himis” house, (b) Detachment of the supporting timber column for the upper storey from the URM wall, (c-d) Illustration of the favourable effect of confinement led by timber lacing noted on similar building typologies (Kahramanmaraş)

#### 7.4. Post-Earthquake Observations on the Local and Global Failure Mechanisms of Historical Constructions

In general, historical constructions, ranging from low-rise to monumental, have flexible floors and weak connections between orthogonal walls, which prevents proper distribution of the lateral seismic forces to the load-bearing URM walls; hence, they do not demonstrate “box-like behaviour” and suffer from localized failure mechanisms [30]. To enhance the diaphragm action, often, the existing timber floors and roof systems are replaced with heavy reinforced concrete (RC) slabs and RC ring beams. Although these interventions provide a stiffer diaphragm, they may not guarantee a better global performance of the building.

Figure 7.8 shows several OOP failure mechanisms of multi-layer unreinforced stone masonry walls strengthened via RC elements. In Figure 7.8a, the RC ring beam became visible upon the

partial collapse of the stone masonry wall. As mentioned earlier, the adopted intervention did not provide sufficient structural integrity and became disconnected from the load-bearing system due to the strong ground shaking. A similar situation is presented in Figure 7.8b, where the adopted RC roof did not prevent the OOP failure of the rubble stone masonry wall, which was detached from the RC beam. Note that the poorly constructed multi-layer URM walls may not resist the new strength demands. Hence, it is necessary to better understand the effectiveness of the implemented intervention plan beforehand.



(a)



(b)

**Figure 7.8: Out-of-plane failure of irregular multi-layer unreinforced masonry walls strengthened with RC beam: (a) St. Petrus and St. Pavlus Church (Adiyaman), (b) a stone masonry building (Antakya)**

The seismic behavior of slender URM masonry structures, including masonry towers, minarets and chimneys, was examined during the reconnaissance visit. A wide range of architectural styles, geometrical properties (*e.g.*, slenderness ratio: height over the base diameter, wall thickness, etc.), and material characteristics used in the construction of slender masonry structures (*e.g.* brick, stone, or combination of both) were noticed (see Figure 7.9). Different partial and total failure mechanisms are presented in Figure 7.9. The diagonal cracks initiated from the opening and propagating along the mortar joints were noted at the lower section of the masonry tower (Hötüm Dede Türbesi, located in Adiyaman), shown in Figure 7.9a. It is important to highlight that the seismic behavior of slender URM structures is highly dependent on the dominant frequency of the base excitation, which can trigger a global over-turning mechanism or partial collapse of the spire (or upper part of the minaret), as can be seen in Figure 7.9b. Furthermore, joint sliding and cracking developed diagonally through the height of the masonry tower (Handanbey Mosque, Gaziantep) that can be observed in Figure 7.9d. The

current (damaged) state the minaret may pose a threat to the adjacent structure in the case of an aftershock unless it is stabilized via reversible interventions as performed in another nearby minaret (Alaüddevle Mosque, Gaziantep), shown in Figure 7.9c.

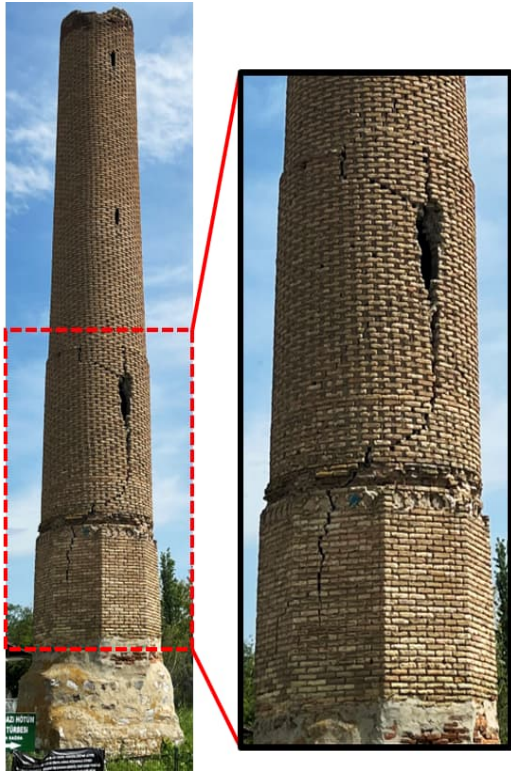
The beneficial effect of metal ties was noted on many occasions, as shown in Figure 7.10, where the strengthened masonry arch-pier systems resisted the strong ground motion. If properly connected, the adopted steel ties improve structural integrity and prevent local failures. Typically, the failures were noted either at the tie-rod connection (Figure 7.10a) or the mortar joints nearby to the tie-rod connection, which can be observed in Figure 7.10b. Overall, the implementation of steel ties was found very effective once the load carrying capacity of tie-rod connections was ensured to resist expected seismic loads (see Figure 7.10c).

Various damage conditions were observed in URM domes and vaults, shown in Figure 7.11. The damage and structural stability of URM domes are directly influenced by the boundary conditions (i.e., displacement and rotation of the supporting walls and buttresses). In Figure 7.11a, the collapse of a masonry dome is presented, which suffered from excessive deflection of the supporting wall in the outward direction. Moreover, the crack at the intrados of the vaults was noted due to the rocking behavior of the structural systems that induce flexural tensile stresses both at the intrados and extrados, given in Figure 7.11b.

The walls and towers of Gaziantep Castle were severely damaged, where most URM walls failed due to local disintegration and stone unit separation, as seen from Figure 7.12a-c. The majority of the standing parts of the castle were noticed to be the original construction.

It is worth mentioning that the stability of slender multi-layer URM walls can easily be lost if the replaced masonry units are not properly attached to the structure, or if any connecting elements, such as through stones, are not used. This was a common problem noted throughout the reconnaissance visit, where the bricks or blocks detached from the original structure stemming from disregarding the structural role of the masonry units during restoration or reconstruction.

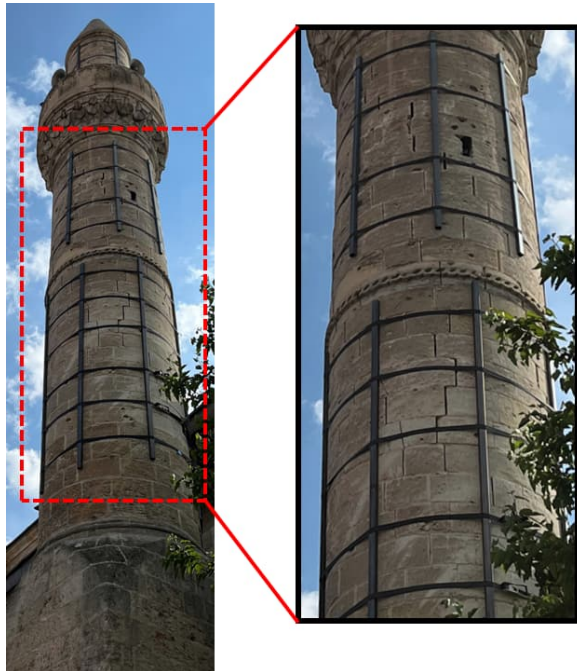
Different failure mechanisms can be noticed from the “as-is” condition of the towers, shown in Figure 7.12d, where IP and OOP and combined IP-OOP failure modes were observed.



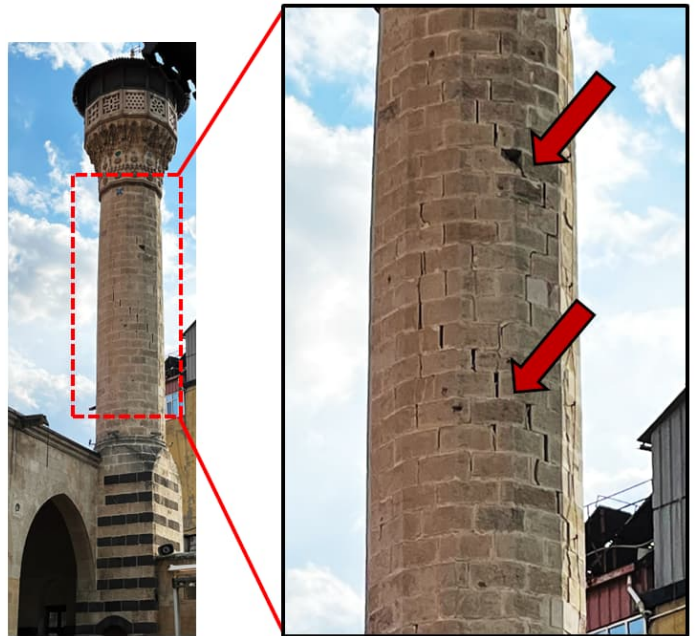
(a)



(b)

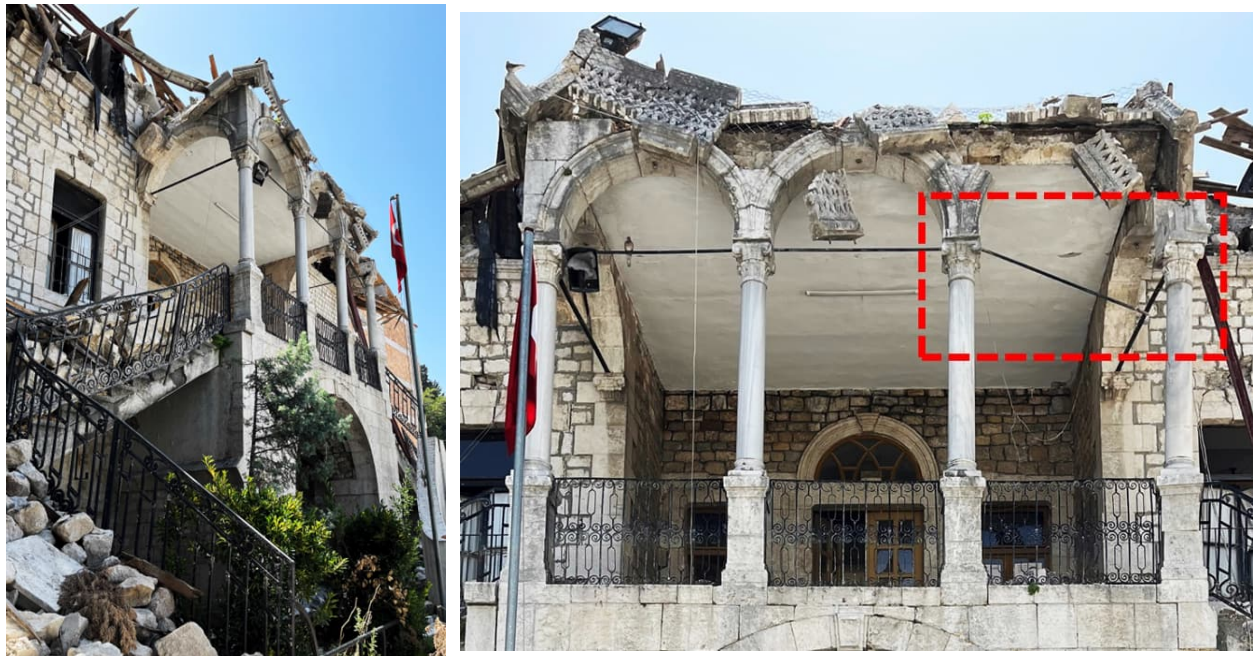


(c)



(d)

**Figure 7.9: Different failure mechanisms observed in slender masonry structures**



(a)



(b)

(c)

**Figure 7.10: The use of metal ties in different structures (a) failure of the tie-rod connection, (Ata Koleji – Antakya); (b) Damage at masonry where the connections (Roman Catholic Church – Iskenderun), and (c) Steel ties connecting inner pier-arch systems to peripheral walls (St. Petrus and St. Pavlus Church - Adiyaman).**



(a)



(b)

**Figure 7.11: (a) The collapse of a masonry dome due to tilting at the support masonry wall (the tomb of Mahmut El-Ensari, Adiyaman) and (b) cracks at the intrados of an unreinforced masonry vault (Tomb of Abuzer Gaffari, Adiyaman).**



(a)



(b)

**Figure 7.12: Out-of-plane, in-plane, combined OOP-IP, and local wall disintegration failures observed at the Gaziantep Castle (Gaziantep)**



(c)



(d)

**Figure 7.13 (Cont'd): Out-of-plane, in-plane, combined OOP-IP, and local wall disintegration failures observed at the Gaziantep Castle (Gaziantep)**

While this chapter mainly discusses partial collapse, many historic buildings and cultural heritage presented total collapse or were severely damaged. In Figure 7.14, two examples are provided where the main body of the structures turned to rubble. Only two façades of the Roman Catholic church were standing in a vulnerable condition needing stabilization (Figure 7.14a). Another example is the severely damaged and collapsed Ulu Mosque, as shown in Figure 7.14b. Although several retrofitting details were noticed in both structures (see Figure 7.14b – tie-rods were implemented), it was clearly insufficient to prevent total collapse, suggesting further investigations regarding the cause of inadequate strengthening solutions.

## 7.5. Final Remarks

Overall, a wide range of traditional and historical masonry buildings were examined that were affected by the Kahramanmaraş Earthquakes. According to the observations made during the reconnaissance visit, the following outcomes are derived:

- Most URM buildings did not suffer from severe damage or collapse, having good or high material quality and traditional seismic strengthening techniques, such as well-connected multi-layer walls, large and regular cut corner blocks, proper connection between the

orthogonal walls and floor-wall connections, among others, implemented into their structural system.

- Re-visiting the traditional seismic strengthening techniques for rural, old and heritage buildings and enhancing the practical knowledge when constructing URM structures would be beneficial to eliminate further losses in the region. A significant number of historic buildings have partially or fully collapsed either due to the lack of appropriate seismic retrofitting, inappropriate interventions or poor maintenance.



(a)



(b)

**Figure 7.14: Total destruction of a masonry church (Roman Catholic Church – Iskenderun) and mosque (Ulu Mosque, Adiyaman).**

- Post-earthquake observations indicate that the most traditional timber frame with masonry infill constructions performed well. This construction technique should be protected and further investigated as earthquake resistant system for low-rise residential buildings.
- The implementation of RC beams and slabs into the old URM wall systems should be considered carefully since it may cause unwanted failures due to their incompatibility of

the existing load-bearing wall system. To make sure the provided rigid diaphragm action enhances the seismic performance, first, the construction quality of URM walls should be assessed since the added mass may cause higher seismic demands. Therefore, the compatibility of the proposed intervention plan should be checked, and necessary structural computations should be done prior to its implementation.

- Seismic retrofitting via steel tie rods was found to be very effective, often noted at the arch-pier systems. However, monitoring of their condition needs to be done, especially for historical buildings, since the failure at the steel-tie connections was noted on several occasions.

## 8. Lifelines

Yavuz Kaya, Jason Dowling, Emre Insel, and Martin Zaleski

### 8.1. Performance of Roadway Network

The team used the roadway network for travelling to affected areas. Damage on roads was mainly caused by failure of soil support and surface rupture (see figures in chapters 3 and 5 of this report). At the time of the teams' mission, major highways and roads were partially repaired. However, we were able to observe road surface failures due to the reasons mentioned above.

### 8.2. Performance of Bridges

The team inspected bridges as they travelled throughout the effected region. Approximately one hundred bridges were inspected, and report logs created within the field reporting applications used by the team, with many instances of damage noted. In general, however, the performance of the transportation structures during the strong shaking was very good. The predominant factors noted to affect the performance of different structural configurations were geotechnical conditions, articulation details and detailing (to the extent it could be observed), and examples are presented in this section.

It was intended to inspect a random general sampling of the bridges in the earthquake region, and the majority of the structures inspected were in the cities and towns visited, or along, or a short detour off, the connecting routes. The remainder were sought out based on investigation and discussion with others in the region.

For convenience of discussion, the inspected structures can be distributed into three groups based on the observations in the field and common performance characteristics: typical highway underpasses, pedestrian bridges and other bridges.

#### 8.2.1. Typical Highway Underpasses

Highway underpasses share structural and performance traits that lend themselves to quick speed of construction and robust seismic performance. From our observations, typical highway underpasses, such as that shown in Figure 8.1, have the following shared structural characteristics (with slight idiosyncratic variations):

- a pair of simple-spans
- central wall pier, abutments with wingwalls and approach embankments
- elastomeric/rubber bearings
- precast girders and CIP deck
- transverse shear keys at abutments and pier
- link deck at central pier and expansion joints at abutments.



**Figure 8.1: Typical Highway Underpass**

The clear majority of the many observed typical highway underpasses performed extremely well during the earthquakes, with no observed damage. Where damage was seen, it was typically spalled/cracked shear keys, indicating that the spans had displaced temporarily or permanently during the shaking. At two bridges we observed complete shear key failure. One of these cases is shown in Figure 8.2, where the two exterior shear keys of the central wall pier can be seen to have failed, rotated outwards and are hanging 180° out of alignment with their original orientation. The interior shear keys are badly damaged, but sufficient reinforcing remained in place to prevent the girders from unseating during the shaking.



**Figure 8.2: Damaged shear keys at a Typical Highway Underpass.**

The second highway underpass where shear key failure was observed, was a structure under construction at the time of the earthquakes. The superstructure unseated and collapsed onto the highway below. The collapse was cleared away quickly, and only the partially complete abutment and failed shear keys remained visible at the time of our visit as shown in Figure 8.3.



**Figure 8.3: Shear key damage at abutments of bridge under construction.**

Varying degrees of approach settlement was also observed in many instances. The observed settlement was typically relatively minor and did not inhibit, or minor effort only was required to restore, functionality. An approach embankment failure was noted at one structure, which resulted in severe lateral spreading and complete loss of functionality as shown in Figure 8.4, which shows relative displacements of adjacent segments of asphalt of greater than a metre in places.



**Figure 8.4: Approach Embankment Failure at a Typical Highway Underpass in Gaziantep.**

### **8.2.2. Pedestrian Bridges**

The observed pedestrian bridges were widely varying in their configuration and structure, but shared the distinguishing trait that their relatively lightweight superstructure aided good seismic performance and very little damage during the earthquakes. The majority of the pedestrian bridges were encountered in urban settings and were most often steel access towers and superstructures. An example of a typical pedestrian bridge is shown in Figure 8.5, near Kahramanmaraş.



**Figure 8.5: Example Pedestrian Bridge near Kahramanmaraş**

There are very few instances of damage observed to pedestrian bridges, and in all cases was related to approach settlement, or non-structural, such as railing, façade panel or escalator damage. Figure 8.6 shows a steel pedestrian bridge in Antakya that had damaged/collapsed railings and façade panels.



**Figure 8.6: Damaged Pedestrian Bridge in Antakya**

### 8.2.3. Other Bridges

The typical highway underpass and pedestrian bridge groupings are convenient and logical given the obvious structural and performance similarities associated with each. Beyond these two groups, the variety of observed structure types and individual performance idiosyncrasies do not lead to any other obvious distinctions, and hence a wide variety of structures are discussed in this section.

Other bridge types inspected include:

- RC frame bridges
- multiple simple-span RC river bridges
- multiple simple-span urban viaduct bridges
- continuous steel girder viaducts
- mixed steel and concrete girder structures
- historic masonry bridges
- RC arch bridges
- continuous trapezoidal box girder viaducts
- variable depth (balanced cantilever) CIP bridges

#### Viaducts

The mountainous topography common throughout much the affected region necessitate large viaducts and tunnels for highways. An example is shown in Figure 8.7, one of a series of five closely spaced viaducts, outside of Nurdağı, Gaziantep. These structures generally performed well during the earthquakes, and the damaged observed was most frequently restricted to the approaches and joints.



**Figure 8.7: Viaduct outside Nurdağı, Gaziantep**

One 266 m long viaduct inspected (Nurdağ Viyadüğü) had, in addition to approach settlement and joint damage, shear key damage, flexural cracking and spalls in multiple columns, permanent residual deflection/drift in one column and residual superstructure span displacement at the joints. The viaduct was one of a pair of similar structures that had unknown foundation conditions (although rock outcropped adjacent to the bridge single RC column bents, three continuous curved steel girder spans (with four web lines and adjoining bottom flange plates) and two simple precast concrete box girder spans (four box girder lines), modular joints at the abutments and intermediate expansions joints.

### **Modular Joints**

The longer bridges tended to incorporate multiple modular joints. This is true for viaducts, which, with their longer continuous spans are suited to the application of modular joints, but also for longer multiple simple-span structures, which often featured link slabs making adjacent spans thermally continuous and grouping thermal movement to a smaller number of the total of piers and abutments.

There were many instances of damage at modular joints, most often involving larger than anticipated joint movements and/or settlement at approaches. Many of the joints that were damaged on the larger highways had been temporarily repaired to reinstate traffic quickly after the earthquakes, and in one case the joint replacement was under construction. An example of the frequently observed damage scenario is shown in Figure 8.8, which shows the temporary repair asphalt, evidence of approach settlement at barriers and damage to the utilities and ducting. Other damaged joints frequently featured spalled concrete and deformed railings due to pounding.



**Figure 8.8: Damage at a viaduct abutment modular joint (not visible under temporary repair asphalt) and barrier**

### Girder Damage

The earthquake loading damaged at least five girders on a pair of 5-span concrete bridges in Antakya. The spans were all simple, with seven prestressed concrete girders and each pier/abutment had four shear keys. One of the damaged girders is shown in Figure 8.9, which shows a destroyed web near the support, due to overloading the girder in weak axis bending when the girder pounded into the shear key.



**Figure 8.9: Damage to precast girder, abutment and drainage pipe, Antakya**

Many of the shear keys were also damaged on these bridges, and many spans had permanent displaced offsets. Observations suggest that the web of one of the girders had been damaged when it was subject to weak-axis bending due to the large vertical accelerations and its constructed condition with a misaligned bearing – there was a 50mm or so misalignment between the girder and bearing centerlines, and constructed geometry was such that it could have not impacted a shear key, hence the horizontal force that is thought to have caused the damage came from the horizontal component of the vertical accelerations that resulted from the unintended eccentric loading.

### Liquefaction Damage

There were many observed instances of liquefaction throughout the region, which will be more thoroughly reported in the geotechnical sections of this report (Section 5). Here, we will focus on a single site only, Demirköprü, as shown in Figure 8.10, which was subject to the effects of liquefaction and a significant amount of lateral spreading.



**Figure 8.10: Liquefaction damage at Demirköprü**

The twin Demirköprü structures were built in 1990 and are 62 m long with three simple-spans, hammerhead river piers and seven girder lines with elastomeric bearings. The area all around the bridges liquefied, and sand boils and lateral spreading were widespread. The approaches settled by approximately 500 mm from a distance of about 200 m to the east, they also moved slightly south. The eastbound lane approach embankment settled much more than the westbound lanes.

The southern structure was reopened 14 hours after the earthquake, the east abutment was the only structural damage, and both approaches had settled and spread, but fill near abutments and asphalt over pavement cracks allowed vehicles to pass.

The east abutments have four 914 mm piles, and they have settled and rotated by approximately 23°. The west abutment of the northern bridge was also rotated towards the water and to the north, there were large cracks in the piles at cap level. The two river piers of the north bridge have rotated and tilted. The gaps between the girders of adjacent spans landing in the river piers opened and contained permanent deformations horizontally and vertically, due to pier translations and rotations.

Girder on bearing alignment, shear key cracks and the north bridge west abutment pile permanent deformations indicate that the two structures rotated clockwise in plan somewhat.

The channel faces were made of grouted riprap, which was destroyed on the east face. A sand boil was seen adjacent to one rotated pile, and lateral spreading cracks were seen below the riprap just above water level.

A drainage channel crossed under the east approach. It was fractured on either side of the bridge and at the median where it was blocked. The extent of lateral spreading is particularly evident to the north adjacent to the building, which appears to be damaged, and tilted.

Prior to the earthquake, the bridges appear to have been in generally good condition. Substructures looked excellent, but superstructures showed signs of deterioration and corrosion at sidewalks and abutment joints (what remained to be seen). The south structure showed cover spalling and extensive rebar corrosion on the outside face of the sidewalk cantilevers, and there were local spalls and rebar corrosion near abutments.

### **Historic Masonry Bridges**

An example of an historic masonry bridge (that had been refurbished in 2019) is shown in Figure 8.11. The spandrel wall had partially collapsed in one location during the earthquake. This is the only example of structural damage observed among inspected masonry structures.



**Figure 8.11: Masonry Bridge (Tarihi Batiayaz Köprü)**

### **8.2.4. Summary List**

Figure 8.12 lists the majority of the structures inspected (some undamaged duplicate structures are omitted for brevity).

**Figure 8.12: Bridge Summary List**

Location	Bridges inspected and observed earthquake damage
Antakya	<ul style="list-style-type: none"> <li>- 4-span CIP RC urban bridge</li> <li>- single-span RC urban bridge: RC wall beside abutment collapsed</li> <li>- 2-span CIP RC urban bridge: adjacent RC wall collapsed</li> <li>- 3-span prestressed girder urban bridge, with decorative towers and cables</li> <li>- 4-span parallel CIP girder urban bridges: minor shear key damage</li> <li>- twin 4-span parallel CIP girder urban bridge: minor shear key damage</li> <li>- twin 5-span urban bridges, with 7-prestressed girders and 4 shear keys: webs destroyed (one due to vertical acceleration), lots of shear key damage</li> <li>- Historic stone arch: spandrel at abutment collapsed</li> <li>- Pedestrian Bridges: <ul style="list-style-type: none"> <li>- Steel low arch: façade and railing damage</li> <li>- 6-span continuous steel: abutment settled 100mm due to lateral spreading</li> <li>- 5-span continuous steel</li> <li>- 3-span through truss steel</li> <li>- Tall circular steel arch with cables supporting deck</li> </ul> </li> </ul>
Iskenderun	<ul style="list-style-type: none"> <li>- Multi-span steel pile and CIP dock pier with approach span: liquefaction-induced damage at approach with differential settlement</li> <li>- Pedestrian Bridges: <ul style="list-style-type: none"> <li>- RC arch</li> </ul> </li> </ul>
Demirköprü	<ul style="list-style-type: none"> <li>- Twin 3-span highway river bridges: extensive liquefaction-induced settlement and lateral spreading of both approaches, with permanent deflections and rotations at the piles and piers, with pile, shear key and abutment damage</li> </ul>
Kahramanmaraş	<ul style="list-style-type: none"> <li>- Single-span urban highway underpass, with 70-prestressed I-girders: shear key damage</li> <li>- Single-span highway underpass (under construction): shear keys, sidewall failed, girders unseated</li> <li>- 5-span RC frame (carries drainage channel under highway)</li> <li>- Pedestrian Bridges: <ul style="list-style-type: none"> <li>- 2-span continuous steel, with stairs and escalators: escalator railing damage</li> <li>- 2-span continuous steel, with stairs (under construction)</li> </ul> </li> </ul>
Nurdagi	<ul style="list-style-type: none"> <li>- Twin viaducts # 1: parallel viaduct bridges, precast girders and RC piers</li> <li>- Twin viaducts # 2: parallel viaduct bridges, 3-spans of continuous steel girders and 2-spans of simple precast concrete trapezoidal box (four per span), on concrete piers: the joints at the abutments failed, as did the joint between the steel and concrete spans; the west pier had concrete cracking above grade, the second pier showed signs of soil failure around the column that failed as the column moved laterally in the earthquake, and the third (tallest) pier had a steel jacket retrofit, it tilted visibly to the west</li> <li>- Twinned #3 viaducts: tall piers, continuous steel superstructure; concrete footings constructed in excavations in rock face, rock face had rock anchors and concrete facing with imbedded reinforcing mesh.</li> </ul>

	<ul style="list-style-type: none"> <li>- Twinned viaducts # 4: tall piers, 5-span continuous steel superstructure; concrete footings constructed in excavations in rock face, rock face had rock anchors and concrete facing with imbedded reinforcing mesh: west modular joint damaged, and temporarily repaired with asphalt; east joint seals torn, and barrier and sidewalk cover plates damaged; utilities embedded in concrete damaged at joint; minor cracking/spalling at foundation excavation cut slope retaining concrete</li> <li>- #5 Viaducts: parallel viaduct bridges, precast girders and RC piers, each 8 simple spans, 3 modular joints: modular joints failed at each abutment and temporarily repaired with asphalt; vertical and lateral permanent offsets at abutment approach barriers; parapet concrete damaged at all joints; utilities embedded in sidewalk concrete damaged, minor cracking at the hinge zones at the bases of the concrete piers</li> </ul>
Gaziantep	<ul style="list-style-type: none"> <li>- Typical Highway Underpass Bridges:             <ul style="list-style-type: none"> <li>- Five two-span precast concrete girder highway underpasses: shear keys damaged, bearings damaged, single seal joints damaged; permanent offsets at bearings (elastomeric bearings in shear with displacement equal to height, ruptured bearings; approach failed under lateral spreading for one of the five</li> <li>- 2-span urban precast concrete girder highway underpasses</li> </ul> </li> </ul>
Pazarcik:	<ul style="list-style-type: none"> <li>- Pedestrian Bridge:             <ul style="list-style-type: none"> <li>- 2-span steel ped bridge</li> </ul> </li> </ul>
Celikkoy	<ul style="list-style-type: none"> <li>- Pedestrian Bridge:             <ul style="list-style-type: none"> <li>- 2-span steel ped bridge</li> </ul> </li> </ul>
Sambayat	<ul style="list-style-type: none"> <li>- Twin 11-span precast concrete simple spans, with large RC pier footings and lots of riprap: many cracked/spalled shear keys (spacing between shear keys and girders was even, such that in some cases only 2 of 15 girders contacted shear keys), and minor settlement of abutments</li> <li>- Twin 6-span precast concrete simple span, with large RC pier footings: many cracked/spalled shear keys; major settlement of abutments, with 150mm vertical offset at damaged utilities</li> </ul>
Adiyaman	<ul style="list-style-type: none"> <li>- CIP single span 3-girder bridge with diaphragms</li> <li>- 3-span CIP bridge, joint damage temporarily repaired with asphalt; continuous structure with short backspan, and what look like inclined tension members tying abutment to base of piers.</li> <li>- Pedestrian Bridges:             <ul style="list-style-type: none"> <li>- 2-span steel bridge</li> <li>- Four identical single-span bridges in a park: one of which has settlement at approach</li> </ul> </li> </ul>
Golbasi	<ul style="list-style-type: none"> <li>- 3 single-span CIP bridges unaffected by the widespread devastating liquefaction</li> </ul>
Malatya	<ul style="list-style-type: none"> <li>- 3-span continuous CIP trapezoidal box girder (two) bridge, with tall CIP piers: both shear keys spalled and sidewalk joint cover plates buckled throughout</li> </ul>

	<ul style="list-style-type: none"> <li>- long urban tunnel made of five closely spaced single-span bridges; retaining walls are made of shotcrete soil walls with facade concrete panels: many of which had fallen off</li> <li>- 4-span RC bridge, minor shear key cracking/spalling only</li> <li>- twin 8-span 6-girder simple-span concrete bridges with common abutments</li> <li>- 11-span concrete girder (closely spaced) bridge: only one shear key on either side, over railway tracks</li> </ul>
Eskikoy	<ul style="list-style-type: none"> <li>- Melet bridge, a beautiful old (and deteriorating) masonry arch bridge; lots of rockfalls on the road down to the river where the bridge is</li> </ul>
Ibrahimsehir	<ul style="list-style-type: none"> <li>- Twin 6-span box girder simple-span bridge</li> <li>- <i>Typical</i> Highway Underpass Bridges: <ul style="list-style-type: none"> <li>- 2-span urban precast concrete girder highway underpasses</li> </ul> </li> </ul>
Kocatepe	<ul style="list-style-type: none"> <li>- <i>Typical</i> Highway Underpass Bridges: <ul style="list-style-type: none"> <li>- 2-span precast concrete girder highway underpasses</li> </ul> </li> </ul>
Belkis	<ul style="list-style-type: none"> <li>- 3-span box girder highway bridge over made channel, with large skew, single bearing under each box and no joints at abutments</li> </ul>
Meteler	<ul style="list-style-type: none"> <li>- 1197m long twin concrete box girder bridges</li> </ul>
Birecik	<ul style="list-style-type: none"> <li>- 5-span CIP arch bridge with steel tension straps on the top of the arches, CIP spandrel columns and a drop-in span between arches</li> <li>- Adjacent 14-span continuous CIP bridge on large CIP piers</li> </ul>
Halfeti	<ul style="list-style-type: none"> <li>- Pedestrian Bridge: <ul style="list-style-type: none"> <li>- Cable bridge</li> </ul> </li> </ul>
Kadikendi	<ul style="list-style-type: none"> <li>- twin 2-span concrete bridges with tall RC piers and tall stepped abutments</li> </ul>
Şanlıurfa	<ul style="list-style-type: none"> <li>- 3-span continuous CIP bridge, with guided pot bearings and no shear keys, spans over single span bridge over channel below</li> <li>- Single-span concrete bridge over channel</li> <li>- Single-span concrete bridge over channel, with skew</li> <li>- CIP arch bridge with masonry facade, crossing channel, with long back spans: crack at back-span where wall changed angle</li> <li>- 2-arch masonry bridge, next to market (old and deteriorated)</li> <li>- Pedestrian Bridges: <ul style="list-style-type: none"> <li>- 7-arch masonry bridge, rebuilt/rehabilitated after damage about 20yrs ago</li> <li>- Five simple-span steel bridges in park above channel, all survived flood loading</li> </ul> </li> </ul>

### 8.3. Airports and Ports

Iskenderun port experienced a significant fire during the immediate aftermath of the earthquakes. Local media reported that the fires were caused by the ignition of toppled containers. Combined with damage to structures, the port was out of commission for approximately two months. At the time of the team's visit the port was operational, however access to the port was restricted. Remnants of charred debris was still visible through the fenced areas of the port at the time of the reconnaissance.



**Figure 8.12: Earthquake and fire damage at the Iskenderun Port (image from *Dunya Gazetesi*)**

Hatay airport was constructed on the former Amik Lake, and it began its operation in 2007. The runway of Hatay Airport was damaged due to surface rupture. This caused the airport to be out of commission for seven days following the earthquake. The structural damage to airport buildings was reported to be minimal by the local media.

#### **8.4. Pipelines**

The team visited a 24" diameter natural gas pipeline that follows the north side of the lake at Gölbaşı, which experienced significant embankment landsliding and liquefaction. Based on visual observation, most of the pipeline was trenched into bedrock on the inboard (north) side of the pipeline right-of-way construction grade, which has been repurposed as a scenic drive, pedestrian promenade, and lakeshore access. There was one location where the pipeline appeared to deviate from this norm and crossed ground that might have been subject to seismic ground failure. Although the team did not observe charred ground or other signs of a pipeline explosion, residents of Gölbaşı reported seeing a fireball several hundred metres high on the north side of the lake, which could be consistent with a gas pipeline rupture.

## 9. Recovery and Reconstruction Efforts

Helene Tischer and Cheryl Sewell

### 9.1. Environmental Impact

While not the main purpose of the reconnaissance team, our visit allowed us to observe the emergency response efforts, in particular solutions to shelter a large proportion of the population, as well as allow to re-establish commercial activities.

At the time of our visit, roughly three months after the earthquake, emergency rescue activities had been concluded, and life seemed to be returning to some sort of normality. In the worst affected areas, entire neighborhoods were abandoned. While there was little evidence of retrofit work, other than small interventions apparently carried out without professional guidance, we observed demolition works in progress or completed in most if not all towns and cities visited. Impressive piles of debris, in new dumping sites commonly seen off the highways, gave testimony of the amount of work already accomplished.

In many urban centres a large extent of the collapsed buildings had been removed. Huge volumes of debris and rubble, resulting from the collapse and demolition of buildings, need to be managed. The team observed the ongoing effort to stockpile debris on sites where buildings had previously stood. From these stockpiles the debris was being loaded into dump trucks and hauled away. It will be a major challenge to remove and manage the excessive volume of debris.



**Figure 9.1: Debris stockpiles on sites where buildings previously stood in Iskenderun.**

embodied carbon in which exists in concrete. With the extent of demolition and debris management, the aftermath of these earthquakes will result in a huge negative carbon impact on the environment.



**Figure 9.2: Building demolition and debris removal, Gölbaşı**

There is a serious need to make changes to construction practices and improve adherence to building code requirements to ensure that newly constructed buildings are more resilient to earthquakes.

## **9.2. Emergency Response, and Temporary Shelters**

### **9.2.1. Tent Camps and Container Settlements**

The acute lack of housing seemed to have been relieved by the distribution of tents, identified with logos of national and international relief agencies. The team observed these both in rural and urban settings, in gardens, public spaces, lining the road, and in greater numbers in newly established tent cities on the outskirts of population centers. Some examples are presented in Figure 9.3.

As a more robust solution, the use of modified containers seemed to be more widespread, see Figure 9.4. New fenced communities were being constructed in several of the visited locations.

Tents and containers were also observed to be used to allow for the re-establishment of commerce and food distribution at some locations. In severely affected areas, sanitation provided through dry latrines was observed.



**Figure 9.3: Tents in urban and rural settings serving as temporary housing**





***Figure 9.4: More semi-permanent housing constructed out of containers***

## References

- 1) The World Bank (2023). <https://www.worldbank.org>.
- 2) UNDP (2023). Türkiye Earthquakes, Recovery and Reconstruction. United Nations Development Program (UNDP) Report in collaboration with the Government of Türkiye. pp. 218.
- 3) Barka and Reilinger, 1997
- 4) City Population, "City Population - Iskenderun, Hatay," [Online]. Available: [https://www.citypopulation.de/en/turkey/hatay/TR63106\\_\\_iskenderun/](https://www.citypopulation.de/en/turkey/hatay/TR63106__iskenderun/). [Accessed 03 06 2023].
- 5) Earthquake Engineering Research Institute, "February 6, 2023 Türkiye Earthquakes: Report on Geoscience and Engineering Impacts," Earthquake Engineering Research Institute, 2023.
- 6) Türkiye Earthquake Reconnaissance and Research Alliance, "Reconnaissance Report on February 6, 2023 Kahramanmaraş-Pazarcık (Mw=7.7) and Elbistan (Mw=7.6) Earthquakes," Türkiye Earthquake Reconnaissance and Research Alliance, 2023.
- 7) Google Earth, "Aerial Imagery of Iskenderun Cay District," 16 2 2023. [Online]. Available: [earth.google.com/web/](http://earth.google.com/web/). [Accessed 2023 06 09].
- 8) City Population, "City Population - Golbasi Adiyaman," [Online]. Available: [https://www.citypopulation.de/en/turkey/adiyaman/g%C3%B6lba%C5%9F%C4%B1/1048\\_\\_g%C3%B6lba%C5%9F%C4%B1/](https://www.citypopulation.de/en/turkey/adiyaman/g%C3%B6lba%C5%9F%C4%B1/1048__g%C3%B6lba%C5%9F%C4%B1/). [Accessed 09 06 2023].
- 9) Google Earth, "Aerial Imagery of South Shoreline of Lake Gölbaşı," 6 03 2023. [Online]. Available: [earth.google.com/web/](http://earth.google.com/web/). [Accessed 06 06 2023].
- 10) S. Türkmen, H. Tağa and E. Özgüler, "Effect of Construction Material on Dam Type Selection of the Büyük Karacay Dam (Hatay, Turkey)," Geotechnical and Geological Engineering, 2013.
- 11) Turkish Society on Dam Safety, "Pazarcık (Mw 7.7) Ve Elbistan (Mw 7.6) Earthquakes with date of Feb. 06, 2023 Impacts on Dams in the Region and Possible Problems in the Future," Turkish Society on Dam Safety, Çankaya, Ankara, 2023.
- 12) R. W. Briggs, W. D. Barnhart, J. A. Thompson Jobe, C. B. DuRoss, A. E. Hatem, R. D. Gold, J. D. Mejstrik and S. Akçiz, "Preliminary fault rupture mapping of the 2023 M7.8 and M7.5 Türkiye Earthquakes.," United States Geological Survey DOI: <https://doi.org/10.5066/P985I7U2> , 2023.
- 13) H. Sucuoğlu, "New Improvements in the 2018 Turkish Seismic Code," International Workshop on Advanced Materials and Innovative Systems in Structural Engineering: Seismic Practice, 2018.
- 14) Turkish Seismic Code (2019). Disaster and Emergency Management of Türkiye, (AFAD).
- 15) Turkish Seismic Code (2007). Disaster and Emergency Management of Türkiye, (AFAD).

- 16) G. o. Türkiye, “Türkiye Earthquakes Recovery and Reconstruction Assessment,” Government of Türkiye, 2023.
- 17) Earthquake Engineering Research Center, METU, “Mw = 7.6, Kahramanmaras-Turkiye Earthquakes,” Preliminary Reconnaissance Report, p. 91, 2023.
- 18) M. Saatciogul, D. Mitchell, R. Tinawi, J. N. Gardner, A. G. Gillies, A. Ghobarah, D. L. Anderson and D. Lau, “August 17, 1999, Kocaeli (Turkey) earthquake - damage to structures,” *Canadian Journal of Civil Engineering*, vol. 28, no. 4, pp. 715-737, 2001.
- 19) American Society of Civil Engineers, “ASCE 7-22,” American Society of Civil Engineers, Reston, Virginia, 2022.
- 20) E. Kalkan and S. B. Yuksel, “Pros and cons of multi-Story RC tunnel form (Box-Type) buildings in Turkey,” *The Structural Design of Tall and Special Buildings*, vol. 3, no. 17, pp. 601-617, 2008.
- 21) C. Balkaya and E. Kalkan, “Nonlinear seismic response evaluation of tunnel form building structures,” *Computers and Structures*, vol. 81, no. 3, pp. 153-165, 2003.
- 22) V. Mohseinian, N. Gharaei-Mghaddam and I. Hajirasouliha, “Seismic performance assessment of tunnel form concrete structures under earthquake sequences using endurance time analysis,” *Journal of Building Engineering*, vol. 40, 2021.
- 23) S. Ozden and H. Meydanli, “Seismic response of precast industrial buildings during 1999 Kocaeli earthquake,” in *Skopje Earthquake -40 Years Of European Earthquake Engineering (SE 40EEE)*, Skopje, 2003.
- 24) Earthquake Engineering Research Insitute, Geotechnical Extreme Event Reconnaissance Association amd Earthquake Engineering Association and Earthquake Engineering Foundation of Türkiye, “February 6, 2023 Türkiye Earthquakes: Report on Geoscience and Engineering Impacts,” EERI, 2023.
- 25) G. Ozkula, “Preliminary Earthquake Reconnaissance Report: Turkiye Earthquake Sequence on February 6, 2023,” 2023.
- 26) Google Earth, “Aerial Imagery of Tepehan, Hatay,” 11 2 2023. [Online]. Available: [earth.google.com/web](http://earth.google.com/web). [Accessed 2023 06 10].
- 27) Taftoglou, M., Valkaniotis, S., Papathanassiou, G., Karantanellis, E. (2023). Stellite Imagery for Rapid Detection of Liquefaction Sureface Manifestations: The Case Study of Türkiye-Syria 2023 Earthquakes. <https://www.mdpi.com/journals/remotesensing>.
- 28) Surendran AV, Singh K, Pulatsu B, Gonen S, Biggs D, Erdogmus E. Effect of Opening Size in Unreinforced Masonry Walls Subjected to Lateral Loads: Computational Modeling and Code Comparison. *J Eng Mech* 2023;149:1–11. <https://doi.org/10.1061/jenmdt.emeng-6930>.
- 29) Borri A, Corradi M, De Maria A. The failure of masonry walls by disaggregation and the masonry quality index. vol. 3. 2020. <https://doi.org/10.3390/heritage3040065>.
- 30) Lourenço PB, Mendes N, Ramos LF, Oliveira D V. Analysis of masonry structures without box behavior. *Int J Archit Herit* 2011;5:369–82. <https://doi.org/10.1080/15583058.2010.528824>.